Upscaling of the Two-Phase Flows in Petroleum Reservoirs

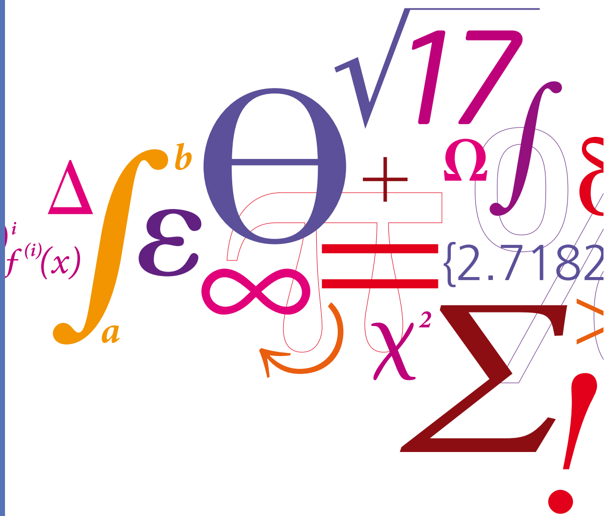

Xuan Zhang
Ph.D. Thesis
September 2011

DTU Chemical Engineering
Department of Chemical and Biochemical Engineering

Upscaling of the Two-Phase Flows in Petroleum Reservoirs

PhD Thesis

Xuan Zhang

September 2011

DTU Chemical Engineering
Department of Chemical and Biochemical Engineering

Copyright©: Xuan Zhang
September 2011

Address: Center for Energy Resources Engineering
Department of Chemical and
Biochemical Engineering
Technical University of Denmark
Søltofts Plads, Building 229
DK-2800 Kgs. Lyngby
Denmark
Phone: +45 4525 2800
Fax: +45 4525 4588
Web: www.cere.dtu.dk

Print: J&R Frydenberg A/S
København
December 2011

ISBN: 978-87-92481-54-2

Preface

The work presented in this thesis is the partial fulfillment of the requirements for the degree of Doctor of Philosophy at the Technical University of Denmark (DTU). The work was carried out at the Center for Energy Resources Engineering (CERE) from September 2008 to September 2011 under the supervision of Associate Professor Alexander Shapiro and Professor Erling H. Stenby. I would like to express my gratitude to all my supervisors.

I feel extremely privileged to have had the opportunity to pursue a PhD at DTU, as well as be enrolled in a very innovative and friendly group, CERE. I am very grateful to DTU and Danish Council of Technology and Production (FTP) for financial support in the framework of the ADORE project.

I also wish to thank Assisstant Professor Kristian Jessen from Mork Family Department in the University of Southern California (USC) for his supervision during my external research stay, as well as Dalad Krapongpang and Muhammad Jay for being my office-mates and good friends when I was working in USC.

Moreover, I want to thank all my colleagues at CERE for three-year enjoyable and fruitful time and Lars Gregersen, COMSOL, for kind consulting as regards the setting up the 2D displacement simulations.

Kongens Lyngby, September 2011

Xuan Zhang

Summary

This thesis presents a semi-analytical upscaling method for solving two-phase immiscible incompressible flows in layered porous media with very good inter-layer communication. Waterflooding of petroleum reservoirs is discussed as an example for this method. This method applies asymptotic analysis to the 2D waterflooding equations and generates multiple 1D equations for water saturation in a multi-layer reservoir model. Cases in absence of gravity and presence of gravity are studied. Although this method is derived from 2D models of reservoir, it can be used for reduction of the 3D problems to the series of 1D problems by application of the streamline methods. The commercial finite element solver COMSOL is used to simulate the complete 2D waterflooding problems as comparisons to the presented semi-analytical upscaling method.

This thesis consists of eight chapters. They are summarized below:

Chapter 1 introduces the background of the subject of fluid flow in porous media and one of its basic applications, waterflooding of petroleum reservoirs. Multi-dimensional Buckley-Leverett displacement theory is explained. Motivation and objectives of the PhD project are described in this chapter. List of publications and conference proceedings is also included.

Chapter 2 includes a review of the development of pseudo functions is followed by a short description of the generalization of reservoir models. This chapter also includes a review of the upscaling methods for multiphase flow in layered porous media.

Two extreme cases result from the layered reservoir model. The first case is that the barriers between layers are impermeable and the inter-layer crossflow is negligible. The second extreme case corresponds to perfect communication between the layers, where the exchange between them is instantaneous (the case of vertical equilibrium). Literature on both cases is discussed in this chapter.

Chapter 3 discusses the Kurbanov-Hearn method, which has previously been applied for upscaling. In our opinion, this method insufficiently takes into account the interaction between the layers. A more general and more precise study on two-phase immiscible incompressible flows in layered reservoir model under absence of gravity is then presented.

The problem is presented and transformed to the dimensionless form. The anisotropy parameter is defined as a measure for the degree of inter-layer communication. An asymptotic analysis based on large value of anisotropy parameter is applied to 2D flow equations. Finally, in a layered 2D model of reservoir, for example a vertical cross section of a reservoir, the asymptotic 2D equation is reduced to a set of 1D homogeneous hyperbolic equations.

The average saturation profiles and oil recoveries generated by our method and that by commercial finite element solver COMSOL are compared.

This chapter also introduces the implementation of complete 2D waterflooding simulation on COMSOL time-dependent PDE module. The settings for boundary and initial conditions are specified. Meshing, solver and the COMSOL-Matlab interface functions are introduced.

Chapter 4 presents a detailed discussion of the water banks and transition zones in the water saturation distribution profiles for individual layers. The water banks are formed because water tends to flow from the higher to the lower horizontal mobility variation under the existence of the inter-layer crossflow.

Chapter 5 takes the gravity effect into consideration. Two additional dimensionless parameters are needed in this case: the gravity-viscous ratio and fluid density ratio. These parameters describe the buoyancy effect onto segregation. In the multi-layer reservoir model, the asymptotic 2D integral-differential equation for saturation is derived and afterwards reduced to a set of 1D equations. When the gravity effect is moderate, this system of equations is hyperbolic. As the gravity effect increases, the system may change into parabolic form. When gravity effect becomes large, the two phases of flow may be completely separated. Our method needs to be modified in order to handle this case.

Chapter 6 shows the implementation of the vertical 1D upscaling method introduced in Chapter 3 and Chapter 5 into streamline-based reservoir simulation. In this way, we are able to solve the complete 3D problem by means of multiple 1D equations without transforming the problem into time-of-flight (TOF) domain. Unlike the conventional streamline simulation method, our 1D equations are written in terms of the path of streamlines, which is the space domain. Thus cases with gravity effect can be solved directly, without application of operator splitting. Results by our vertical 1D method along streamlines fit well with the results by 3D finite difference method.

Chapter 7 presents the conclusions from the thesis.

Chapter 8 presents suggestions for further development of the work carried out in this PhD project.

The work presented in this thesis has resulted in three journal publications and two conference proceedings so far.

Resumé

Denne afhandling præsenterer en semi-analytisk opskalering metode til løsning af to-fase blandbar inkompressibel flow i lagdelt porøse medier med god inter-lags kommunikation. Som eksempel undersøges waterflooding via denne metode. Metoden anvender asymptotisk analyse på 2D waterflooding ligninger, og genererer derved et set af 1D ligninger for vand mætningen i en multilags reservoir-model. Både situationer med og uden tyngdekraft undersøges. Selv om denne metode er udledt på baggrund af en 2D reservoir model, kan den, ved at benytte strømlinjer, anvendes til løsning af 3D problemer, der derved er reduceret til løsning af et set af 1D ligninger. Den semi-analytiske opskaleringsmetode sammenlignes med finite element løsninger af det fuldstændige 2D waterflooding problem implementeret i det kommercielle finite element program COMSOL. Denne afhandling består af otte kapitler. Disse kapitler er sammenfattet nedenfor:

Kapitel 1 introducerer baggrunden for flow i porøse medier og en af dens grundlæggende applikationer, waterflooding i Enhanced Oil Recovery (EOR), og forklarer Buckley-Leverett forskydningsmekanismen, front advance teori.. Motivation og formålet af ph.d.-projektet er beskrevet i dette kapitel. Lister over publikationer og konference biddrag er også inkluderet.

Kapitel 2 omfatter en gennemgang af udviklingen af pseudo-funktioner efterfølges af en kort beskrivelse af generaliseringer af reservoir modeller. Dette kapitel omfatter også en gennemgang af opskalering metoden til multifase flow i lagdelte porøse medier.

Den lagdelte reservoir-model giver anledning til to yderliggående situationer. Den første situation er, at barriererne mellem lagene er uigennemtrængelige og derved er inter-lags crossflow uden betydelig. I den anden situation er der perfekt kommunikation mellem lagene, det vil sige, at der er øjeblikkelig udvekslingen mellem lagene (situation med vertikal ligevægt). Baggrundslitteraturen for begge situationer undersøges også i dette kapitel.

Kapitel 3 starter med en grundig diskussion af Hearn metoden. Det er vores opfattelse, at Hearn metode ikke i tilstrækkelig grad tager hensyn til samspillet mellem lagene. En mere generel og mere præcis undersøgelse af modeller for to-fase blandbar inkompressibel flow i lagdelte reservoir uden tyngdekraft præsenteres.
Først, bringes problemet på en dimensionsløs form. En anisotropisk parameter indføres som mål for graden af inter-lags kommunikation. Dernæst, foretages en asymptotisk analyse af 2D-flow ligningerne for store værdi af anisotropisk parameter, således at den vertikale trykgradient kan negligeres. Til sidst, reduceres de asymptotiske 2D ligninger til et sæt af 1D homogene hyperbolske ligninger for en lagdelt 2D-model af reservoiret, for eksempel, et lodret tværsnit af et reservoir. Resultater af gennemsnitlige mætnings

profiler og olie inddrivelse fundet via vores metode sammenlignes med finite element resultaterne.

Dette kapitel introducerer også implementeringen af de komplette 2D waterflooding ligninger i COMSOL's tidsafhængige PDE modul. Indstillingerne for grænsen betingelser og begyndelses betingelser er specificeret. Desuden beskrives meshing er og COMSOL-Matlab grænseflade funktioner.

Kapitel 4 præsenterer en indgående drøftelse af vand bank og overgangszonens indflydelse på vand mætning fordelings profilen i de enkelte lag. Dette skyldes, at vand har en tendens til at flyde fra højere til lavere horisontal mobilitet variation under eksistensen af inter-lags crossflow.

I Kapitel 5 tages der højde for tyngdekraftens indflydelse på systemerne der blev undersøgt i kapitel 3. Det antages at anisotropi parameteren er stor. Når der tages højde for tyngdekræften er der behov for yderligere to dimensionsløse parametre, tyngde-viskositetsforholdet og væske densitetsforholdet. Disse tre effekter arbejder sammen som en del af opdriften og spiller en afgørende rolle i flow adskillelse. I multilags reservoir-modellen kan de asymptotiske 2D integro-differentialligninger reduceres til et sæt af 1D ligninger. I tilfældet hvor effekten af tyngdekraften er lille, er ligningssystemet hyperbolsk. Når værdien af effekten af tyngdekraften stiger, kan systemet skifte til parabolske form. Når effekten af tyngdekraften bliver store, kan det forekomme at de to faser af flowet er fuldstændigt adskilte. Vores metode skal ændres med henblik på at håndtere dette tilfælde, hvilket ikke er omhandlet i denne afhandling.

I Kapitel 6 gennemføres den vertikale 1D opskalering metoden introduceret i kapitel 3 og kapitel 5 for strømlinje simuleringer. Vi kan derved løse et fuldt 3D-problem ved hjælp af et set af 1D ligninger uden at omdanne problemet til time-of-flight (TOF) domænet. I modsætning til den konventionelle strømlinje simulerings metode, er vores 1D problemer skrevet langs strømlinjerne, det vil sige, i reel rummet. Derved kan situation der tager højde for tyngdekraften løses direkte, uden anvendelse af operator splitting. Resultater af vores lodrette 1D metode passer godt overens med resultaterne af 3D finite difference resultater.

Kapitel 7 indeholder en konklusion af afhandlingen.

Kapitel 8 præsenterer forslag til videreudvikling af dette ph.d.-projekt.

Arbejdet præsenteret i denne afhandling har givet anledning til tre tidsskrifts publikationer og to Konferencebidrag.

Table of Contents

List of Tables

List of Figures

Nomenclature

A Area of cross section of streamtube

B Intermediate variable, function of F; $\int_0^Y \frac{\partial F}{\partial X} dY'$

C Integration constant function of dimensionless pressure

d Number of streamline

E_a Anisotropy ratio

E_g Gravity-viscous ratio

E_ρ Density ratio

F Fractional flow of water

g Gravitational acceleration constant; 10[m/s^2]

G Function of F

h Height of layers of reservoir

H Height of the reservoir model

k Absolute permeability

K Dimensionless permeability

kr Relative permeability

L Length of the model of reservoir

M End point mobility ratio (oil to water)

N Total number of layers in the reservoir

p Pressure

P Dimensionless pressure

q Volume rate

s Saturation

t Time

T Dimensionless time

u Velocity of each phase

U Total velocity of water and oil

$\bar{U}$ Dimensionless total velocity of water and oil

v_{inj} Injection velocity

V_{inj} Dimensionless injection velocity

V^{st} Volume of streamtube

x Coordinate along reservoir

X Dimensionless coordinate along reservoir

y Coordinate orthogonal to reservoir

Y Dimensionless coordinate orthogonal to reservoir

z Horizontal coordinate orthogonal to x

Greek letters

α Fraction of height of layers

β Mean value of probability

σ Variance of probability

θ Number of background grid block

λ Mobility of fluid

Λ Dimensionless mobility

μ Viscosity

M Dimensionless viscosity

ξ Arc length of streamlines

ρ Density of fluid

τ Time-of-flight

ϕ Porosity

Φ Dimensionless porosity

φ Probability density function

Subscripts

d, e Number of streamline

i Irreducible

ini Initial

inj Injection

m, n, j Number of the layer

o Oil

pvi Pore volume injected

pro Production

r Residual

w Water

x, X Direction along a reservoir

y, Y Direction orthogonal to a reservoir

z Horizontal direction orthogonal to x

0 Scale of variables

θ Number of background grid block

Superscripts

gb Grid block

irr Irregular grids on streamline

reg Regular grids on streamline

sl Streamline

st Streamtube

* Average

Chapter 1 Background

The purpose of this chapter is to introduce the background of the subject of fluid flow in porous media and one of its basic applications, waterflooding of the petroleum reservoirs. The objectives of this Phd project are presented.

1.1 Introduction

Simultaneous two-phase immiscible flows in natural porous media arise in a number of processes important in nature and industry. These processes may be subdivided into two categories: (i) steady state, i.e., all properties of the system are time invariant at all points, and (ii) unsteady state, i.e., properties change with time. In steady state, the saturation of the medium with respect to all phases of the fluid contained in the system is constant at all (macroscopic) points. Hence, there is no displacement of any fluid by any of other fluids in the pores for steady state flows. Scheidegger (1974), Craig (1971), EL-Sayed and Dullien (1977) give examples of studies of these phenomena. On the other hand, in unsteady state, saturation at a given point in the system varies. Displacement phenomena fall in this category (Dullien (1979), Dake (1978), Bear (1972)).

The theory of displacement is of great interest in engineering, for example chemical engineering (LNAPL (Light Non-Aqueous Phase Liquids) and DNAPL (Dense Non-Aqueous Phase Liquids), Longino and Kueper (1996)), carbon dioxide sequestration in the aquifers (Pau et al. (2010)), medical and biochemical engineering, i.e. biological membrane and filters (Dullien (1979)), geosciences (Tyler and Wheatcraft (1990), (1992); Bird et al. (2000)) and petroleum engineering (see references below). Much of the study is driven by the needs of the petroleum industry and their desire to understand the dynamics of multiphase flow (Hunt (2005)).

Probably, one of the oldest and the most widely studied industrial processes in petroleum engineering is the process of waterflooding, or displacement of oil by water in petroleum reservoirs. This is the most widely used method and fundamental physical process for secondary oil recovery.

The efficiency of an oil recovery method is to a large extent determined by physical mechanism at the microscopic level, e.g. how the phases: oil, water and gas distribute in the pore space of the geological rock. Melcher (1920), Burdine et al. (1949), Bondino et al. (2010) provide some of the studies about flows in pore-scale porous media. Prediction of macroscopic (field scale) properties of petroleum reservoir, such as water cut, oil recovery curve, inter-layer communication and so on, directly determines the selection of the recovery methods. The front advance theory by Buckley and Leverett (1941) characterizes the macroscopic displacement mechanism in porous media.

1.2 Multi-Dimensional Buckley-Leverett Displacement Mechanism

1.2.1 Model Description

Consider an anisotropic heterogeneous petroleum reservoir developed by waterflooding. Assumptions for this reservoir model are:

1. There is no fault, dip or bending on the reservoir geometry.
2. The variation of reservoir properties orthogonal to the reservoir areal extent is larger than that along the areal extent.
3. No leakage or inflow at the outer boundary of the reservoir. There is only inflow from injector and outflow from producer.
4. Fluids velocity and pressure obey Darcy's law.
5. Water and oil fill the whole porous volume.
6. All properties of reservoir, like absolute permeability k_x, k_y, k_z, porosity ϕ, irreducible water saturation s_{wi}, residual oil saturation s_{or} and end point relative permeabilities kr_{wor}, kr_{owi}, may vary in space, but not with time.
7. Isothermal system as fluctuations in temperature is regarded minimal (Sarkar et al. (1994))
8. Incompressible fluids. That indicates constant density of each fluid (Sarkar et al. (1994); Orr (2007)).
9. Immiscible fluids.
10. Negligible capillary forces and gravity.
11. Constant viscosity of fluids.
12. No fluids are absorbed in the porous medium of the reservoir.
13. Chemical reactions are not considered.
14. Relative permeabilities of water and oil depend on water saturation s_w monotonically, obeying Corey power law for relative permeabilities (Corey and Rathjens (1956))

$$kr_w = kr_{wor}\left(1 - s_{or} - s_{wi}\right)^{-2}\left(s_w - s_{wi}\right)^2 \tag{1.1}$$

$$kr_o = kr_{owi}\left(1 - s_{or} - s_{wi}\right)^{-2}\left(1 - s_w - s_{or}\right)^2 \tag{1.2}$$

1.2.2 The Buckley-Leverett Theory

Buckley and Leverett (1941) presented the well known frontal advance theory. The original work was confined onto unidirectional incompressible flow through a small element of sand within continuous sand body. Along the same line of Buckley-Leverett original theory, the general mass balance equation of for water phase in a multi-dimensional waterflooding process can be written as:

$$\phi \frac{\partial s_w}{\partial t} + \nabla \cdot \vec{u}_w = 0 \tag{1.3}$$

Where s_w, ϕ, represent water saturation, porosity (may vary in space). $\vec{u}_w$ represent water velocity, which is a multi-dimensional vector. Total velocity of oil and water are defined as the sum of water velocity and oil velocity.

$$\vec{U} = \vec{u}_w + \vec{u}_o \tag{1.4}$$

Since we assume that water and oil fill the whole porous volume, water saturation and oil saturation should result in a sum of unit and the total velocity of these two phases should obey the continuity-incompressibility equation

$$\nabla \cdot \vec{U} = 0 \tag{1.5}$$

According to Darcy's law, the phase velocities are proportional to the pressure gradient (which is the same in both phases due to negligible capillary forces). The proportionality coefficient for water phase, λ_w is equal to $k \cdot kr_w / \mu_w$, where k, kr_w are absolute permeability and relative water permeability, and μ_w is viscosity of water. Absolute permeabilities and, therefore, water mobilities λ_w may be different in horizontal and vertical directions as well as at different position of reservoir. When gravity is not involved, we have

$$\vec{u}_w = -\lambda_w \nabla p = F\vec{U} \tag{1.6}$$

The velocity of oil phase is expressed in the similar way.

$$\vec{u}_o = -\lambda_o \nabla p = (1-F)\vec{U} \tag{1.7}$$

where F is the fractional flow of water in the total flowing stream, defined as in terms of relative permeabilities kr_w, kr_o and viscosities μ_w, μ_o :

$$F = \frac{kr_w / \mu_w}{kr_w / \mu_w + kr_o / \mu_o} \tag{1.8}$$

The concept of fractional flow is introduced by Leverett (1941). When relative permeabilities kr_w, kr_o are monotonic functions of s_w, F is also monotonic function of s_w.

Substitution of expressions of velocities into flow equations leads to a closed system for water saturation s_w and pressure p .

$$\phi \frac{\partial s_w}{\partial t} + \nabla \cdot \left(-\lambda_w \nabla p\right) = 0 \tag{1.9}$$

$$\nabla \cdot (-\lambda \nabla p) = 0 \tag{1.10}$$

where total mobility λ is defined as the sum of water mobility and oil mobility:

$$\lambda = \lambda_w + \lambda_o \tag{1.11}$$

A generalization of these equations onto the action of gravity is presented in Chapter 5.

For one-dimensional waterflooding problems in homogeneous media, the Buckley-Leverett theory introduces the transformation of Eq. (1.3):

$$\frac{\partial x}{\partial t} = \frac{U}{\phi} \left(\frac{\partial F}{\partial s_w} \right) \bigg|_t \tag{1.12}$$

The analytical solution for problems described by Eqs. (1.3), (1.12) can be found in Bedrikovetsky (1993).

Welge (1952) present the simplified method to the Buckley-Leverret frontal advance equation. This method consists of integrating the saturation distribution over the distance from the injection point to the front, obtaining the average water saturation behind the front.

1.3 Objectives

Since it is not possible to obtain very detailed information about the heterogeneous reservoir, and computations accounting for all the peculiarities of reservoir structure are prohibitively time-consuming, upscaling techniques are needed to get the pseudo properties of the reservoirs: pseudo relative permeabilities and pseudo fractional flow functions. These functions are used in the framework of the traditional Buckley-Leverett theory of waterflooding (Buckley and Leverett (1941)). They define average effective properties on a large scale, based on small-scale properties and their distributions. Similar problems arise in other processes mentioned above, since they often occur in heterogeneous porous media of the not-totally known structure.

This PhD project is aiming at development of a semi-analytical upscaling method. Many petroleum reservoirs may be approximated by layered models where the variation of reservoir properties orthogonal to the reservoir's areal extent is larger than that in the direction of the areal extent. The inter-layer communication may be large or small. In some previous works, the waterflooding schemes in layered reservoirs were simplified, for example, by assuming piston-like displacement fronts (Dykstra and Parsons (1950) and Dietz (1953)), interchangeable layers (Hearn (1971), Kurbanov (1961), Kurbanov and Atanov (1972)), while Bedrikovetsky (1993) makes the most complete account of all the cases. These assumptions are too strong and sometimes result in unrealistic solutions, such as step-wise saturation profile and inaccurate prediction of oil recovery, compared to full-scale numerical simulations.

The previous works give motivation for this PhD project to find a more general way for upscaling two-phase immiscible flows in layered porous media, involving the gravity effect. Inter-layer communication is quantified by a parameter of anisotropy ratio, similarly to Yortsos (1991), (1992), Zapata and Lake (1981), Yokoyama and Lake (1981). Asymptotic analysis is applied to 2D flow equations based on large value of anisotropy ratio, which means large inter-layer communication. Unlike Martin (1968) and Yortsos (1991), we only consider the zero order term in the asymptotic expansion of pressure. Furthermore, in a well-defined layered 2D model of reservoir, the system can be expressed by multiple 1D equations. This is the most important part of the PhD project.

Cases in absence of gravity are studied first (Chapter 3). The way of derivation in cases in presence of gravity is a little different from that for cases without consideration of gravity. This is written in Chapter 5. 2D water saturation profile, vertically averaged saturation profile, recovery curves are given in these two chapters. Chapter 4 presents a detailed discussion on water bank and transition zone on the water saturation distribution profile of individual layers, which is because that water tends to flow from the higher to the lower horizontal mobility variation under the existence of inter-layer crossflow.

Complete 2D simulation for waterflooding needs to be carried on as a comparison to the pseudo 1D method. The commercial computer finite element solver COMSOL is used to do the 2D simulation. The PDE Module of COMSOL is selected instead of the Earth Science Module, since it is more flexible and can handle anisotropic permeability field. The implementation of 2D waterflooding simulation is introduced in Chapter 3.

Although this vertical 1D upscaling method is derived originally from a 2D model of reservoir, it can solve specific 3D problems by application of streamline simulation (Chapter 6).

1.4 Publications

1. Xuan Zhang, Alexander Shapiro, Erling H. Stenby: Upscaling of Two-Phase Immiscible Flows in Communicating Stratified Reservoirs, Transport in Porous Media (2011)

2. Xuan Zhang, Alexander Shapiro, Erling H. Stenby: Gravity Effect on Two-Phase Immiscible Flows in Communicating Layered Reservoirs, Transport in Porous Media (accepted)

3. Hao Yuan, Xuan Zhang, Alexander A. Shapiro, Erling H. Stenby: Crossflow and water banks in viscous dominant regimes of waterflooding, Journal of Petroleum Science and Technology (accepted)

1.5 Conference Proceedings

1. Xuan Zhang, Alexander Shapiro, Erling H. Stenby: COMSOL Implementation for Upscaling of Two-Phase Immiscible Flows in Communicating Layered Reservoir. In: COMSOL Conference 2010 Paris (2010)

2. Xuan Zhang, Alexander Shapiro, Erling H. Stenby: Upscaling of Two-Phase Immiscible Flows in Communicating Stratified Reservoirs. In: 12th European Conference on the Mathematics of Oil Recovery, September 2010, Oxford, UK

Chapter 2 Overview of Previous Works

There are many upscaling methods, focusing on different scales of reservoir model, analytical/numerical methods and even the way for gridding. This chapter focuses on reviewing upscaling methods for a layered reservoir model.

2.1 Necessity for Upscaling

As written in section 1.2, upscaling techniques are needed to account for heterogeneity of the reservoirs and reduction of the computational time by solving flow equations (Eqs. (1.9)-(1.10)) on the coarse grids.

In single-phase flow, the important parameters to upscale are the natural properties of reservoir: permeability and porosity. When multiphase flow occurs, relative permeability plays an important role. In such cases, the upscaling techniques aim to obtain pseudo relative permeabilities and furthermore pseudo fractional flow functions (Guedes and Schiozer (1999)). The upscaled properties and pseudo functions define average effective properties on a large scale, based on small-scale properties and their distributions. They should replicate the fine scale characterization, to large degree, in terms of key flow behavior, for example overall flow rate, water cut, recovery (Chen et al. (2003)).

2.2 Pseudo Functions

Pseudo functions can be applied in the framework of the solution scheme of the Buckley-Leverett theory (Eq.(1.12)). There are many methods for generation of the pseudo functions. Barker and Thibeau (1996) present a critical review of the use of pseudo relative permeabilities for upscaling. Discussion on advantages and drawbacks of the methods and suggestions for improvement are given.

Kyte and Berry (1975) propose the most common method to calculate dynamic pseudocurves. Average pressure is applied to coarse grids. Although this method is widely used, it does not produce good results for strongly heterogeneous porous media. It also may result in negative or infinite values of relative permeabilities. Stone (1991) describes the first method using total mobility to avoid calculation of average pressure in the method given by Kyte and Berry (1975) and similar methods. This method is built for a black-oil model in the absence of gravity and capillary forces. It can be applied to a non-communicating layered reservoir model. Jacks et al. (1972) present dynamic pseudofunctions to model a 3D reservoir with a 2D reservoir simulator, taking into account oil zone, transition zone and water zone. Coats et al. (1971) derive pseudo functions basing on the assumption of vertical equilibrium. Capillary forces and gravity are accounted for in this work. They are assumed to be equalized in the vertical direction, corresponding to capillary-gravity dominating regime. Hearn (1971); Kurbanov (1961); Kurbanov and Atanov (1972), following the work by Hiatt (1958) provide a method for rearranging layers in order to get pseudo relative permeability curves. Gravity and capillary forces are not considered in this method.

2.3 Reservoir Models

Geological modeling is highly important for reservoir simulation. The main difficulty is to take proper account of the various large- to small-scale heterogeneities, because each type of the heterogeneity influences fluid flows and hence recovery efficiency. Weber and Genuns (1990) present a framework for treating reservoir heterogeneities and constructing reservoir simulation models. This work is based on Weber (1986), which describes various degrees of heterogeneity at various scales and classifies them into seven types, from large-scale faults to microscopic features. Weber and Genuns (1990) generalize the large-scale features into three basic reservoir types: layer-cake model, jigsaw-puzzle model and labyrinth model.

According to Weber and Genuns (1990), the stone properties of the layer-cake reservoir models do not have major discontinuity or changes in horizontal extent. The thickness of layers should be more or less constant or with gradual changes. Boundaries between layers should coincide with major changes in rock properties or baffles to flow. Jigsaw-puzzle reservoir models are composed of a series of rock bodies that fit together without major gaps between them. Large jumps in rock properties can occur between the rock units. The labyrinth reservoir models are characterized by complex arrangement of pods and lenses of porous media. The continuity of rock is often direction-dependent. It is usually hard to model labyrinth reservoirs in a realistic way, but statistical modeling can be applied.

2.4 Upscaling Methods for Layered Model of Reservoir

In order to simplify the computational tasks and provide manageable methods for upscaling, certain simplifying assumptions about the structure of the porous medium should be made. Due to the stratified characteristics of the earth shell, property variation for many oil reservoirs or other natural porous medium is usually larger in vertical direction than that in horizontal direction. Thus it is reasonable to adapt a layer-cake, stratified structure for these reservoirs. In order to design analytical or semi-analytical upscaling methods, the reservoir layers are often assumed to be homogeneous. The Buckley-Leverett flow equations for waterflooding (Eqs.(1.9)-(1.10)) can be applied to each layer with constant parameters. This is, definitely, an oversimplification made for computational purposes.

Two extreme cases result from the stratified reservoir model. The first case is that the barriers between layers are impermeable and the inter-layer crossflow is negligible. Alternatively, this is the case when the permeability across the layers is much lower than that along the layers. The second extreme case corresponds to perfect communication between the layers, where the exchange between them is instantaneous (the case of vertical equilibrium). This case is usually connected to the viscous dominant regime of displacement, where viscous forces prevail over capillary and gravity forces.

The Dykstra-Parsons method (Dykstra and Parsons (1950)) is one of the widely applied upscaling methods for the first case, non-communicating layers. Other main assumptions of the method are: piston-like displacement of oil by water, all layers are individually homogeneous, constant total injection rate, and injector-producer pressure drop for all layers is the same. Velocities of displacement front in each layer are given by this method. Stiles (1949) applies a similar method to calculate water cut and oil recovery accounting for variation of permeability. However, this method only works where the end point mobility ratio of the displacing and displaced phase is equal to unity. The main drawback of the Dykstra-Parsons method is the assumption about piston-like displacement in each layer.

Modifications and extensions have been introduced to the original Dykstra-Parsons method. Reznik11 et al. (1984) extend the original Dykstra-Parsons discrete solution to continuous, real time basis. The assumption about piston-like displacement is retained in this work. Stevens (1985) completes a semi-analytical investigation of the effect of trailing zone on the results based on the original Dykstra-Parsons method. Mahfoudhl and Enlck (1990) model polymer flooding in stratified porous media in the way of Dykstra-Parsons displacement mechanism, considering also free gas saturation.

The Buckley-Leverett theory is coupled with the Dykstra-Parsons theory by Kufus and Lynch (1959). This method is only valid for unit viscosity ratio of the two phases. Snyder and Ramey (1967) apply the Buckley-Leverett theory to waterflooding in non-communicating layer-cake reservoir models. This leads to better prediction for the flow performance after breakthrough than in the original Dykstra-Parsons method.

The Hearn-Kurbanov method (for brevity often termed the Hearn method) has been developed for the second extreme case of layered reservoir models, the communicating layers (Hearn (1971); Kurbanov (1961); Kurbanov and Atanov (1972)). As in the original Dykstra-Parsons technique, the Hearn-Kurbanov method is designed for manual calculations and sacrifices accuracy in favor of simplicity. It involves additional assumptions, like piston-like displacement in each layer and interchangeable layers. Not all the assumptions are verified by direct computations (see the analysis below). The Hearn-Kurbanov method is based on the work by Hiatt (1958), who applied the material-balance method to a multilayer system and then integrated the continuity flow equation to get the coverage of displacing fluid. An essential analog of Hiatt's method is the theory developed by Warren and Cosgrove (1963). Permeability is assumed to be of log-normal distribution along the dimensionless height of the reservoir and porosity is assumed to be of normal distribution. The average saturation and average fractional flow function are obtained by some simple integration of porosity and permeability along cross-sections.

Katz (1962) generalizes these two extreme cases, of the non-communicating and fully communicating layers, by application of harmonic and arithmetic mean value of permeability respectively, with the height of a layer as weighting factor. He considers these two cases as the two limits of flow behavior under the same properties of the medium and the flow itself. Obviously, he also assumes that the order of layers does not affect the saturation distribution or the final oil recovery curve.

El-Klhatib (1985) rearranges the layers in a reservoir model in the similar way as Hearn and investigates how the end point mobility ratio of the two phases affects water cut and recovery efficiency. This work describes the effect from the crossflow on performance of a multiphase flow in perfectly communicating layered porous systems under favorable and unfavorable end point mobility ratios. El-Klhatib (1999) focusses on the log-normal distribution of permeabilities. Pseudo relative permeabilities are derived. They are only functions of saturation and heterogeneity. Phenomena at high end point mobility ratios (oil to water) are treated in a different way, since they may produce multiple values of saturation by the method of El-Klhatib.

Yortsos (1991) develops a quantitative justification for the methods developed for non-communicating and fully communicating layered porous systems, which is in agreement with the works of Zapata and Lake (1981) and Lake (1989). In the paper of Yortsos, strict expansion of the two-dimensional displacement problem under assumption of the vertical equilibrium results in an integral-differential equation for saturation. Along the same lines there is the work by Lake and Hirasaki (1981) on tracer dispersion in stratified systems, as well the various viscous fingering models, such as Koval (1963), Todd and Longstaff (1972) and Fayers (1984). While they have only an empirical basis, the numerical evidence is in many cases supportive of their applicability.

Chapter 3 Two-Phase Immiscible Flows with Negligible Gravity and Capillary Forces

This chapter presents the study of two-phase immiscible incompressible flows in layered reservoir model under absence of gravity. The Hearn method is discussed in details. Its problems are pointed out.

Asymptotic analysis based on the assumption of perfect inter-layer communication is applied to general 2D flow equations so that vertical pressure gradient is approximated to be zero. For a layered 2D model of reservoir, for example a vertical cross-section of a reservoir, the asymptotic 2D equation is reduced to a set of 1D homogeneous hyperbolic equations. Results of average saturation profiles and oil recoveries generated by our method and that by commercial finite element solver COMSOL are compared. These results are published in Zhang et al. (2011).

This chapter also introduces the implementation of a complete 2D waterflooding simulation on COMSOL. Some of the content is published in Zhang et al. (2010).

3.1 Introduction

In this chapter, a method for reduction of the 2D displacement process to a 1D problem in a layer-cake porous medium is proposed in details. The theoretical development is close to that of Yortsos (1991), but differs from it in a number of important details. Unlike in the work by Yortsos, who leaves the time to be a dimensional variable, we carry out the complete asymptotic analysis similar to Martin (1968) and, further, to Kanevskaya (1988) and Bedrikovetsky (1993). We consider the case of viscous dominant displacement.

Similarly to the previous works, it turns out that the main parameter responsible for the inter-layer communication is the anisotropy ratio, which is dependent on the geometry of the 2D reservoir model and permeability field. A small value of anisotropy ratio corresponds to poorly communicating layers, which can be solved by Dykstra-Parsons method, while a large value of anisotropy ratio is shown to correspond to fast exchange and negligible pressure gradient across the layers, which is the main assumption of the so-called vertical equilibrium. With the only assumption about negligible vertical pressure gradient it becomes possible to derive explicit analytical expressions of total velocities along layers and orthogonal to layers. This serves as the basis for the 1D model.

We consider waterflooding of petroleum reservoir as our basic (default) example, keeping in mind, however, that the considered methods, with certain modifications, may be applied to other processes.

The results of our 1D method are well comparable with the results of the full 2D simulations in a multilayer reservoir. This indicates a possibility of replacing the long and elaborate multidimensional simulations by our fast 1D simulation, at least for the viscous dominant displacement regime. Another application of our approach is production of the pseudo fractional flow functions on the basis of known permeability distributions. The solution of the problem with constant boundary conditions is self-similar, and the pseudo fractional flow function may be calculated as a function of average saturation along the solution. Thus, we suggest a more precise and substantiated alternative to the Hearn method.

The chapter is organized as follows. Sections 3.2 shows theory of this 1D method. A detailed model formulation is written in Section 3.2.1, including all assumptions applied in this thesis. Section 3.2.2 discusses the Hearn method, showing its inaccuracy by specific cases. Mathematic explanation of the problems in the Hearn method is given. Section 3.2.3 presents the detailed transformation of the description for a 2D waterflooding problem from dimensional form to dimensionless form. Section 3.2.4 brings the application of asymptotic analysis to the dimensionless system. A closed equation for water saturation is obtained with known injection velocity. So far, the problem is still in the space of two dimensions. In Section 3.2.5, this 2D problem is reduced to multiple 1D homogeneous hyperbolic equations in a layered model of reservoir. The number of the 1D equations is equal to the total number of layers in the reservoir model. Section 3.3 is devoted to a detailed comparison of the computational results with 2D simulations in different layer geometries. Flow performance in non-communicating layered is also provided as comparison. Conclusions are drawn in Section 3.4.

3.2 Theory

We carry out asymptotic analysis of two-phase two-dimensional flows in the regime of viscous dominant following Martin (1968), Kanevskaya (1988) and Bedrikovetsky (1993).

3.2.1 Model Description

In this chapter, we consider a vertical cross-section plane of the reservoir model defined in section 1.2.1. Length is denoted as L and height as H. Coordinate x is directed horizontally along length L and y vertically upwards along height H. Water is injected at $x=0$ (inlet) along x direction. Production well is located at $x=L$ (outlet). Further assumptions for this 2D model are:

1. It is a rectangular geometry, which means its height H is constant along its length L.
2. Injection velocity is constant.
3. Injection is uniform across the height H.
4. Production pressure is constant.
5. Top ($y=H$) and bottom ($y=0$) are impermeable.

The studies presented in Chapter 3, 4, 5 and 6 are all based on the waterflooding model described here.

3.2.2 Dimensionless Description of 2D Waterflooding without Gravity

Consider a two-dimensional case of Eqs. (1.9) – (1.10)

$$\phi\frac{\partial s_w}{\partial t}+\frac{\partial}{\partial x}\left(-\lambda_{wx}\frac{\partial p}{\partial x}\right)+\frac{\partial}{\partial y}\left(-\lambda_{wy}\frac{\partial p}{\partial y}\right)=0 \tag{3.1}$$

$$\frac{\partial}{\partial x}\left(\lambda_x\frac{\partial p}{\partial x}\right)+\frac{\partial}{\partial y}\left(\lambda_y\frac{\partial p}{\partial y}\right)=0 \tag{3.2}$$

Let us rewrite the system equations in dimensionless form by introducing dimensionless variables according to the rules

$$\begin{gathered}\phi=\phi_0\Phi,\, t=t_0T,\, x=LX,\, y=HY,\, p=p_0P,\, \mu=\mu_w\mathrm{M}\\ k_x=k_{0x}K_X,\, k_y=k_{0y}K_Y,\, \lambda_x=\left(k_{0x}/\mu_w\right)\Lambda_X,\, \lambda_y=\left(k_{0y}/\mu_w\right)\Lambda_Y\end{gathered} \tag{3.3}$$

All the capital letters represent dimensionless variables. The subscript 0 presents scale for specific parameters. It should be remarked that p_0 is a characteristic pressure difference, but not a characteristic pressure. X and Y are normalized length and height, so they vary from zero to unity. ϕ_0 and k_0 are selected as the vertical averaged value of ϕ and k respectively.

$$\phi_0 = \frac{\int_0^H \phi\, dy}{H} \tag{3.4}$$

$$k_{0j} = \frac{\int_0^H k_j\, dy}{H} \quad (j = x, y) \tag{3.5}$$

The main time scale t_0 is the characteristic for the displacement propagation along the reservoir, which means the scales of time, porosity, pressure, length and mobility to obey the relation

$$\frac{\phi_0}{t_0} = \frac{k_{0x} p_0}{\mu_w L^2} \rightarrow t_0 = \frac{\mu_w \phi_0 L^2}{k_{0x} p_0} \tag{3.6}$$

By substitution of the dimensionless variables (Eqs.(3.3)-(3.6)) into Eqs.(3.1)-(3.2), we obtain the dimensionless expression for waterflooding system in terms of water saturation s_w and dimensionless pressure P.

$$\Phi \frac{\partial s_w}{\partial T} - \frac{\partial}{\partial X}\left(\Lambda_{wX} \frac{\partial P}{\partial X} \right) - E_a \frac{\partial}{\partial Y}\left(\Lambda_{wY} \frac{\partial P}{\partial Y} \right) = 0 \tag{3.7}$$

$$\frac{\partial}{\partial X}\left(\Lambda_X \frac{\partial P}{\partial X} \right) + E_a \frac{\partial}{\partial Y}\left(\Lambda_Y \frac{\partial P}{\partial Y} \right) = 0 \tag{3.8}$$

Where E_a is defined as the anisotropy ratio of the reservoir.

$$E_a \equiv \frac{k_{0y}L^2}{k_{0x}H^2} \tag{3.9}$$

Dimensionless mobility, for example, Λ_{wX} and Λ_{oX} are correspondingly written as

$$\Lambda_{wX} = K_X kr_w \tag{3.10}$$

$$\Lambda_{oX} = K_X kr_o / \mathrm{M}_o \tag{3.11}$$

According to the definition of viscosity scale (Eq.(3.3)), M_o is actually the ratio of oil viscosity to water viscosity.

Another way to express the same system is by introducing dimensionless total velocities defined as:

$$\bar{U}_X = -\Lambda_X \frac{\partial P}{\partial X} \tag{3.12}$$

$$\bar{U}_Y = -E_a \Lambda_Y \frac{\partial P}{\partial Y} \tag{3.13}$$

By this definition (Eqs.(3.3),(3.12)), dimensionless total velocity $\bar{U}_X$ and dimensional total velocity U_x should hold the relation:

$$\bar{U}_X = \frac{L\mu_w}{p_0 k_{0x}} U_x \tag{3.14}$$

Furthermore, dimensionless injection velocity V_{inj} is proportional to dimensional injection velocity v_{inj} in the similar way as shown in Eq.(3.14).

$$V_{inj} = \frac{L\mu_w}{p_0 k_{0x}} v_{inj} \tag{3.15}$$

In the case of negligible gravity and capillary force, water velocity should be the product of total velocity and water fractional flow F (Eq.(1.8)), which is a monotonic function of water saturation.

$$\bar{U}_{wj} = F\bar{U}_j \quad \left(j = X, Y\right) \tag{3.16}$$

So alternatively, the dimensionless water flooding system can also be written as

$$\Phi \frac{\partial s_w}{\partial T} + \frac{\partial}{\partial X}\left(F\bar{U}_X\right) + \frac{\partial}{\partial Y}\left(F\bar{U}_Y\right) = 0 \tag{3.17}$$

$$\frac{\partial \bar{U}_X}{\partial X} + \frac{\partial \bar{U}_Y}{\partial Y} = 0 \tag{3.18}$$

The 2D waterflooding system described by Eqs.(3.12), (3.13), (3.17), (3.18) aims to solve for water saturation s_w, dimensionless pressure P and dimensionless velocities $\bar{U}_X, \bar{U}_Y$. These four equations will be implemented in COMSOL to simulate the process of 2D waterflooding. Eqs. (3.17)-(3.18), are set as main equations for this system, while Eqs. (3.12), (3.13) are treated as intermediate functions dependent on water saturation s_w and dimensionless pressure P.

Boundary conditions for the system expressed by Eqs.(3.12), (3.13), (3.17), (3.18) are:

1. Normal flux at top ($Y = 1$) and bottom ($Y = 0$) is zero due to the assumption of impermeable boundary at top and bottom of the reservoir. That leads to $F\bar{U}_Y\big|_{(X,0,T)} = F\bar{U}_Y\big|_{(X,1,T)} = 0$ for Eq. (3.17) and $\bar{U}_Y(X,0,T) = \bar{U}_Y(X,1,T) = 0$ for Eq.(3.18).

2. Water saturation s_w and dimensionless injection velocity are known at inlet $X = 0$: $s_w(0,Y,T) = 1 - s_{or}$, where s_{or} is residual oil saturation. $F\bar{U}_X\big|_{(0,Y,T)} = V_{inj}$ for Eq. (3.17) and $\bar{U}_X(0,Y,T) = V_{inj}$ for Eq.(3.18).

3. Production pressure is known at outlet $X = 1$: $P(1,Y,T) = P_{pro}$.

Initial conditions are: $s_w(X,Y,0) = s_{wi}$, $P(X,Y,0) = P_{ini}$. s_{wi} is irreducible (or connate) water saturation, P_{ini} is the initial dimensionless pressure inside the reservoir.

3.2.3 Discussion on the Hearn Method: Results and Problems

The Hearn method evaluates pseudo relative permeability curves for a layered reservoir model. It can be applied to 2D simulation of fluid displacement where vertical sweep is primarily affected by permeability variation. This method assumes perfect inter-layer communication, interchangeable layers, uniform end point relative permeability and piston-like displacement front. It is an approaximation of Buckley-Leverett theory. It is more applicable to waterflooding than to gas injection where the density difference can be large.

A layered reservoir model (Fig 3.1) is applied in this method. Each layer is assumed to be homogeneous and isotropic. The main idea is to rearrange the layers in the order of decreasing values of $k_m/\phi_m \Delta s_m$, where $\Delta s_m = 1 - s_{wi,m} - s_{or,m}$. k_m, ϕ_m, $s_{wi,m}$, $s_{or,m}$ represent absolute permeability, porosity, irreducible water saturation, residual oil saturation in layer m.

To apply the method, the average water saturation and relative permeabilities at the outflow end are computed after breakthrough of each layer. Then the pseudo relative permeability curves and the pseudo fractional flow function are produced. For a system with N discrete layers (Fig 3.1), the Hearn method should give, in principle, a piecewise linear fractional flow curve to produce N displacement fronts. A system with continuously distributed permeability produces a smooth concave pseudo fractional flow function as, for example, shown by El-Khatib (1999) for a special case of the log-normal distributed permeabilities.

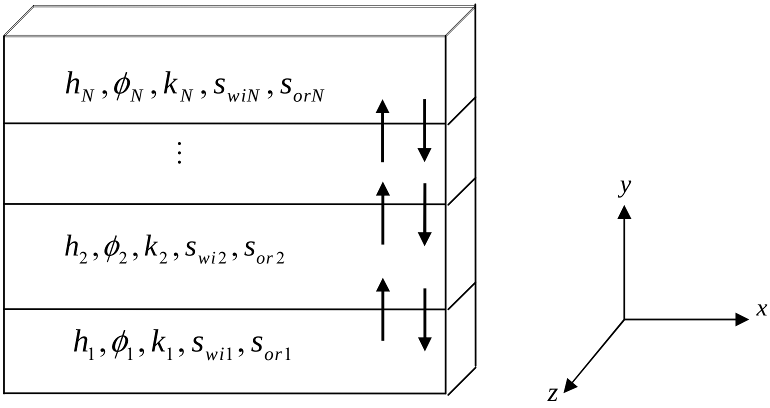

Fig 3.1 Stratified reservoir model. $\uparrow\downarrow$ denotes crossflow between layers. The top and bottom of reservoir are assumed to be impermeable, which means no inflow or outflow there.

The Hearn method is not precise. As an example, consider a 2D displacement problem in a two-layer reservoir, with a very good communication between layers (anisotropy ratio equal to 1000). The parameters of this problem (of the layers and fluids) are listed in Tables 3.1 and 3.2. All calculations are based on the dimensionless parameters that lead to $M = 1.33$ in Table 3.2, where M is the end point mobility ratio (oil to water) and defined as

$$M = \frac{kr_{owi}/\mu_o}{kr_{wor}/\mu_w} = \frac{kr_{owi}/\mathrm{M}_o}{kr_{wor}} \tag{3.19}$$

The rule of derivations for dimensionless parameters from dimensional parameters is written in Eqs.(3.3)- (3.6) and (3.9).

L (characteristic length, m)	1000
H (characteristic height, m)	100
p_0 (characteristic pressure difference, Pa)	1×10^{6}
ϕ_0 (characteristic porosity)	0.2
k_{0x} (characteristic permeability, m^2)	1×10^{-13}
k_{0y} (characteristic permeability, m^2)	1×10^{-12}
μ_w (characteristic viscosity, $\frac{N\cdot s}{m^2}$)	1×10^{-3}
t_0 (characteristic time, s)	$\frac{L^2\phi_0\mu_w}{k_{0x}p_0}=2\times10^{9}$
v_{inj} (injection velocity, m/s)	1×10^{-7}

Table 3.1 Dimensional parameters of the two-dimensional model of reservoir.

Dimensionless parameters	Layer 1	Layer 2
Fraction of thickness α	0.33	0.67
Irreducible water saturation s_{wi}	0.05	0.2
Residual oil saturation s_{or}	0.25	0.2
Relative water permeability at residual oil	0.8 (0.4)	0.8 (0.4)

saturation kr_{wor}		
Relative oil permeability at irreducible water saturation kr_{owi}	0.8	0.8
Permeability in x-direction K_X	0.6	1.2
Dimensionless porosity Φ	1	
Dimensionless dynamic viscosity of oil M_o	3 (1.5)	
Dimensionless injection rate V_{inj}	1	

Table 3.2 Dimensionless parameters for the two-layer model. The values in brackets correspond to the mobility ratio (oil to water) $M = 1.33$, other values correspond to $M = 0.33$.

The 2D problem is solved by application of COMSOL. The characteristic saturation distribution in the two layers, in the course of displacement, is presented in Fig 3.2, which shows that for well communicating layers there are no sharp fronts in each layer, but one smooth front across all layers. The saturation profiles assumed by the Hearn method and obtained in 2D simulation are shown in Fig 3.3a. The saturation profile for the 2D simulation is calculated by averaging of the saturation across the reservoir. It is clearly seen that the profiles are different: while the Hearn profile has two distinctive displacement fronts, the profile from the 2D simulation is smooth. The oil recovery from the 2D simulation is also different from the oil recovery predicted by the Hearn method (Fig 3.3c).

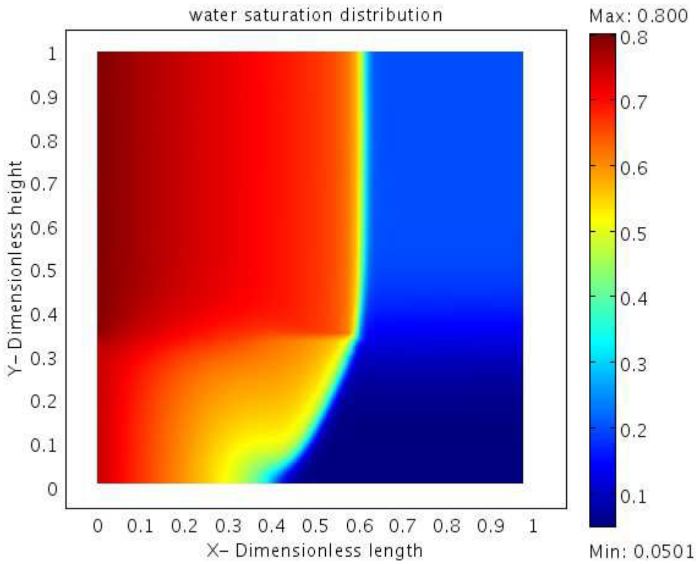

Fig 3.2 Water saturation profile of 2D waterflooding simulation by COMSOL, at time=0.25 PVI (Pore Volume Injected). This model consists of two well communicating layers, with E_a equal to 1000. The surface of this figure represents the value of water saturation. Horizontal axis is the dimensionless length of reservoir and vertical axis is the dimensionless height. $M = 1.33$

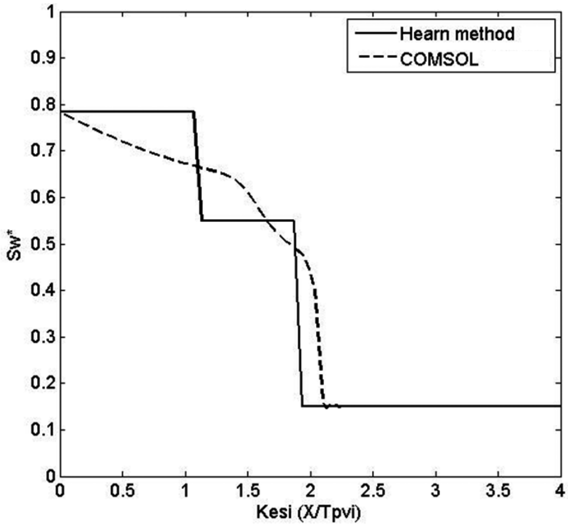

(**a**)

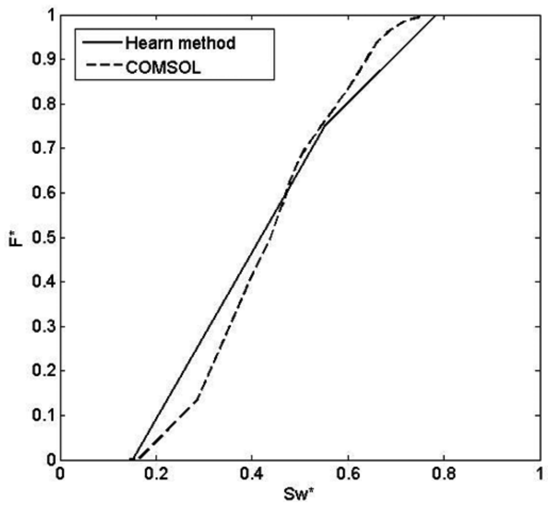

(**b**)

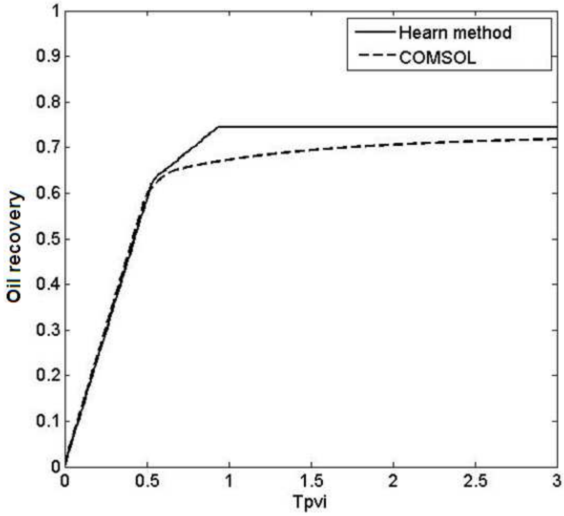

(**c**)

Fig 3.3 Comparisons of Hearn method and 2D simulation by COMSOL with $E_a = 1000$, $M = 1.33$ (Fig 3.2). (**a**) Average water saturation profile, (**b**) Pseudo-fractional flow function, (**c**) Oil recovery. Solid lines represent the result obtained by the Hearn method. Dashed lines represent the result by COMSOL 2D simulation.

One of the assumptions of the Hearn method is that the layers may be exchanged without affecting the averaged flow pattern. This assumption is not precise, either. The 2D simulation shows that different orders of layers result in different saturation profiles (Fig 3.4). Dimensionless parameters are from Table 3.3.

Dimensionless parameters	Values
Fraction of thickness α	0.2;0.3;0.5
Irreducible water saturation s_{wi}	0.1;0.2;0.15
Residual oil saturation s_{or}	0.15;0.1;0.2
Relative water permeability at residual oil saturation kr_{wor}	0.8
Relative oil permeability at irreducible water saturation kr_{owi}	0.8
Permeability in x-direction K_X	0.59;1.47;0.885
Dimensionless porosity Φ	1
Dimensionless dynamic viscosity of oil M_o	3
Dimensionless injection rate V_{inj}	1

Table 3.3 Dimensionless parameters for the three-layer system. $M = 0.33$.

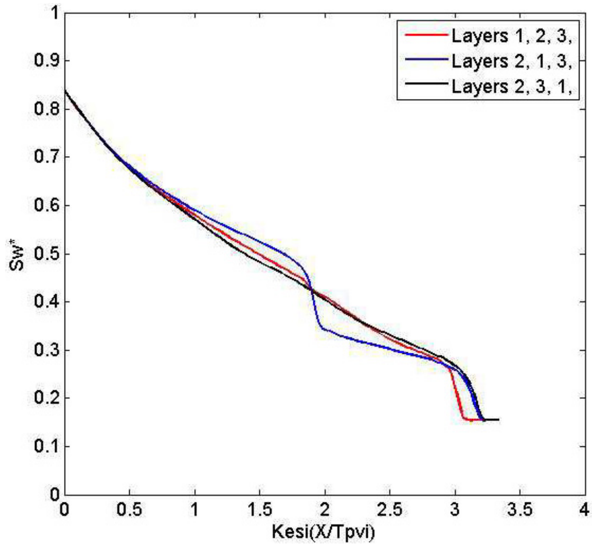

Fig 3.4 Average water saturation profiles simulated by COMSOL of 3-layer communicating system, $E_a = 1000$. The layers are arranged in the different orders.

Sometimes the Hearn method may produce results contradicting physical intuition and common sense. To the best of our knowledge, this has not been discussed in the literature. Let us consider characteristic examples.

Assume for simplicity that all porosities and residual saturations of the layers are the same. In this case, according to the Hearn procedure, the layers should be arranged in decreasing order of their permeabilities k_m (for definiteness, the higher permeable layers at the bottom, so that water moves faster there, as in Fig 3.5). The permeability dependence $k(y)$ in the system of rearranged layers is a monotonously decreasing function from the bottom of a reservoir to the top H. The procedure of rearranging the layers may introduce an additional source of imprecision into the Hearn approximation, as will be shown below in the numerical calculations for the three-layer case.

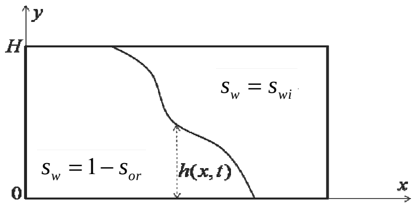

Fig 3.5 Illustration of the rearrangement of layers in the Hearn method.

Let us denote by $h(x,t)$ the vertical distance to the position of the advanced front (see Fig. 3.5). The average water saturation s_w^* of the vertical cross-section in position x is calculated as

$$s_w^* = (1-s_{or})\frac{h}{H} + s_{wi}\frac{H-h}{H} \tag{3.20}$$

In view of the linear dependence between $s_w^*(x,t)$ and $h(x,t)$, it is convenient to express the relative permeabilities not in terms of s_w^*, but in terms of h. Since in the Hearn method the horizontal pressure gradient is assumed to be the same in all layers, we obtain the following expressions for average water and oil relative permeabilities kr_w^*, kr_o^* (Bedrikovetsky (1993)):

$$kr_w^*(h) = \frac{kr_{wor}}{k^*}\frac{\int_0^h k(z)dz}{H}$$

$$kr_o^*(h) = \frac{kr_{owi}}{k^*}\frac{\int_h^H k(z)dz}{H}$$

where k^* is average absolute permeability across the layers of reservoir, defined as

$$k^* = \frac{\int_0^H k(z)dz}{H}$$

Here kr_{wor}, kr_{owi} are the relative permeability of water at residual oil saturations and the relative permeability of oil at irreducible water saturation. By the Hearn method they are assumed to be the same for all reservoir layers. Correspondingly, the fractional flow function may be represented as:

$$F^*(h) = \frac{kr_w^*(h)/\mu_w}{kr_w^*(h)/\mu_w + kr_o^*(h)/\mu_o} = \frac{a(h)}{(1-M)a(h) + Mk^*}$$

$$a(h) = \frac{\int_0^h k(z)dz}{H}$$

The idea of the Hearn method is to replace the solution of the two-dimensional displacement problem by solution of the one-dimensional Buckley-Leverett problem with the pseudo fractional flow function $F^*(s_w^*) = F^*(h(s_w^*))$ (where the dependence $h(s_w^*)$ is determined from Eq.(3.20)). As known from the general theory of the quasi-linear hyperbolic equations (Gelfand (1959)), the displacement may be "smooth" or may contain discontinuities of the saturations depending on the shape of function $F^*(s_w^*)$. If this dependence (or, equivalently, dependence $F^*(h)$) is convex, the displacement is "smooth", otherwise it contains displacement fronts.

This rule must be correlated with a type of heterogeneity which must be described. If a (model) reservoir consists of N discrete layers, it is to be expected that the Hearn approximate solution will have N discrete fronts. This corresponds to a dependence $F^*(s_w^*)$ having N convexities (or N straight-linear cuts) (Fig 3.6a). For a smooth distribution of permeabilities (for example log-normal), a smooth increase of the water saturation on the production site may be expected. A gradual increase of s_w^* may only be modeled with a concave dependence $F^*(s_w^*)$ excluding the appearance of the displacement fronts (Fig 3.6b).

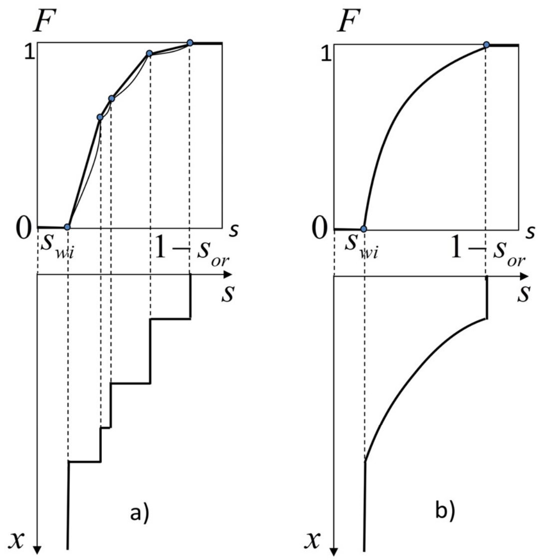

Fig 3.6 Solutions of the Buckley-Leverett problems with pseudo fractional flow functions for (**a**) A layer-cake reservoir, (**b**) A reservoir with a smooth permeability distribution.

Let us check whether $F^*(s_w^*)$ has the necessary type of concavity or convexity. Since interdependence of s_w^* and h is linear, it is enough to differentiate $F^*(h)$. The second derivative of this function has the form of

$$(F^*)''(h)=\frac{M^2\left(k^*\right)^2 k'(h)+M\left(1-M\right)k^*\left[k'(h)a\left(h\right)-2k^2\left(h\right)\right]}{\left[\left(1-M\right)a\left(h\right)+Mk^*\right]^3}$$

Let us consider the N-layer case where permeability is piecewise constant, i.e. $k'(h)=0$. For such a case the previous expression is simplified to

$$(F^*)''(h) = -\frac{2M\left(1-M\right)k^*k^2\left(h\right)}{\left[\left(1-M\right)a\left(h\right)+Mk^*\right]^3}$$

F^* is convex, as required, only for the favorable mobility ratio, $M>1$, since the denominator $\left[\left(1-M\right)a+Mk^*\right]^3 = \left[a+M\left(k^*-a\right)\right]^3$ is always larger than zero. If, on the contrary, $M<1$, then F^* becomes locally concave, which produces additional non-physical rarefaction waves in addition to the expected fronts. It might be argued that the case $M<1$ may result in instability and viscous fingering, which smoothens the saturation profiles. However, such phenomena are not taken into account by the initial Hearn model of displacement.

Analysis is much more difficult for the case of continuous variation of $k(h)$. Assume, for example, that for some conditions $F^*(h)$ is convex as required. Consider the variation of permeability $k(h) \to k(h)+\delta\sin(Dh)$, where δ is small enough in order not to destroy the increase of permeability with depth, but D is large. This transformation may locally change the sign of $(F^*)''$ and produce multiple fronts and rarefaction waves where they are not expected.

In the original Hearn paper (Hearn (1971)) the pseudo relative permeabilities were calculated at a number of points and interpolated in between them. Clearly, the result depends on the way of interpolation. It is obvious that the result converges as the number of "sample layers" increases. However, this does not remove the concavity problem. Under unfavorable mobility ratios, it may happen that some layers are not represented by the correspondent displacement fronts in the solution of the upscaled Buckley-Leverett problem.

In order to illustrate it, let us consider an example of a two-layer reservoir (analysis for the case of multiple layers is possible, but much more cumbersome). The reservoir layers have permeabilities k_1, k_2 $(k_1 > k_2)$, and thicknesses h_1, h_2, correspondingly. Assume for simplicity that the endpoint relative permeabilities and residual saturations are equal for both layers. An adequate upscaled solution should contain two displacement fronts representing the two layers. On the plane $(h, F(h))$ the first front corresponds to the jump from $(h_1, F(h_1))$ to (0,0), the second from $(h_1+h_2, 1)$ to $(h_1, F(h_1))$, where F is the upscaled fractional flow function. The inclinations of the corresponding jumps are $D_1 = F(h_1)/h_1$

and $D_2 = (1 - F(h_1)) / h_2$, correspondingly. If $D_1 > D_2$, both jumps appear in the solution. Otherwise, if $D_1 < D_2$, the solution of the upscaled problem is piston-like, and on the plane $(h, F(h))$ the only jump is depicted by the straight line connecting $(h_1 + h_2, 1)$ and (0,0). Straightforward computations involving the above formulae for pseudo-relative permeabilities show that

$$F(h_1) = \frac{k_1 h_1}{k_1 h_1 + M k_2 h_2}$$

Thus, condition $D_1 > D_2$ is equivalent to

$$k_1 > M k_2$$

This is not always the case. Moreover, unlike the examples above, this inequality may be violated under favorable mobility ratios, $M > 1$. Thus, consistency of the Hearn procedure should be verified in each particular case, and the conclusion may be nontrivial.

This analysis shows that the original Hearn scheme has obvious deficiencies and may result in a non-physical behavior of the predictions of displacement. In our opinion, the reason is that the Hearn method insufficiently takes into account the interaction between the layers. A more consistent approach basing on asymptotic analysis is discussed in the following sections of the thesis.

3.2.4 Asymptotic Analysis

There may be two asymptotic cases for the system described by Eqs. (3.7)-(3.8): 1) E_a is a small parameter and 2) E_a is a large parameter. The first case corresponds to poor inter-layer communication. In this case the flow becomes quasi one-dimensional, and the flows of different values of Y (different "layers") become independent of each other. Thus, we recover the system corresponding to the Dykstra-Parsons method (Dykstra and Parsons (1950)).

The second case, describes very good communication between the layers. In Eq.(3.8), the term $\frac{\partial}{\partial Y}\left(\Lambda_Y \frac{\partial P}{\partial Y}\right)$ becomes small in this case compared to $\frac{\partial}{\partial X}\left(\Lambda_X \frac{\partial P}{\partial X}\right)$. When E_a becomes asymptotically large, it can be reduced to

$$\frac{\partial}{\partial Y}\left(\Lambda_Y \frac{\partial P}{\partial Y}\right) \approx 0 \quad \text{or} \quad \Lambda_Y \frac{\partial P}{\partial Y} \approx C$$

where the integration constant C is a function of X, T only.

As talked above, boundary condition for $\bar{U}_Y$ at top and bottom of the dimensionless square geometry is that $\partial P/\partial Y = 0$, so C is zero. Asymptotically, we have

$$\frac{\partial P}{\partial Y} = 0 \tag{3.21}$$

Thus, the pressure is invariable in the Y-direction. This is the main assumption of the Hearn-Kurbanov method (Hearn (1971); Kurbanov (1961); Kurbanov and Atanov (1972)), corresponding to absolute communication of the layers. This plays as the basis of the assumption of vertical equilibrium (Zapata and Lake (1981); Coats. et. al (1971); Yortsos (1991), (1992)).

In the original Hearn method, it was implicitly assumed that $\bar{U}_X$ depends only on T and, maybe, Y, so that the conservation law holds for each "layer" (each value of Y). This assumption is, however, too strong and results in the imprecision of the method and some problems described above. Unlike the case of non-communicating layers, the masses of water and oil are not conserved in each layer, but in the reservoir as a whole. A more rigorous approach to this problem is further described.

3.2.5 General Integral Relations

The goal of this section is to derive general relations which are independent of the expansion. They should hold whatever model/approximation is selected.

Consider Eq. (3.18) and integrate it over Y from 0 to 1:

$$\frac{\partial}{\partial X}\int_0^1 \bar{U}_X\, dY + \int_0^1 \frac{\partial \bar{U}_Y}{\partial Y}\, dY = 0 \tag{3.22}$$

The first integral in Eq. (3.22) can be viewed as the averaged dimensionless total velocity or the total dimensionless flux passing the cross-section line $(X,0) \to (X,1)$. When there is no other source except injector and producer in the domain of reservoir (as assumed in this thesis), this is equal to the dimensionless injection velocity.

$$\int_0^1 \bar{U}_X dY = V_{inj} \tag{3.23}$$

We should be aware that the validity of Eq. (3.23) is also due to the regular geometry of the 2D reservoir model that height H is constant along length L (Section 3.2.1). Otherwise $\int_0^1 \bar{U}_X dY$ is only equal to averaged dimensionless total velocity and all following equations involving the term V_{inj} should be replaced by averaged dimensionless total velocity. The exceptions from Eq. (3.23) is presented in streamline simulation (Chapter 6).

In view of impermeability of top and bottom, the second integral in Eq.(3.22) is reduced to

$$\bar{U}_Y(1) - \bar{U}_Y(0) = 0 \tag{3.24}$$

Thus, $\partial V_{inj} / \partial X = 0$ and the overall injection velocity is only time-dependent.

Now, let us do the same integration to Eq. (3.17). The last term will be dropped out, for the same reason as in Eq.(3.24). We obtain

$$\frac{\partial}{\partial T}\int_0^1 \Phi s_w dY + \frac{\partial}{\partial X}\int_0^1 \bar{U}_X F dY = 0$$

The first integral results in the average water saturation s_w^*, because according to our rule of scaling the dimensionless porosity (Eqs. (3.3)-(3.4)) we have $\int_0^1 \Phi dY$ equal to 1.

$$s_w^* = \frac{\int_0^1 \Phi s_w dY}{\int_0^1 \Phi dY} = \int_0^1 \Phi s_w dY \tag{3.25}$$

The second integral is the average flow of water. Thus, the average fractional flow of water F^* is

$$F^* = \frac{1}{V_{inj}}\int_0^1 \bar{U}_X F dY \tag{3.26}$$

3.2.6 Derivation of the Approximation

It was proven in Section 3.2.4 (Eq. (3.21)) that P is independent of Y within the order of $1/E_a$. Thus, the pressure gradient along the reservoir $\partial P/\partial X$ is the same for all the values of Y (all the layers).

Substituting the Darcy equation Eq. (3.12) into Eq. (3.23) and accounting for independence of $\partial P/\partial X$ on Y, we obtain

$$\frac{\partial P}{\partial X} = -\frac{V_{inj}}{\int_0^1 \Lambda_X dY}$$

Further substitution of this relation into Eq. (3.12) gives the explicit expression for dimensionless total velocity $\bar{U}_X$ in terms of V_{inj}.

$$\bar{U}_X = \frac{\Lambda_X}{\int_0^1 \Lambda_X dY} V_{inj} \tag{3.27}$$

This equation indicates that the velocity at each height Y (each layer) is proportional to the mobility at this height; the term in the denominator is the average mobility along the whole height. Eq. (3.27) is substituted into the continuity equation (Eq.(3.18)), which makes it possible to express $\bar{U}_Y$ explicitly:

$$\frac{\partial \bar{U}_Y}{\partial Y} = -V_{inj} \frac{\partial}{\partial X} \frac{\Lambda_X}{\int_0^1 \Lambda_X dY} \rightarrow \bar{U}_Y = -V_{inj} \frac{\partial}{\partial X} \left[\frac{\int_0^Y \Lambda_X dY'}{\int_0^1 \Lambda_X dY} \right] \tag{3.28}$$

Substitution of Eqs. (3.27)-(3.28) into the equation for saturation (Eq.(3.7)) results in

$$\Phi \frac{\partial s_w}{\partial T} + V_{inj} \frac{\partial}{\partial X} \left\{ \frac{F \Lambda_X}{\int_0^1 \Lambda_X dY} \right\} - V_{inj} \frac{\partial}{\partial Y} \left\{ F \frac{\partial}{\partial X} \left[\frac{\int_0^Y \Lambda_X dY'}{\int_0^1 \Lambda_X dY} \right] \right\} = 0 \tag{3.29}$$

This is a closed equation for saturation $s_w(X, Y, T)$, since injection velocity V_{inj} is known from the boundary conditions. Both pressure and velocity are excluded. It should be stressed that the only assumption made for derivation of this equation is the assumption about the pressure independence on the vertical coordinate. Other assumptions of the Hearn method (like exchangeability of the layers or a piston-like character of displacement) are not applied.

The interpretation of Eq. (3.29) is as follows: variation of s_w at height Y is due to horizontal transfer (in X-direction) plus vertical exchange. The flux of water along X-direction is expressed as $V_{inj} F \Lambda_X / \int_0^1 \Lambda_X dY$. Apart from the fractional flow function F, it includes the "vertical distribution function" $\Lambda_X / \int_0^1 \Lambda_X dY$ expressing redistribution of flows at different height due to pressure interaction. The specific form of the vertical exchange term $-V_{inj} \frac{\partial}{\partial Y} \left\{ F \frac{\partial}{\partial X} \left[\frac{\int_0^Y \Lambda_X dY'}{\int_0^1 \Lambda_X dY} \right] \right\}$ provides the continuity expressed by Eq.(3.8).

The integral-differential equation (Eq.(3.29)) is difficult to solve in a general form. In the next subsection we show that for a layer-cake stratified reservoir there is a discrete treatment for it, reducing it to a system of quasi-linear hyperbolic equations (modified Buckley-Leverett equations for each layer).

3.2.7 A Layer-Cake Reservoir

Consider a layer-cake model of reservoir consisting of N layers of the height h_m $(m = 1,...,N)$, so that $\alpha_m = h_m / H$ is the height fraction of the mth layer in the total height of reservoir (Fig 3.1). We assume that all the properties of flow and reservoir do not vary across each layer. Thus, the derivative with respect to Y can be approximated by the difference between two layers, for example, between layer m and layer $(m-1)$, divided by the height fraction, for example α_m. Integrals over Y are replaced by sums. In this way the integral-differential equation (Eq.(3.29)) is reduced to a system of 1D quasi-linear hyperbolic equations. The number of the equations is equal to the number of layers in the reservoir model, N. The expressions for dimensionless total velocities (Eq. (3.27)-(3.28)) are changed to:

$$\bar{U}_{X,m} = \frac{\Lambda_{X,m}}{\sum_{n=1}^{N} \Lambda_{X,n} \alpha_n} V_{inj}$$

$$\bar{U}_{Y,m} = -V_{inj} \frac{\partial}{\partial X} \left[\frac{\sum_{n=1}^{m} \Lambda_{X,n} \alpha_n}{\sum_{n=1}^{N} \Lambda_{X,n} \alpha_n} \right] \tag{3.30}$$

The ways for calculating average water saturation (Eq.(3.25)) and average fractional flow of water (Eq. (3.26)) are replaced by

$$s_w^* = \sum_{n=1}^{N} \alpha_n s_{w,n} \Phi_n \tag{3.31}$$

$$F^* = \frac{1}{V_{inj}} \sum_{n=1}^{N} \alpha_n F_n \bar{U}_{X,n} \tag{3.32}$$

Eq. (3.29) is replaced by a set 1D quasi-linear hyperbolic equations with regard to water saturations in all layers, $s_{w,1},...,s_{w,N}$:

$$\Phi_m \frac{\partial s_{w,m}}{\partial T} + V_{inj} \frac{\partial}{\partial X} \left\{ \frac{F_m \Lambda_{X,m}}{\sum_{n=1}^{N} \alpha_n \Lambda_{Xn}} \right\} + \frac{V_{inj}}{\alpha_m} \left\{ G_m \left(-\frac{\partial}{\partial X} \frac{\sum_{n=1}^{m} \alpha_n \Lambda_{X,n}}{\sum_{n=1}^{N} \alpha_n \Lambda_{X,n}} \right) - G_{m-1} \left(-\frac{\partial}{\partial X} \frac{\sum_{n=1}^{m-1} \alpha_n \Lambda_{X,n}}{\sum_{n=1}^{N} \alpha_n \Lambda_{X,n}} \right) \right\} = 0$$

(3.33)

The values of G_{m-1} and G_m are the fractions of water in the expressions for water flows between the layers *m* and $m-1$. A question arises, whether they should be chosen equal to F_m, F_{m-1}, or something else (let us say, $(F_m + F_{m-1})/2$). We select these values according to the explicit discretization scheme with the possible reversion of the flux. When expression for $\bar{U}_{Y,m}$ (Eq. (3.30)) is positive, the corresponding term in the flow equation term describes the outflow from layer m to layer $m+1$. In this case it is logical to set $G_m = F_m$. However, if $\bar{U}_{Y,m}$ is negative, this term describes the inflow from layer $m+1$ to layer *m*. Then it should be set $G_m = F_{m+1}$. The value of G_{m-1} is determined in a similar way.

An initial condition and a boundary condition are needed for solving each hyperbolic equation generalized by Eq.(3.33). The initial condition is: $s_{w,m}(X,0) = s_{wi,m}$, where $s_{wi,m}$ is initial (most commonly, irreducible) water saturation in layer *m*. At the inlet ($X = 0$), we set $s_{w,m}(0,T) = 1 - s_{or,m}$, where $s_{or,m}$ is the residual oil saturation in layer m .

Dimensionless time in porous volumes injected (p.v.i.) is defined as

$$T_{pvi} = \frac{V_{injected}}{V_{pore}} = \frac{\int_0^T V_{inj} dT'}{\sum_{m=1}^{N} \alpha_m \Phi_m} = \int_0^T V_{inj} dT' \tag{3.34}$$

The system of equations (Eq.(3.33)) has a standard hyperbolic form of

$$\frac{\partial s_{w,m}}{\partial T_{pvi}} + A_m(s_{w,1},...,s_{w,N}) \frac{\partial B_m(s_{w,1},...,s_{w,N})}{\partial X} = 0$$

If the boundary and the initial conditions of the system are constant, it allows for a self-similar solution depending on the self-similar variable $\xi = X / T_{pvi}$ (Gelfand (1959)). Correspondingly, both average saturation s_w^* (Eq. (3.31)) and average fractional flow F^* (Eq.(3.32)) become functions of ξ. If s_w^* depends on ξ monotonously (which is usually the case), a single-valued pseudo fractional flow function $F^*(s_w^*)$ may be defined along the path. Alternatively, it may be found by numerical computation of the average saturations and fractional flow functions at the outlet (or any other cross-section). This is the essence of the suggested method for upscaling and obtaining the pseudo fractional flow curve. A similar method may be applied for derivation of the pseudo relative permeabilities.

Direct calculation of this system seems to be prohibitively complicated, hindering application of the common analytical solution methods like the method of characteristics. Additionally, it is non-trivial to formulate the conditions on the shocks (displacement fronts), since the system is not represented in the divergent form (Gelfand (1959)). However, the system allows for a straightforward numerical solution.

3.3 Numerical Study

In this section, 2-layer and 10-layer reservoir models of discrete permeability field and 10-layer model of continuous (log-normal) permeability are studied to test the 1D method introduced in the previous section. For each case, two end point mobility ratios (oil to water) are implemented, that are $M = 0.33$ and $M = 1.33$, where M is defined in Eq.(3.19). These two values correspond to unfavorable (or unstable) waterflooding and favorable (or stable) waterflooding respectively. Average water saturation s_w^* is given by Eq.(3.31) , while average fractional flow function F^* is given by Eq. (3.32) and oil recovery is given by Eq.(1.3).

All results are compared with the complete 2D simulation of waterflooding, which is carried out by application of the commercial finite element solver COMSOL, by solving the system of Eq.(3.12), (3.13), (3.17), (3.18). Implementation of the 2D simulation in COMSOL is presented in subsection 3.3.2.

Dimensional parameters of the 2D reservoir model, which is taken as a vertical cross-section plane in this thesis, are listed in Table 3.1. They result in $E_a = 1000$ and $V_{inj} = 1$. Most 2D simulations run in COMSOL are based on this value of E_a, unless otherwise specified.

3.3.1 Practical Aspects of Numerical Computations

An explicit finite difference method is applied to solve systems Eq.(3.33). The distance step is chosen to be $\Delta X = 0.01$ and the time step to be $\Delta T = 0.0025$. The method is implemented in the Intel Fortran program. Convergence is checked by varying the distance and the time steps.

3.3.2 COMSOL Implementation

3.3.2.1 Introduction

COMSOL Multiphysics is a powerful interactive software for modeling and solving many kinds of scientific and engineering problems based on partial differential equations (PDEs). It contains predefined modules, like chemical engineering modules, acoustics modules. It is also possible to build specific models in the PDE module of COMSOL. Finite element method is applied in COMSOL to solve all the problems.

The application of COMSOL for simulation of multiphase flow in porous media has been done in previous works. Diaz-Viera et al. (2008) implement a black-oil model for multiple components. The model is based on the oil phase pressure and total velocity formulation with the capillary pressure taken into account. Lopez-Falcon et al (2008) model the growth and decay of microorganisms and nutrients through porous media. This is also a multiphase, multicomponents system. Bjørnarå and Aker (2008) investigate various types of equation system formulations for modeling two-phase flow in porous media using the finite element method, including five different formulations for 2D simulations and one for 1D. Huang (2010) model two-phase flow through strongly heterogeneous porous media. This work simulates oil-water system in discrete fractured porous media and discrete vuggy porous media. Halder and Datta (2009) present a thorough study on boundary conditions of heat transfer and mass transfer in porous media.

COMSOL is also used in other petroleum-related subjects. Suarez-Rivera (2006) implement a petroleum-geomechanics problem in COMSOL, stability of wells under hydraulic stress. Ekström and Linden (2005) simulate oil discharge and transport in natural river. This work gives the oil concentration curve, which is dependent on time and space, taking into account the absorption of oil by river bed.

Our problem is close to Bjørnarå and Aker (2008) and Diaz-Viera et al. (2008), but our reservoir model is two dimensional, while theirs are only one dimensional. Huang (2010) apply a 2D model, though it assumes the model of porous media is highly discontinuous. Most of previous studies assume the phases of flow are immiscible. It is therefore reasonable to believe that COMSOL can solve problems of 2D immiscible two-phase flow.

3.3.2.2 Implementation of Equations

In our study, COMSOL multiphysics PDE mode for time dependent analysis in the coefficient form is used for Eq. (3.17) with s_w as independent variable and PDE time dependent mode in general form is used for Eq. (3.18) with P as independent variable. The reason that we say s_w and P are independent variables for the system is that dimensionless velocities $\overline{U}_X, \overline{U}_Y$ are functions of s_w and gradient of P (Eqs. (3.17)-(3.18)). The reason for implementing intermediate variables $\overline{U}_X, \overline{U}_Y$ instead of explicit equations for P and s_w (Eq. (3.7)-(3.8)) is that it is easier and more logical to set up boundary conditions. Geometry should be chosen as 2D.

All dimensionless parameters, like anisotropy ratio E_a, dimensionless permeabilities, dimensionless oil viscosity M_o, height fraction of each layer α_m and dimensionless total injection rate V_{inj} are defined in "Constants".

The values of $s_{or}, s_{wi}, kr_{wor}, kr_{owi}, \Phi, K_X, K_Y$ are defined in "Scalar expression", because they may vary in different layers. The expressions for velocities $\overline{U}_X, \overline{U}_Y$ (Eqs.(3.12)-(3.13)), which are intermediate variables in this work, are also implemented in "Scalar expression".

They system of equations (Eqs.(3.12), (3.13), (3.17), (3.18)) is a pure convective transport system for water saturation s_w (but not for dimensionless pressure P). It is a discontinuous problem and can be very difficult, sometimes even impossible, to solve by the finite element method. A possible remedy for this is to use stabilization techniques, for instance artificial diffusion (Bjørnarå and Aker (2008)). In our problem, we set the diffusion coefficient c (COMSOL parameter) to be 1×10^{-2}, which is a very small value compared to other parameters in the system, in the equation setting for Eq. (3.17). No artificial diffusion is added to Eq. (3.18). When the system is built on real parameters, artificial diffusion should be set in accordance with other parameters. That means artificial diffusion should not prevail the main transport mechanism in the system. Diaz-Viera et al. (2008) is one of the examples.

Initial and boundary conditions are set in the same way as mentioned in Section 3.2.3. Two details should be stressed. Firstly, production pressure P_{pro} should be equal to initial pressure P_{ini} to ensure the continuity of pressure. Secondly, the condition of convective outflow is applied to saturation equation (Eq. (3.17)), which means (artificial) diffusion is set to be zero at outlet (Bjørnarå and Aker (2008)).

3.3.2.3 Mesh and Solver

Quadrate mesh of maximum size 0.02 is applied in our work. Thus around $50\times 50=2500$ elements are taken in calculation. Time-dependent Direct UMFPACK solver is used. Time step is determined by the solver automatically. Convergence is checked by varying the element size.

3.3.2.4 Data Processing

After the calculation is finished in COMSOL, we export the structure and data to MATLAB and calculate average saturation of water and average fractional flow of water in MATLAB by using the COMSOL-MATLAB interface command “postinerp”.

Oil recovery is obtained by integrating $(s_w - s_{wi})/(1-s_{wi})$ over the whole flow, that is $[0,1]\times[0,1]$, by using the COMSOL postprocessing function “subdomain integration”.

3.3.3 A Two-Layer Reservoir

For analysis of the peculiarities of displacement in a stratified reservoir we have performed a series of computations for waterflooding in a two-dimensional two-layer reservoir. Dimensionless parameters are listed in Table 3.2. The 2D saturation distribution is shown in Fig 3.2 and 3.7. They are generated by COMSOL.

3.3.3.1 Comparison with 2D Simulations

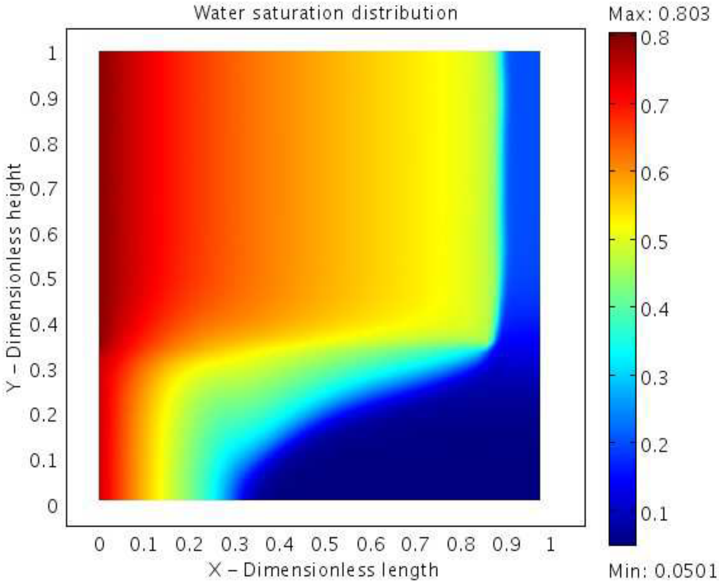

Fig 3.7 Water saturation profile for 2D waterflooding simulation, at time=0.25 p.v.i. The horizontal axis is the dimensionless distance along the reservoir, and the vertical axis is the dimensionless height (across the reservoir). $M = 0.33$.

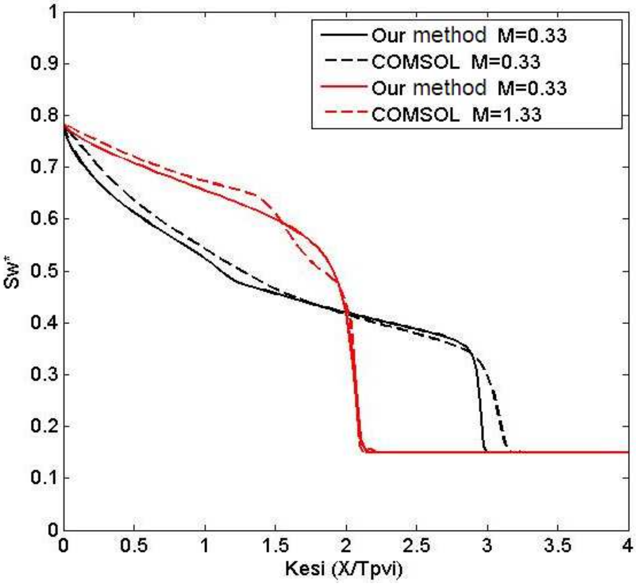
Our method M=0.33
COMSOL M=0.33
Our method M=0.33
COMSOL M=1.33
Sw*
Kesi (X/Tpvi)

(a)

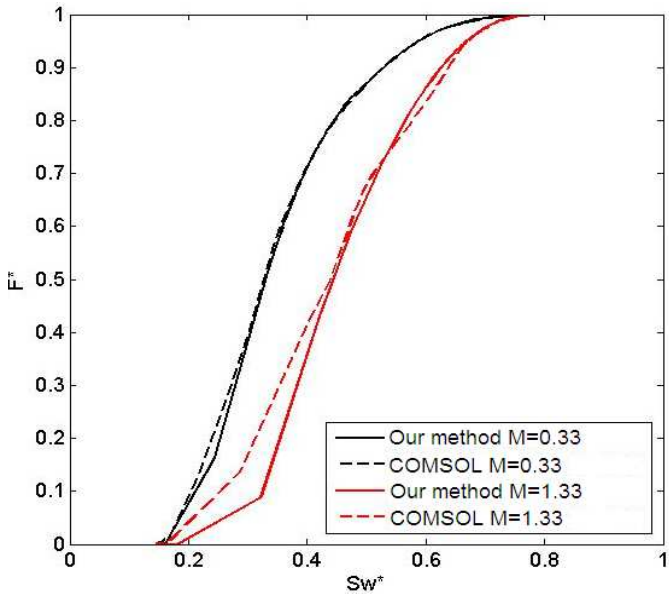
Our method M=0.33
COMSOL M=0.33
Our method M=1.33
COMSOL M=1.33
F*
Sw*

(b)

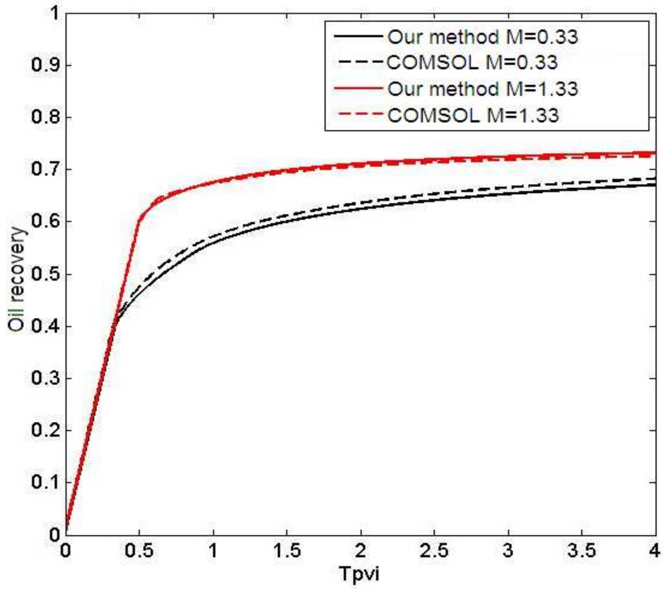

(**c**)

Fig 3.8 Comparison of the results obtained by our method and by the 2D simulation for a reservoir consisting of two communicating layers. Solid lines represent the results of our method; dashed lines the results of the 2D simulation with $E_a = 1000$. Black and red lines represent the results for an unfavorable ($M = 0.33$) and a favorable ($M = 1.33$) mobility ratio, respectively. (**a**) Average water saturation profiles, (**b**) pseudo fractional flow functions, (**c**) oil recovery curves.

From Fig 3.8, it is seen that our 1D simulation gives close results to those of the 2D simulation, or, anyway, much closer than the results obtained with the original Hearn-Kurbanov method (cf. Fig 3.2). The pseudo fractional flow curves are slightly different, but the positions of the displacement fronts (the inclinations of the tangent lines form initial saturation points) and the behavior of the curves at high saturations are similar (Fig 3.8b). Therefore, similar saturation profiles can be expected, which is also confirmed by the calculations (Fig 3.8a). The difference between the saturation profiles obtained by one- and two-dimensional computations is within the degree of approximation, and the displacement fronts (and therefore the breakthrough times) are predicted with good accuracy. It should be noted, however, that there is some qualitative difference between the saturation profiles for the case $M = 1.33$.

In order to test the applicability of our model to a less viscous dominant regime than that given by $E_a = 1000$, we have carried out the simulations at lower values of E_a, equal to 50, 3 and 1. Other parameters are from Table 3.2. As seen from Fig. 3.9c, for values of E_a larger than 50 our method produces oil recovery curves, which are similar to those of the 2D simulation. At lower values of E_a (3 or below) the saturation profiles contain a more expressed second displacement front (Fig 3.9a), becoming closer to the case of the non-communicating layers (Fig 3.10a). However, the arrival of the major displacement front and, therefore, the breakthrough time is still calculated with reasonable accuracy, and the oil recovery curves do not differ significantly, especially, at a late stage.

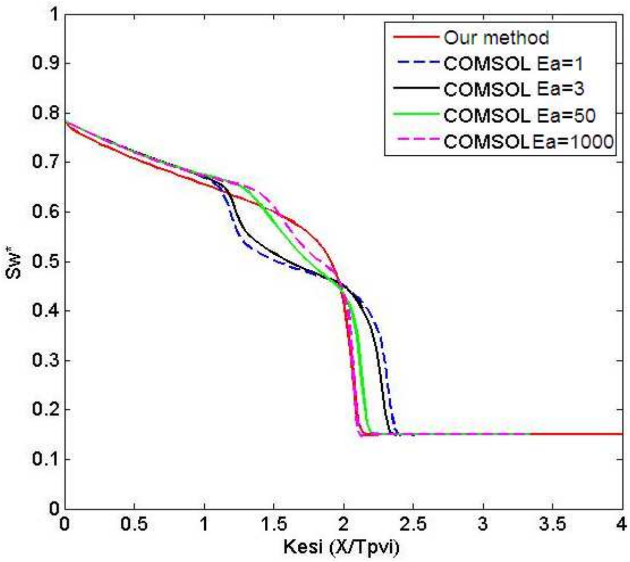

(a)

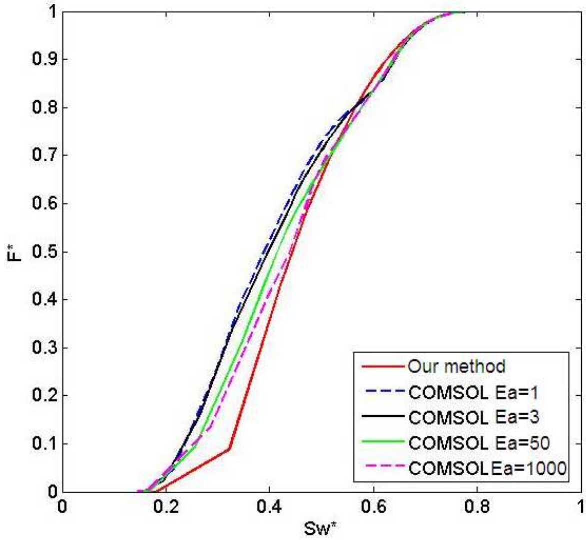

(b)

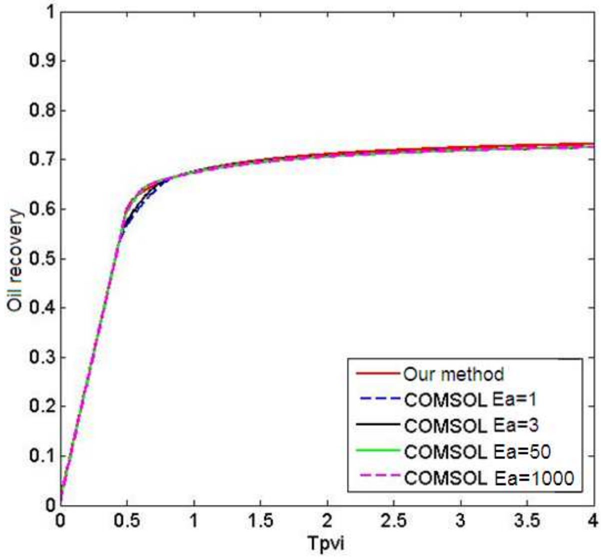

(c)

Fig 3.9 Comparisons of our method and 2D simulation of different levels of communication between layers, where $M = 1.33$. The level of communication between layers is described by the anisotropy ratio E_a. The larger value of E_a, the better communication between layers. (**a**) Average water saturation profile, (**b**) Pseudo-fractional flow function, (**c**) Oil recovery.

3.3.3.2 Communicating versus Non-Communicating Layers

On the basis of 1D simulations, we have compared the displacement results for the communicating layers with those of the non-communicating layers $(E_a \to 0)$. The corresponding profiles of flow behaviors are shown in Fig 3.10. Parameters are from Table 3.2.

For the case of non-communicating layers, there are two independent displacement water fronts (dashed lines in Fig 3.10a). The pseudo fractional flow function has a complex shape, a combination of two s-shaped curves ("one for each layer") (dashed lines in Fig 3.10b). Meanwhile, in the case of communicating layers, individual fronts are "smoothed" by crossflow, so that there is only one front in the saturation profile (solid lines in Fig 3.10a). The pseudo fractional flow functions (solid lines in Fig 3.10b) have a characteristic s-shape, similar to the shape of the fractional flow function in the classical Buckley-Leverett theory for a homogeneous porous medium. Hence, like in the classical theory, the solution of the self-similar displacement problem will contain the only displacement front (Bedrikovetsky (1993)).

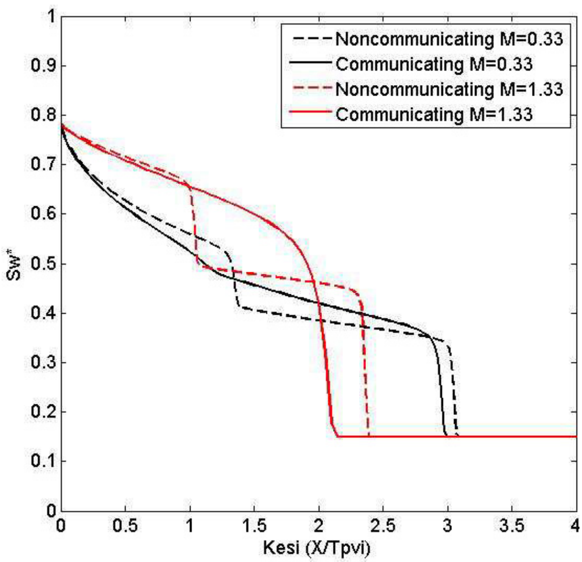

(a)

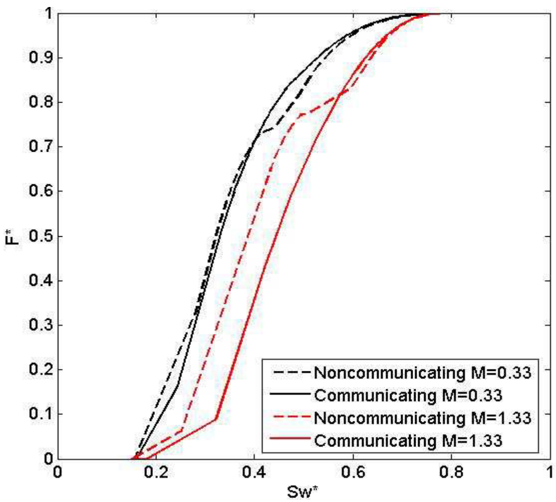

(**b**)

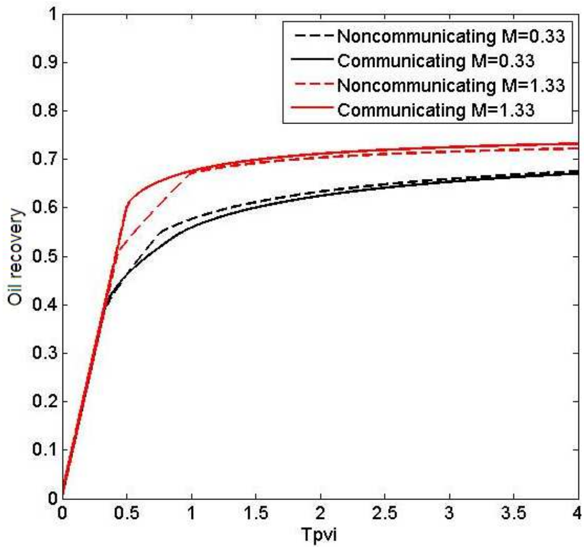

(**c**)

Fig 3.10 Comparisons of communicating and non-communicating stratified reservoirs. This model consists of two layers. Solid lines are the results of communicating case; dashed lines are the results of non-communicating case, where there is no crossflow and total velocity $\bar{U}_X$ is independent on X position and $\bar{U}_Y$ is zero everywhere. Black lines are the results of unfavorable mobility ratio ($M = 0.33$), red lines are the results of favorable mobility ratios ($M = 1.33$). (**a**) Average water saturation profiles, (**b**) Pseudo-fractional flow, (**c**) Oil recovery.

At a favorable mobility ratio, that is $M > 1$, communication between the layers increases oil recovery and delays breakthrough (red solid line in Fig 3.10c, compared to non-communicating layers, red dashed line in Fig 3.10c). At an unfavorable mobility ratio, $M < 1$, communication between the layers decreases the oil recovery (black solid line in Fig 3.10c, compared to non-communicating layers, black dashed line in Fig 3.10c), and breakthrough happens earlier.

3.3.4 Three-Layer Reservoir: Effect of Layer Exchange

We also implement our upscaling method into some three-layer communicating stratified reservoirs. The property of each specific layer remains the same, but the layers are arranged in different orders. The parameters of this problem are listed in Table 3.3. We only test the case of unfavorable mobility ratio, $M = 0.33(< 1)$. Results are shown in Fig. 3.11.

When the layers are arranged in different orders, the saturation profiles can be quite different (Fig 3.11a), as well as the pseudo fractional flow functions (Fig 3.11b) can be. For recoveries of different layer orders, time of the breakthrough and oil recovery may also be different (Fig 3.11c). Our method, as well as 2D simulations, produces also the different results for the different layer arrangements. We can reproduce the saturation profiles for arrangement 2-1-3 qualitatively similarly (with the two displacement fronts) and with a good quantitative accuracy. The saturation profiles for arrangement of the layers in order of 1-2-3 are not that close qualitatively, but are still close quantitatively.

This simulation shows that, when crossflow exists, layers structured in different orders usually lead to different flow patterns, even though the property of each layer remains the same. One of the assumptions of the Hearn procedure is not fully applicable.

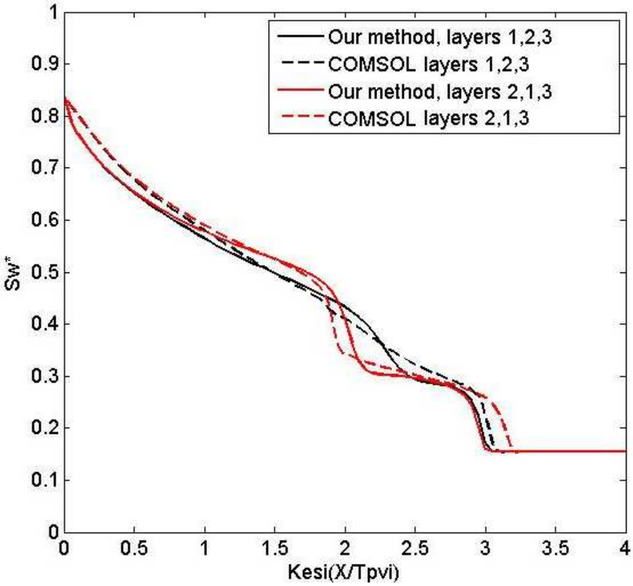
Our method, layers 1,2,3
COMSOL layers 1,2,3
Our method, layers 2,1,3
COMSOL layers 2,1,3
Sw*
Kesi(X/Tpvi)

(**a**)

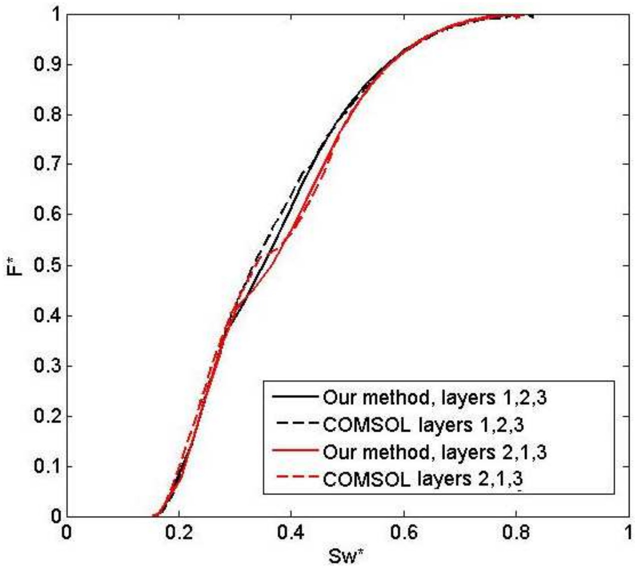
Our method, layers 1,2,3
COMSOL layers 1,2,3
Our method, layers 2,1,3
COMSOL layers 2,1,3
F*
Sw*

(**b**)

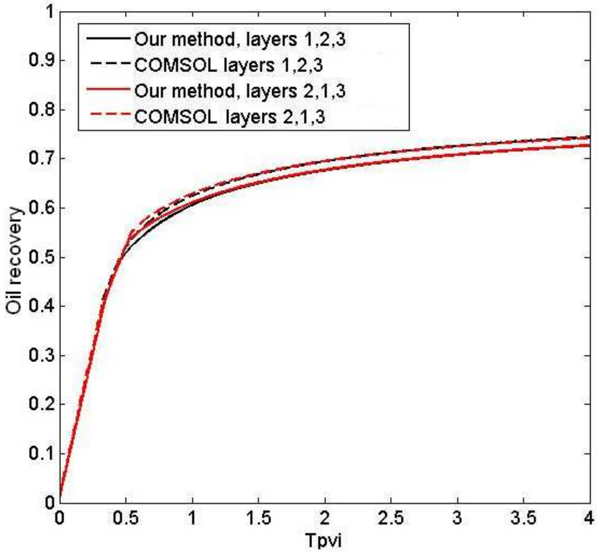

(**c**)

Fig 3.11 Comparisons of our method and 2D simulation, 3-communicating-layer system. Black lines are the results of the case that layers are structured in the order 1,2,3; red lines are the results of the case that layers are of the order of 2,1,3. Solid lines are the results of our method; dashed lines are the results by COMSOL with $E_a = 1000$. (**a**) Average water saturation profile, (**b**) Pseudo-fractional flow function, (**c**) Oil recovery.

3.3.5 Ten-Layer Reservoir

We have considered a reservoir consisting of ten layers. The parameters of the layers are given in Table 3.4. Results are shown in Fig. 3.12. It is seen that the saturation profiles computed by our model and obtained as a result by the 2D simulation are close. The same is valid for the fractional flow functions and the oil recovery curves. In the case of $M < 1$ the displacement profile is smooth and, thus, the arrival of the water to the production site is gradual. The displacement in the case of $M > 1$ is more stepwise. This might be expected, since the case $M > 1$ corresponds to a more stable displacement.

Dimensionless parameters	Value
Fraction of thickness α	0.1; 0.2; 0.05; 0.05; 0.1; 0.1; 0.1; 0.1; 0.1; 0.1
Irreducible water saturation s_{wi}	0.15; 0.05; 0.05; 0.1; 0.1; 0.1; 0.2; 0.2; 0.2; 0.15
Residual oil saturation s_{or}	0.05;0.06;0.07;0.1;0.12;0.13;0.22 0.25;0.3;0.15
Relative water permeability at residual oil saturation kr_{wor}	0.6;0.95;0.8;0.7;0.7;0.7;0.9;0.95; 0.69;0.9 (0.3;0.47;0.4;0.35;0.35;0.35;0.45; 0.47;0.34;0.45)
Relative oil permeability at irreducible water saturation kr_{owi}	0.6;0.95;0.8;0.7;0.7;0.7;0.9;0.95; 0.69;0.9
Permeability in x-direction K_X	0.93;1.12;0.465;0.465;0.744;1.39 0.279;1.023;1.674;1.209
Dimensionless porosity Φ	1
Dimensionless dynamic viscosity of oil M_o	3(1.5)
Dimensionless injection rate V_{inj}	1

Table 3.4 Dimensionless parameters for the ten-layer model. The values in brackets correspond to the mobility ratio (oil to water) $M = 1.33$, the other values correspond to $M = 0.33$.

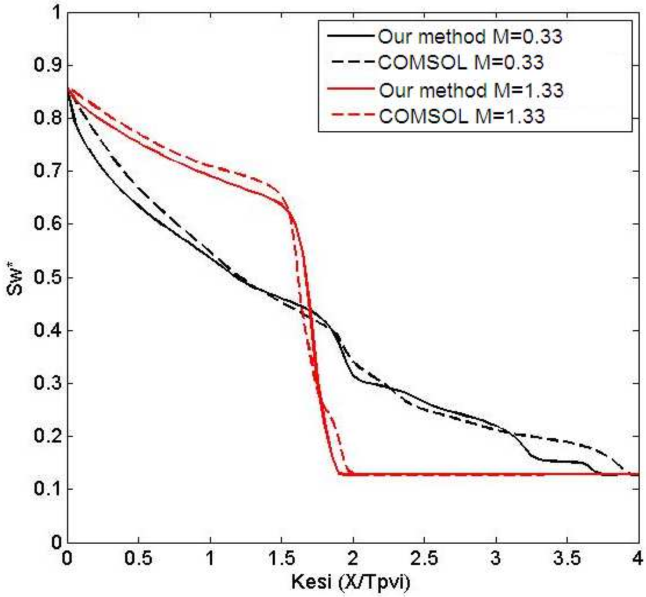
Our method M=0.33
COMSOL M=0.33
Our method M=1.33
COMSOL M=1.33
Sw*
Kesi (X/Tpvi)

(a)

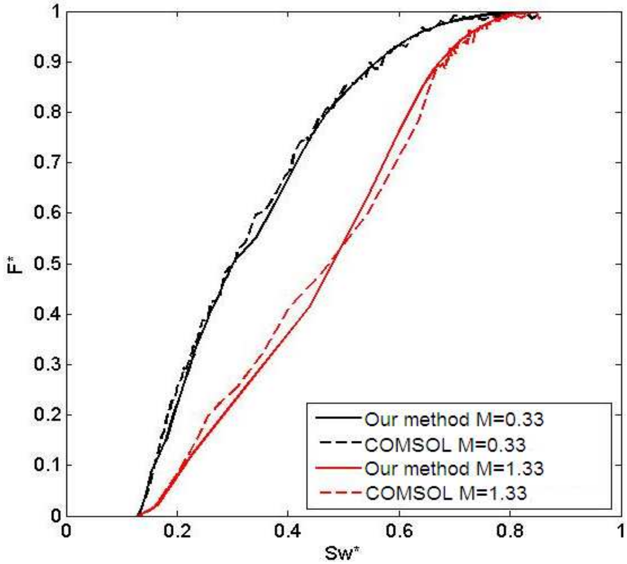
Our method M=0.33
COMSOL M=0.33
Our method M=1.33
COMSOL M=1.33
F*
Sw*

(b)

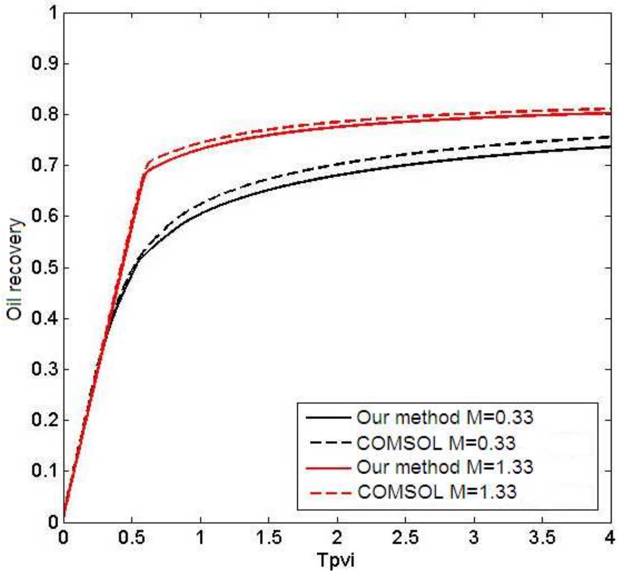

(**c**)

Fig 3.12 Comparison of the results obtained by our method and by the 2D simulation, for a reservoir consisting of ten communicating layers. Solid lines show the results obtained by our method; dashed lines the results of the 2D simulation. Black lines correspond to an unfavorable mobility ratio, red lines to a favorable mobility ratio. (**a**) Average water saturation profiles, (**b**) pseudofractional flow functions, (**c**) oil recovery curves.

3.3.6 Log-Normal Distributed Permeability

In this section, we consider a special case of continuous distribution of permeability, log-normal distribution. We assume that the permeability increases along the height of the reservoir.

The log-normal probability distribution density φ of permeability k is given by

$$\varphi(\ln k) = \frac{1}{\sqrt{2\pi}\sigma} \exp\left[-\frac{(\ln k - \beta)^2}{2\sigma^2}\right] \tag{3.35}$$

Where β is the mean value of $\ln k$, σ is the variance of the distribution density φ, according to the definition of normal distribution.

The relation between k and the dimensionless height of the reservoir Y is

$$Y(k) = \int_{\ln k}^{+\infty} \varphi(\ln k') d(\ln k') \tag{3.36}$$

For normal distribution, Eq.(3.35), the integration (Eq.(3.36)) with respect to $\ln k$ from $\beta - 3\sigma$ to $\beta + 3\sigma$ goes up to 0.97. Hence, it is sufficient to set the calculation range of $\ln k$ to be $[\beta - 3\sigma, \beta + 3\sigma]$, and, therefore, the calculation range of k to be $[\exp(\beta - 3\sigma), \exp(\beta + 3\sigma)]$. In our calculation, this permeability range is divided into ten equal intervals. The value of each interpolation point is substituted into Eq. (3.36) to give a height $Y(k)$. The distance between two adjacent values of $Y(k)$ is treated as a fraction of thickness α_m. Thus, we can solve Eq.(3.33). The parameters of this case are listed in Table 3.5. Results are given in Fig 3.13. Again our method gives results similar to those of the 2D simulation.

Dimensionless parameters	Value
β	$\ln 5$
σ	0.5
Irreducible water saturation s_{wi}	0.1
Residual oil saturation s_{or}	0.1
Relative water permeability at residual oil saturation kr_{wor}	0.8 (0.4)
Relative oil permeability at irreducible water saturation kr_{owi}	0.8
Dimensionless porosity Φ	1
Dimensionless dynamic viscosity of oil M_o	3(1.5)
Dimensionless injection rate V_{inj}	1

Table 3.5 Dimensionless parameters for the log-normal distributed permeability model. The values in brackets correspond to the mobility ratio $M = 1.33$, the other values correspond to $M = 0.33$.

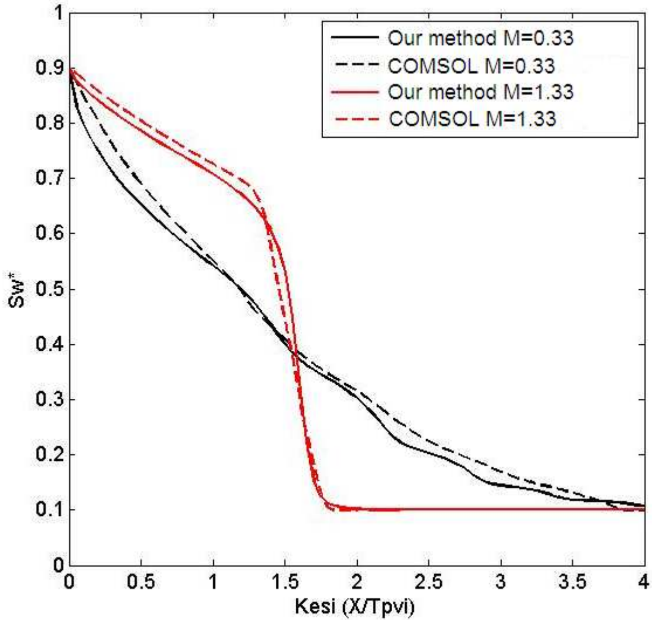
Our method M=0.33
COMSOL M=0.33
Our method M=1.33
COMSOL M=1.33
Sw*
Kesi (X/Tpvi)

(a)

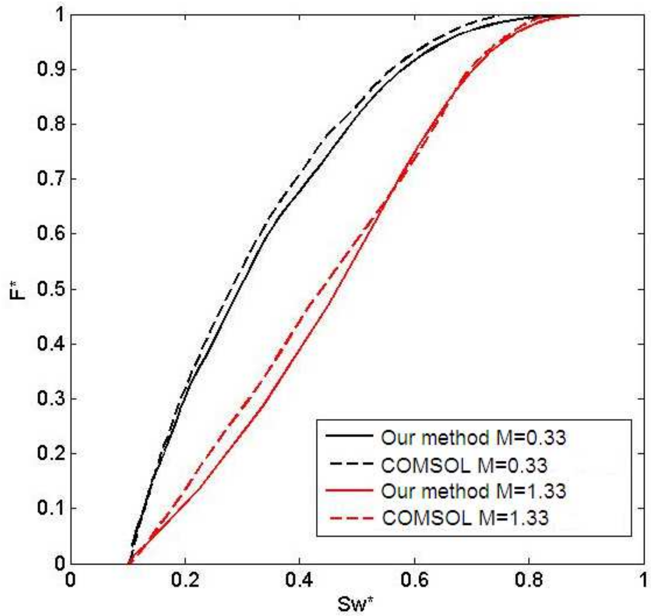
Our method M=0.33
COMSOL M=0.33
Our method M=1.33
COMSOL M=1.33
F*
Sw*

(b)

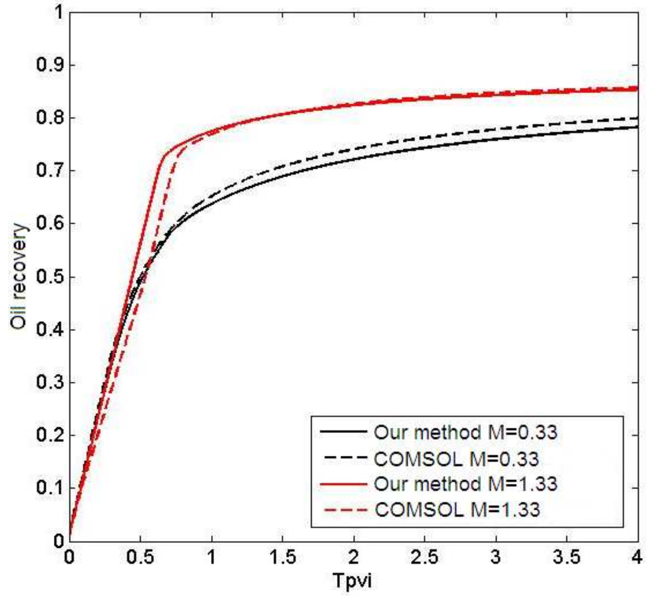

(**c**)

Fig 3.13 Comparison of the results obtained by our method and by the 2D simulation for the reservoir with log-normal permeability distribution. Solid lines represent results by our method; dashed lines represent the results by the 2D simulation. Black lines correspond to an unfavorable mobility ratio, red lines to a favorable mobility ratio. (**a**) Average water saturation profiles, (**b**) pseudofractional flow functions, (**c**) oil recovery curves.

3.4 Summary

We have developed a fast method for 1D simulation of waterflooding in a layer-cake reservoir. It may be used for upscaling of waterflooding in a stratified reservoir of a viscous dominant regime. For the waterflooding problems in well defined multilayer reservoirs, as well as reservoirs with log-normal distributed permeabilities, the results obtained by our method are all very close to the results obtained from the complete 2D displacement simulation. For the anisotropy ratios being 50 and higher, our method gives oil recovery curves very close to those obtained in complete 2D simulations. Even when anisotropy ratios are around 1, the oil recovery curve produced by our method is still similar to the results of the 2D simulations. The saturation profile calculated by our method is slightly different from the 2D simulation result. However, the difference is within the degree of approximation and the positions of the displacement fronts are almost the same.

The method developed for upscaling is advantageous over the classical Hearn method, since it refrains from some of the assumptions of the Hearn method and takes into account mass exchange between the layers. Our approach produces more realistic smooth saturation profiles, and is better at predicting positions of displacement fronts and oil recovery curves. Simulations show that different arrangements of the layers lead to different displacement patterns. Since our method does not rely on assumptions of exchangeability of the layers, it is superior to Hearn's procedure.

For mobility ratios (oil to water) $M > 1$, more oil is produced by waterflooding from a communicating stratified reservoir than from a non-communicating stratified reservoir. For mobility ratios (oil to water) $M < 1$, the effect is opposite. This observed effect of crossflow on oil recovery is in agreement with the work of El-Khatib (1983).

Chapter 4 Water Banks in Viscous Dominant Regimes of Displacement

4.1 Introduction

This chapter follows the publication Yuan et.al (2011). This is a further study on waterfoodling in layered reservoir with perfect inter-layer communication. The study aims at revealing and understanding the inter-layer mass communication.

In Chapter 3, we see clear difference between the averaged saturation profiles, pseudo fractional flow functions, oil recovery curves between the non-communicating reservoir model and the fully-communicating reservoir model (Fig 3.10). This is due to inter-layer cross flow. Figs 3.8a, 3.12a, 3.13a show that under different values of end point mobility ratio (oil to water) M, crossflow may make the distribution of fluids more even or more "dispersive". This leads to different oil recovery curves (Figs 3.8c, 3.12c, 3.13c). El-Khatib (1983) shows that M plays an important role on oil recovery when inter-layer cross flow exists. But no explanation is given.

In this chapter, 2D water saturation distribution and water saturation at the interface between layers are investigated, instead of the vertical average water saturation. Water banks and transition zones are observed. The effect of end point mobility ratio M (Eq.(3.19)) on the formation of water banks and transition zone is examined. The existence of water banks and transition zones is explained.

This chapter is organized in this way: section 4.2 includes the study on a three-layer fully communicating reservoir model, showing water bank and transition zones between layers on the 2D water saturation profile; section 4.3 presents explanation for the existence of water bank and transition zones; section 4.4 draws the conclusion.

4.2 Cases Study

A three-layer reservoir model is applied in this chapter. COMSOL is used to carry on the 2D simulation of fully communicating layered reservoir models. Non-communicating layered models, as comparisons, are simulated by direct calculation of mass balance equation for each layer. Dimensional properties are listed in Table 3.1. Some dimensionless parameters are written in Table 4.1. We use different values of M_o, kr_{owi} and kr_{wor} to get different value of end point mobility ratio M (oil to water) and then examine the effect of M on the formation of water banks and transition zones.

Dimensionless parameters	Value
Fraction of thickness α	0.333,0.333,0.333
Irreducible water saturation s_{wi}	0.1
Residual oil saturation s_{or}	0.3
Dimensionless permeability in x-direction K_X	0.5,1.0,1.5
Dimensionless porosity Φ	1
Dimensionless injection velocity V_{inj}	1
Anisotropy ratio E_a	1000

Table 4.1 Dimensionless parameters of the three-layer reservoir.

4.2.1 $M = 2$

We firstly choose $M_o = 1.5, kr_{wor} = 0.3, kr_{owi} = 0.9$ and have $M = 2$. At T=0.2 pvi, the saturation profiles in the $X - Y$ plane are shown in Fig 4.1 (a) and (b) respectively for the non-communicating and the communicating cases.

In the non-communicating case, a sharp saturation front can be observed in each layer. In the latter case, the displacement profile is even and smooth. The smoothness of the saturation profile in the latter case can be attributed to the almost instantaneous crossflow from more permeable layers to less permeable layers around the displacement fronts.

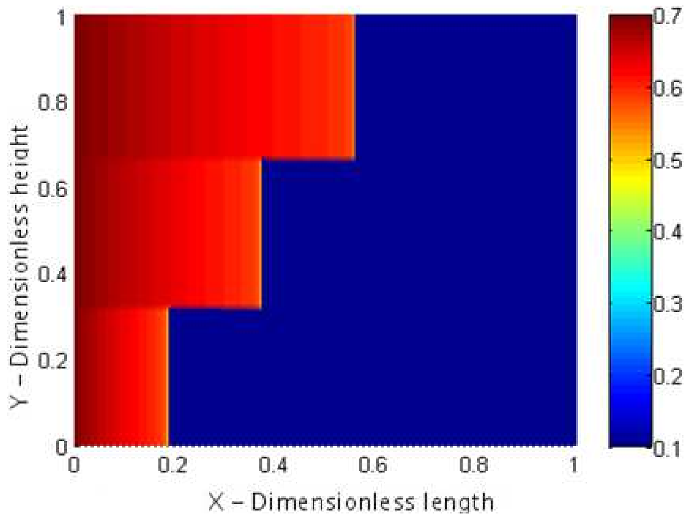

a)

b)

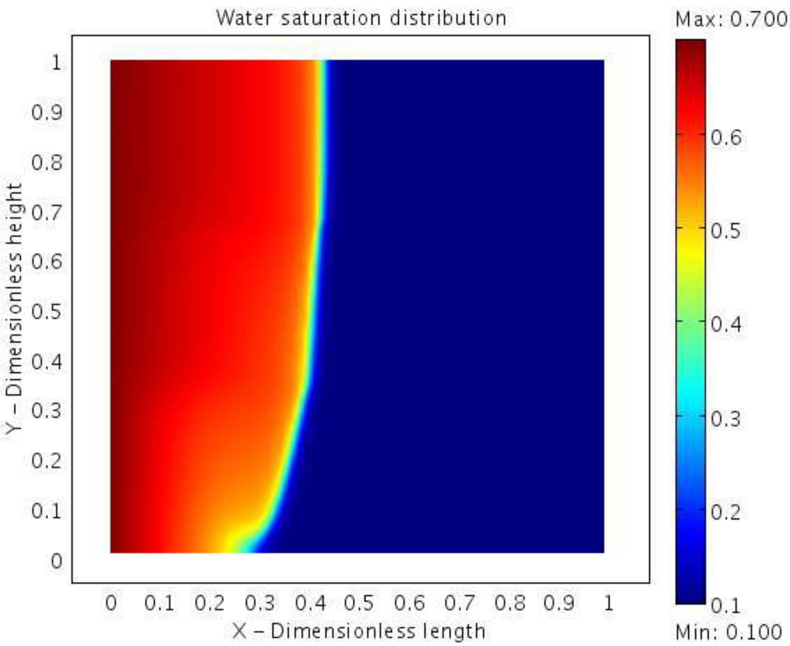

Fig 4.1 2D saturation profiles in $X-Y$ plane, *T*=0.2 pvi, $M=2$ (**a**) non-communicating layer-cake reservoir (by direct calculation of mass balance equation for each layer), (**b**) perfectly communicating layer-cake reservoir (by COMSOL).

4.2.2 $M=1$

Calculations are then carried out with $\mathrm{M}_o=2, kr_{wor}=0.4, kr_{owi}=0.8$ so that *M*=1.0. At *T*=0.2 pvi, the saturation profiles in the $X-Y$ plane are shown in Fig 4.2 (a) and (b) respectively for the non-communicating and the communicating cases. A difference between the two cases is similar to the case of *M*=2. In the communicating case, the displacement profile is less uniform than that with *M*=2. There is a clear transition zone stretching from the more permeable layer to the less permeable layer. Such a transition can be also explained by the crossflow between layers.

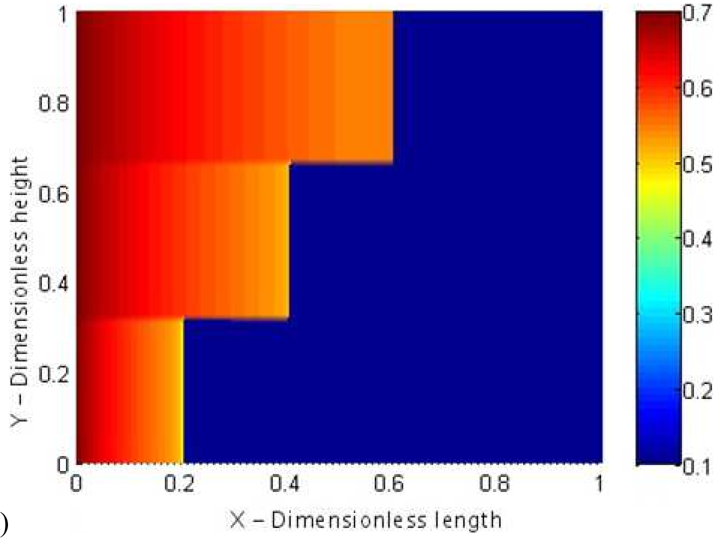

a)

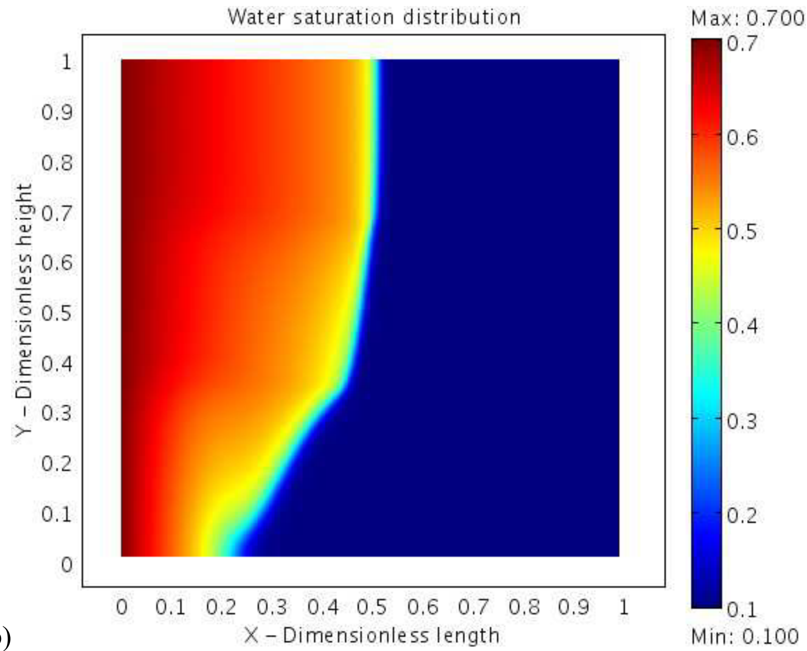

b)

Fig 4.2 2D saturation profiles in $X - Y$ plane, T=0.2 pvi, M=1.0 (**a**) non-communicating layer-cake reservoir (by direct calculation of mass balance equation for each layer), (**b**) communicating layer-cake reservoir (by COMSOL).

4.2.3 $M = 0.25$

Calculations are then carried out with even smaller mobility ratios, *M*=0.25 with $\mathrm{M}_o, kr_{wor}, kr_{owi}$ selected to be 2, 0.8 and 0.4 respectively. At *T*=0.2 pvi, the saturation profiles at different depths and in the $X - Y$ plane are shown in Fig 4.3a and b. The displacement fronts are more non-uniform than those with $M \geq 1$. As pointed out in the figure, a large water bank and a wide transition zone can be observed. The existence of such water banks behind displacement fronts and the transition zone before them may not be observed in the averaged saturation profiles (Zhang et al. (2011)).

In the cases with $M \geq 1$ the saturation distribution does not provide much information about the crossflow between layers since the displacement fronts are relatively even. On the other hand, the displacement profile with *M*=0.25 is highly non-uniform and exhibits a large water bank and a wide transition zone. They are clear evidences of crossflow between layers. They may provide more insights on the focused inter-layer mass communication. Thus, more detailed results with *M*=0.25 are shown below.

Saturation profiles at different time with *M*=0.25 are revealed for the communicating case. Fig 4.4a shows the profiles at the interface between the middle and bottom layers while Fig 4.4b reveals the profiles at the bottom of the reservoir. It can be seen that the water bank evolves and moves towards the producer with time. The end of the water bank closer to the inlet moves along with the displacement front in the bottom layer, as pointed out in Fig 4.4. It indicates that the formation of the water bank is clearly connected with the crossflow between neighboring layers.

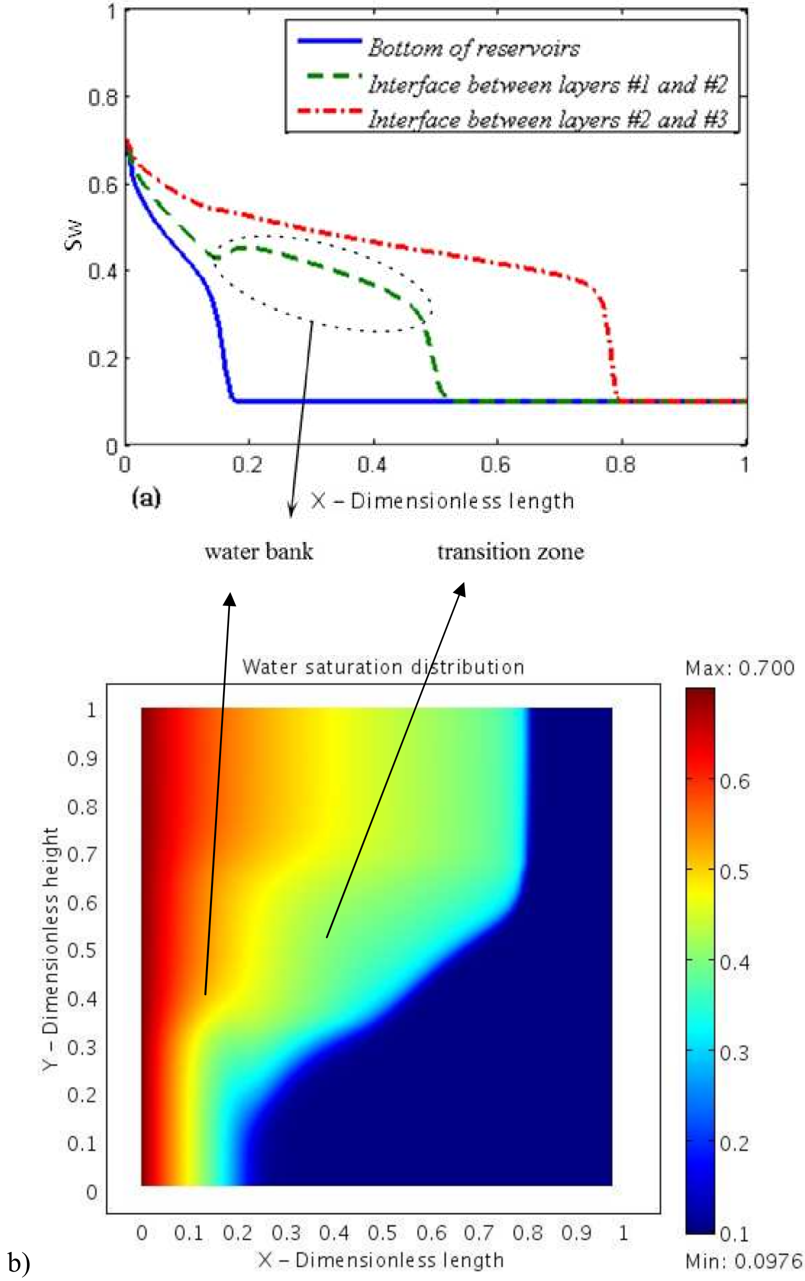

Fig 4.3 (**a**) Saturation profiles at different vertical positions, (**b**) 2D saturation profiles in X-Y plane (by COMSOL). *T*=0.2 pvi, *M*=0.25.

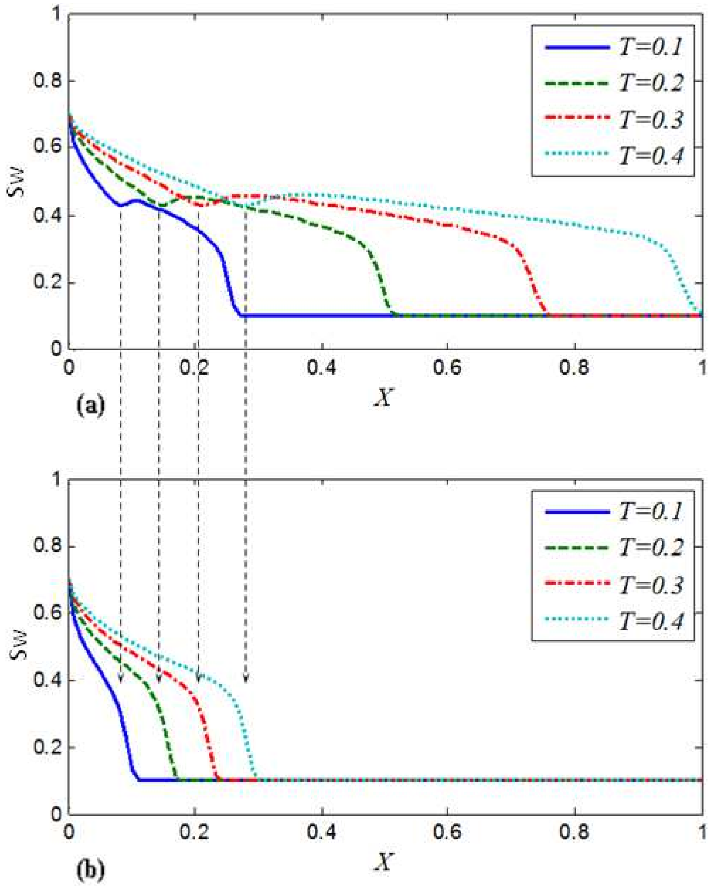

Fig 4.4 (**a**) Saturation profiles at the interface between layer 1 and layer 2, (**b**)Saturation profiles at the bottom of the reservoir. *M*=0.25.

4.3 Explanation for Existence of the Water Bank

The effects of crossflow between layers can be explained in the following sense: Via the interpretation of Eq. (3.28) it is known that the driving force for crossflow is the difference of the horizontal variations of accumulated mobility in different layers. In other words, water tends to flow from the higher to the lower horizontal mobility variation. Such mechanisms may result in uniformity and smoothness of saturation profiles, water banks and transition zones.

The crossflow of water may be illustrated in the following example: (i) At the beginning of water injection, the water saturation behind the displacement fronts drops faster horizontally in the less permeable layer than that in the more permeable layer . Hence water tends to flow from the less permeable layers to the more permeable ones, as seen in Fig 4.5. (ii) Ahead of the slower displacement front, the horizontal mobility variation is close to zero ($s_w \approx s_{wi}$). In the neighboring regions of the more permeable layer, where the displacement front has already passed, the horizontal mobility variation is considerably larger than zero. Thus, water tends to flow from the more permeable layer to the less permeable one. The water bank in Fig. 4.3 and its movement in Fig 4.4 are clear evidences supporting the above mechanisms.

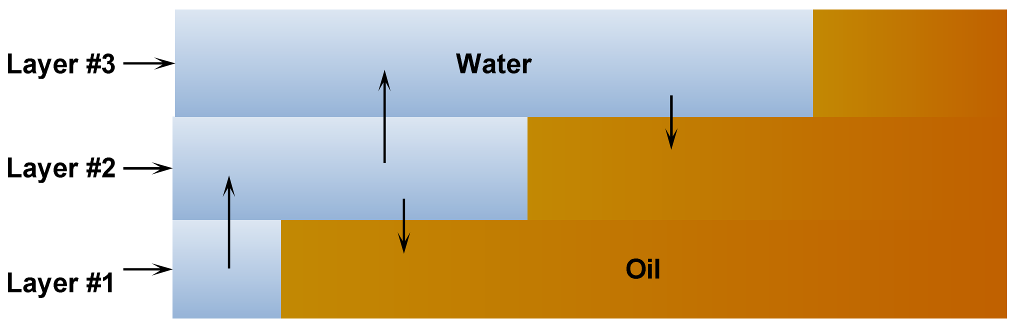

Fig 4.5 Iluustration of the crossflow between reservoir layers, arrows indicate water flow directions.

In order to understand the influence of the mobility ratio on the crossflow, the horizontal mobility variation is rewritten as a function of the mobility derivative with respect to saturation:

$$
\begin{aligned}
\frac{\partial \Lambda_X}{\partial X} &= \frac{d\Lambda_X}{ds_w}\frac{\partial s_w}{\partial X} \\
&= \frac{2K_X kr_{wor}}{\left(1-s_{or}-s_{wi}\right)^2}\left[s_w - s_{wi} - M\left(1-s_w-s_{or}\right)\right]\frac{\partial s_w}{\partial X}
\end{aligned}
$$

It can be seen from this equation that $\frac{\partial \Lambda_x}{\partial X}$ is more sensitive to $\frac{\partial s}{\partial X}$ with smaller values of M. Hence, larger water-oil mobility ratio enhances the crossflow between layers. The clear water bank and the large transition zone in Fig 4.3 and Fig 4.4 may also be attributed to the enhanced crossflow due to the small oil-water mobility ratio.

4.4 Summary

Due to the crossflow between layers the displacement profiles of waterflooding are more even and smoother in a communicating layer-cake reservoir than those in a non-communicating layer-cake reservoir. In a communicating layer-cake reservoir, larger (larger than 1) values of the end-point mobility ratio (oil to water) lead to more even displacement profiles. With small values of the mobility ratio ($M < 1$), water banks behind displacement fronts and transition zones before them may be observed. Analysis of the mathematical model and the modeling results indicates that water tends to flow from the less permeable to the more permeable layers behind displacement fronts, while water tends to flow from the more permeable to the less permeable layers ahead of the slower displacement fronts, forming water banks and transition zones.

Chapter 5 Inclusion of Gravity

The study in this chapter takes gravity effect into consideration in addition to the previous study in Chapter 3 and 4. The effect of capillary forces is not considered. The study is based on the stratified viscous dominant regime, corresponding to the large value of anisotropy parameter. Water is injected parallel to reservoir. Two more dimensionless parameters are needed for description of this regime: the gravity-viscous ratio and the fluids density ratio. As gravity effect becomes large, the two phases of flow may be completely separated by gravity. Our method needs to be modified in order to handle this case.

5.1 Introduction

Gravity effects can significantly affect reservoir performance. Gravity has been beneficial in the accumulation of hydrocarbon in reservoirs, but it may be positive or negative for hydrocarbon recovery. The study about gravity effect on flow behavior in porous media generally contains two parts: free-fall gravity drainage and gravity segregation in the process of displacement. Cardwell and Parsons (1948) follow the work by Muskat and his associates (Muskat and Taylor (1946); Boyer et.al (1947)) and present a theory for estimating the rate of free-fall gravity drainage of a liquid out of a sand column. Dykstra (1978) expand the work by Cardwell and Parsons and derive the equation for recovery. Seven comparisons of recovery are made by the method of Cardwell and Parsons with recoveries determined experimentally.

Gravity segregation in multiphase displacement process is of great significance for petroleum industry. Gravity segregation can occur through two different mechanisms. First, all phases of flow in the reservoir, possible oil, gas and water, move through the same pores.

For the second mechanism, all phases are completely separated that some pores carry only downward flows while others carry only upward flows. These two mechanisms result in substantially different phase velocities (Hales and Cook (2010)). Spivak (1974), related with the first mechanism, test waterflooding and gas flooding in a homogeneous anisotropy three dimensional reservoir model with gravity effect. Qualitative conclusion of the effect from density difference, permeability, production rate on gravity segregation is drawn.

Lamine et al. (2011) presents a locally conservative cell-based multidimensional upwind scheme for hyperbolic flow system with gravity effect in porous media on structured and unstructured grids.

Elliot and Kovscek (2001) and Javad et al. (2011) are numerical and experimental simulation of steam assisted gravity drainage (SAGD) process respectively. This process is driven by the second mechanism of gravity segregation. Rittirong and Kelkar (2010) present an analytical upgridding method to preserve dynamic flow behavior in the displacement process where the two phases of flow are completely separated by gravity.

Dietz (1953), Bear (1972) and Yortsos (1991, 1992) include analysis on both mechanisms. Yortsos (1992) present details of analysis on the second mechanism of gravity dominant displacement and extend the method derived in Yortsos (1991) to the geometry with dip. All his derivations are based on the assumption of vertical equilibrium. Experiments by Hales and Cook (2010) cover the two mechanisms.

Our work in this chapter is similar with Yortsos (1991), with some changes regarding the computations of the inter-layer flow. It is shown in numerical simulations that our method gives results close to full 2D simulation for even relatively moderate anisotropy ratios.

The chapter is organized as follows. Section 5.2 describes the theory of the method, including reformation of dimensional flow equation into dimensionless form in Section 5.2.1, asymptotic analysis on current problem in Sections 5.2.2, derivations about reservoir of layer-cake structure in Section 5.2.3. Section 5.3 is devoted to a detailed comparison of the computational results with 2D simulations in different layered geometries and under different flow regimes. Section 5.3.1 introduces the numerical scheme. Cases of only existence of gravity and both existences of gravity and inter-layer crossflow are studied in Section 5.3.2, 5.3.3 and 5.3.4. Different combinations of gravity-viscous ratio and anisotropy ratio are tested in Section 5.3.5. Conclusions are drawn in Section 5.4.

5.2 Theory

The study carried out in this chapter is based on the reservoir model and assumptions described in Section 1.2.1 and Section 3.2.1. The only difference is that we do not assume negligible gravity in this chapter.

5.2.1 Dimensionless Description of 2D Waterflooding in Presence of Gravity

Mass balance and continuity equations are written in Eqs. (1.3)-(1.5). Darcy velocity in horizontal direction is expressed in Eq. (1.6) for water phase and Eq. (1.7) for oil phase. Since gravity is involved, the expression for vertical Darcy velocity should also include the gravity term:

$$u_{wy} = -\lambda_{wy}\left(\frac{\partial p}{\partial y} + \rho_w g\right)$$

$$u_{oy} = -\lambda_{oy}\left(\frac{\partial p}{\partial y} + \rho_o g\right)$$

where ρ_w, ρ_o are density of water and oil respectively; g is gravity acceleration.

Substitution of expressions of velocities into flow equations leads to a system of equations for water saturation s_w and pressure p .

$$\phi\frac{\partial s_w}{\partial t} + \frac{\partial}{\partial x}\left(-\lambda_{wx}\frac{\partial p}{\partial x}\right) + \frac{\partial}{\partial y}\left[-\lambda_{wy}\left(\frac{\partial p}{\partial y} + \rho_w g\right)\right] = 0 \tag{5.1}$$

$$\frac{\partial}{\partial x}\left(\lambda_x\frac{\partial p}{\partial x}\right) + \frac{\partial}{\partial y}\left(\lambda_y\frac{\partial p}{\partial y}\right) + \frac{\partial}{\partial y}\left(\lambda_{wy}\rho_w g + \lambda_{oy}\rho_o g\right) = 0 \tag{5.2}$$

Total mobilities λ_x, λ_y are defined in Eq. (1.11).

By using Eqs. (3.3)-(3.6), we are able to express Eq. (5.1)-(5.2) in dimensionless form.

$$\Phi\frac{\partial s_w}{\partial T} + \frac{\partial}{\partial X}\left(-\Lambda_{wX}\frac{\partial P}{\partial X}\right) + E_a\frac{\partial}{\partial Y}\left[-\Lambda_{wY}\left(\frac{\partial P}{\partial Y} + E_g\right)\right] = 0$$

$$\frac{\partial}{\partial X}\left(\Lambda_X \frac{\partial P}{\partial X}\right)+E_a \frac{\partial}{\partial Y}\left[\Lambda_Y \frac{\partial P}{\partial Y}+E_g\left(\Lambda_{wY}+E_\rho \Lambda_{oY}\right)\right]=0$$

The dimensionless parameter E_a is defined in Eq. (3.9). Two more parameters are needed to characterize gravity effect.

$$E_g \equiv \frac{\rho_w g H}{p_0} \tag{5.3}$$

is the ratio of the gravity and viscous forces; and

$$E_\rho = \frac{\rho_o}{\rho_w} \tag{5.4}$$

is the density ratio of oil and water.

The system can also be expressed in terms of dimensionless total velocities $\bar{U}_X$, $\bar{U}_Y$, as Eqs. (3.17)-(3.18). Under the presence of gravity, $\bar{U}_X$ is defined in the same way as Eq. (3.13), but $\bar{U}_Y$ should be defined differently.

$$\bar{U}_Y = -\Lambda_Y \frac{\partial P}{\partial Y} - E_g\left(\Lambda_{wY}+E_\rho \Lambda_{oY}\right) \tag{5.5}$$

Dimensionless water velocity can be expressed as:

$$\bar{U}_{wX} = F\bar{U}_X \tag{5.6}$$

$$\bar{U}_{wY} = \bar{U}_Y F - E_g\left(1 - E_\rho\right)\Lambda_{oY} F \tag{5.7}$$

It should be noted that, unlike in the case of absence of gravity, $\bar{U}_{wY}$ is not proportional to $\bar{U}_Y$. The additional term expresses the effect of the buoyancy force: It is proportional to $1 - E_\rho$ and, therefore, to the density difference $\rho_w - \rho_o$.

The system now becomes

$$\Phi\frac{\partial s_w}{\partial T} + \frac{\partial}{\partial X}\left(F\bar{U}_X\right) + E_a\frac{\partial}{\partial Y}\left[\bar{U}_Y F - E_g\left(1 - E_\rho\right)\Lambda_o F\right] = 0 \tag{5.8}$$

$$\frac{\partial \overline{U}_X}{\partial X} + E_a\frac{\partial \overline{U}_Y}{\partial Y} = 0 \tag{5.9}$$

The 2D waterflooding system described by Eq. (3.12), (5.5), (5.8), (5.9) aims to solve water saturation s_w, dimensionless pressure P and dimensionless velocities $\overline{U}_X, \overline{U}_Y$. These four equations will be implemented in COMSOL to simulate the 2D process of waterflooding. Boundary and initial conditions are similar as that for the system of Eq. (3.12), (3.13), (3.17), (3.18).

5.2.2 Asymptotic Analysis

In this chapter, we carry out the asymptotic analysis in a different way from Chapter 3.

From continuity equation Eq.(5.9), $\overline{U}_Y$ can be expressed in terms of $\overline{U}_X$:

$$\overline{U}_Y = -\frac{1}{E_a}\int_0^Y \frac{\partial \overline{U}_X}{\partial X} dY' = \frac{W}{E_a} \tag{5.10}$$

Here expression $-\int_0^Y \frac{\partial \bar{U}_X}{\partial X} dY'$ is denoted as W. From Eq. (5.5) and (5.10) $\partial P/\partial Y$ can be expressed in terms of W.

$$\frac{\partial P}{\partial Y} = -\frac{W}{\Lambda_Y E_a} - E_g\left[F + E_\rho(1-F)\right] \tag{5.11}$$

Dimensionless pressure P is thus the integral of $\partial P/\partial Y$ over Y plus a integration constant $C(X,T)$:

$$P = C(X,T) - \frac{1}{E_a}\int_0^Y \frac{W}{\Lambda_Y} dY' - E_g\int_0^Y \left[F + E_\rho(1-F)\right] dY' \tag{5.12}$$

Referring to Darcy's law Eq. (3.12), the full expression of $\bar{U}_X$ can now be written in terms of partial derivative with respect to X of all three terms on the right side of Eq.(5.12):

$$\bar{U}_X = -\Lambda_X\left(\frac{\partial C}{\partial X} - \frac{1}{E_a}\int_0^Y \frac{\partial}{\partial X}\left(\frac{W}{\Lambda_Y}\right) dY' - E_g\int_0^Y \frac{\partial}{\partial X}\left[F + E_\rho(1-F)\right] dY'\right)$$

For large values of E_a, the term proportional to $1/E_a$ may be neglected compared to other terms, and expression for $\bar{U}_X$ may be reduced to

$$\bar{U}_X = -\Lambda_X \frac{\partial C}{\partial X} + E_g(1-E_\rho)\Lambda_X B \tag{5.13}$$

Here we denote

$$B = \int_0^Y \frac{\partial F}{\partial X} dY' \tag{5.14}$$

Although we neglect the terms proportional to $1/E_a$ in the expression of $\overline{U}_X$, we cannot neglect the value of $\overline{U}_Y$, which is also proportional to $1/E_a$ according to Eq. (5.10). Indeed, the mass balance equation (Eq. (5.8)) includes term $E_a \overline{U}_Y F$, which is comparable to other terms in this equation. Thus, we cannot eliminate terms including $\overline{U}_Y$ from the system.

Now, $\overline{U}_X$ and $\overline{U}_Y$ are both expressed in terms of $\partial C/\partial X$ and $s_w(X,Y,T)$, since B is actually a function of water saturation s_w. $\overline{U}_X$ and $\overline{U}_Y$ can also be expressed in terms of the dimensionless injection velocity. Referring to Eqs. (3.12), (3.23), since the value of $\partial C/\partial X$ is independent of Y, it can be expressed explicitly in terms of V_{inj}:

$$\frac{\partial C}{\partial X} = \frac{-V_{inj} + E_g(1-E_\rho)\int_0^1 B\Lambda_X dY}{\int_0^1 \Lambda_X dY}$$

Now it is possible to rewrite $\overline{U}_X$ and $\overline{U}_Y$ in terms of V_{inj} by substituting the expression for $\partial C/\partial X$ into Eq. (5.13) and (5.10):

$$\overline{U}_X = \Lambda_X \left[\frac{V_{inj}}{\int_0^1 \Lambda_X dY} + E_g(1-E_\rho)\left(B - \frac{\int_0^1 B\Lambda_X dY}{\int_0^1 \Lambda_X dY} \right) \right] \tag{5.15}$$

$$\overline{U}_Y = -\frac{1}{E_a}\int_0^Y \frac{\partial}{\partial X}\left\{ \Lambda_X \left[\frac{V_{inj}}{\int_0^1 \Lambda_X dY} + E_g(1-E_\rho)\left(B - \frac{\int_0^1 B\Lambda_X dY}{\int_0^1 \Lambda_X dY} \right) \right] \right\} dY' \tag{5.16}$$

Substitution of Eqs. (5.15) and (5.16) into Eq. (5.8) gives

$$\Phi\frac{\partial s_w}{\partial T}+\frac{\partial}{\partial X}\left(\frac{\Lambda_X F V_{inj}}{\int_0^1 \Lambda_X dY}\right)-\frac{\partial}{\partial Y}\left[F\int_0^Y \frac{\partial}{\partial X}\left(\frac{\Lambda_X V_{inj}}{\int_0^1 \Lambda_X dY}\right)dY'\right]+E_g(1-E_\rho)\frac{\partial}{\partial X}\left[\Lambda_X F\left(B-\frac{\int_0^1 B\Lambda_X dY}{\int_0^1 \Lambda_X dY}\right)\right]$$
$$+E_g(1-E_\rho)\frac{\partial}{\partial Y}\left\{F\int_0^Y \frac{\partial}{\partial X}\left[\Lambda_X\left(\frac{\int_0^1 B\Lambda_X dY}{\int_0^1 \Lambda_X dY}-B\right)\right]dY'\right\}-$$
$$E_a E_g\left(1-E_\rho\right)\frac{\partial}{\partial Y}(\Lambda_o F)=0$$

(5.17)

This is a closed equation for water saturation $s_w(X,Y,T)$, since V_{inj} is known in our study . The value of B is expressed by Eq. (5.14).

Now let us analyze the terms associated with gravity (proportional to $E_g(1-E_\rho)$) in Eq. (5.17). In the definition of E_g (Eq. (5.3)), the characteristic pressure difference p_0 is usually of the order of several atmospheres to several MPa, and the height of a reservoir is from several ten to several hundred meters. Thus, E_g is usually of the order of 0.1~1 or less. $\left(1-E_\rho\right)$ may be viewed as the ratio of density difference of the two phases (Eq.(5.4)). It is of the order of 0.1. So the product of E_g and $\left(1-E_\rho\right)$ is of the order of 0.01~0.1 or even less. When it is very small, the terms only proportional to $E_g(1-E_\rho)$ can be neglected compared to other terms. However, this is not applied to the term proportional to $E_aE_g\left(1-E_\rho\right)$, which can be large due to large value of E_a. Gravity thus produces buoyancy, which is due to density difference of the two phases of flow, for the lighter phase. In the case of small value of $E_g\left(1-E_\rho\right)$, Eq. (5.17) can be reduced to

$$\Phi\frac{\partial s_w}{\partial T}+\frac{\partial}{\partial X}\left(F\frac{\Lambda_X V_{inj}}{\int_0^1\Lambda_X dY}\right)-\frac{\partial}{\partial Y}\left[F\int_0^Y\frac{\partial}{\partial X}\left(\frac{\Lambda_X V_{inj}}{\int_0^1\Lambda_X dY}\right)dY'\right]-E_aE_g\left(1-E_\rho\right)\frac{\partial}{\partial Y}\left(\Lambda_o F\right)=0$$

(5.18)

Such a reduction, when possible, greatly simplifies analysis and solution of the equation.

5.2.3 A Layer-Cake Reservoir

In a layer-cake model of reservoir described in Section 3.2.7, we can discretize Eqs.(5.17)-(5.18) into multiple 1D quasi-linear equations, by approximating the derivative with respect to Y to be the difference between two layers, for example, between layer m and layer $(m-1)$, divided by the height fraction α_m and replacing integrals over Y by sums. The number of the 1D equation is equal to the number of layers in the reservoir.

Thus the full expressions for dimensionless total velocities (Eqs. (5.15)-(5.16)) are changed to

$$\bar{U}_{X,m}=\Lambda_{X,m}\left[\frac{V_{inj}}{\sum_{j=1}^{N}\Lambda_{X,j}\alpha_j}+E_g(1-E_\rho)\left(B_m-\frac{\sum_{j=1}^{N}B_j\alpha_j}{\sum_{j=1}^{N}\Lambda_{X,j}\alpha_j}\right)\right]$$

$$\bar{U}_{Y,m}=-\frac{1}{E_a}\sum_{j=1}^{m}\frac{\partial}{\partial X}\left(\frac{\Lambda_{X,j}V_{inj}}{\sum_{n=1}^{N}\Lambda_{X,n}\alpha_n}\right)\alpha_j+\frac{E_g}{E_a}(1-E_\rho)\sum_{j=1}^{m}\frac{\partial}{\partial X}\left(\frac{\Lambda_{X,j}\sum_{n=1}^{N}B_n\Lambda_{X,n}\alpha_n}{\sum_{n=1}^{N}\Lambda_{X,n}\alpha_n}-B_j\Lambda_{X,j}\right)\alpha_j$$

(5.19)

Here

$$B_m = \sum_{j=1}^{m} \frac{\partial}{\partial X} F_j \alpha_j \ .$$

The resulting system of one-dimensional equations produced from Eq. (5.17) with regard to water saturations $s_{w,m}$ in all layers is:

$$\begin{aligned}
&\Phi_m \frac{\partial s_{w,m}}{\partial T} + \frac{\partial}{\partial X}\left(F_m \frac{\Lambda_{X,m} V_{inj}}{\sum_{n=1}^{N} \Lambda_{X,n}\alpha_n} \right) + E_g(1-E_\rho)\frac{\partial}{\partial X}\left[\Lambda_{X,m} F_m \left(B_m - \frac{\sum_{n=1}^{N}\Lambda_{X,n} B_n \alpha_n}{\sum_{n=1}^{N}\Lambda_{X,n}\alpha_n} \right)\right] \\
&-\left\{ G_m \sum_{j=1}^{m} \alpha_j \frac{\partial}{\partial X}\left[\frac{\Lambda_{X,j} V_{inj}}{\sum_{n=1}^{N}\Lambda_{X,n}\alpha_n} - E_g(1-E_\rho)\Lambda_{X,j}\left(\frac{\sum_{n=1}^{N}\Lambda_{X,n} B_n \alpha_n}{\sum_{n=1}^{N}\Lambda_{X,n}\alpha_n} - B_j \right)\right] \right. \\
&\left. \quad - G_{m-1} \sum_{j=1}^{m-1} \alpha_j \frac{\partial}{\partial X}\left[\frac{\Lambda_{X,j} V_{inj}}{\sum_{n=1}^{N}\Lambda_{X,n}\alpha_n} - E_g(1-E_\rho)\Lambda_{X,j}\left(\frac{\sum_{n=1}^{N}\Lambda_{X,n} B_n \alpha_n}{\sum_{n=1}^{N}\Lambda_{X,n}\alpha_n} - B_j \right)\right] \right\} / \alpha_m \\
&-E_a E_g \left(1-E_\rho\right)\frac{\Lambda_{o,m}F_m - \Lambda_{o,m-1}F_{m-1}}{\alpha_m} = 0
\end{aligned} \tag{5.20}$$

Similar as the discussion about Eq. (3.33) in Section 3.2.7, when $\bar{U}_{Y,m}$ given by Eq. (5.19) is larger than zero, it describes the outflow from layer m to layer $m+1$. In this case it is logical to set $G_m = F_m$. However, if it is smaller than zero, this term describes the inflow from layer $m+1$ to layer m. Then it should be set $G_m = F_{m+1}$. G_{m-1} is determined in a similar way.

Eq. (5.20) includes second order derivatives with respect to X . For example, the forth term on the left hand side can be expanded as

$$E_g\left(1-E_\rho\right)\frac{\partial}{\partial X}\left(\Lambda_{X,m}F_mB_m\right)=E_g\left(1-E_\rho\right)\left[\frac{\partial\Lambda_{X,m}F_m}{\partial X}\sum_{n=1}^{m}\frac{\partial F_n}{\partial X}\alpha_n+\Lambda_{X,m}F_m\sum_{n=1}^{m}\frac{\partial^2F_n}{\partial X^2}\alpha_n\right]$$

Gravity plays the role of “diffusion”, smearing the averaged displacement front. This effect will be seen on the average saturation profile in Section 5.3.

Eq. (5.20) represents a system of parabolic equations. An initial condition and two boundary conditions at both ends of the interval of interest are needed for each of the equations. The initial condition is: $s_{w,m}(X,0)=s_{wi,m}$, where $s_{wi,m}$ is initial (most commonly, irreducible) water saturation in layer m . At the inlet ($X=0$), we set $s_{w,m}(0,T)=1-s_{or,m}$, where $s_{or,m}$ is the residual oil saturation in layer m . The outlet ($X=L$) is an open boundary, where after water breaks through water saturation $s_{w,m}$, velocities $\overline{U}_{wX,m}$, $\overline{U}_{wY,m}$ and velocity derivatives $\partial\overline{U}_{wX,m}/\partial X$, $\partial\overline{U}_{wY,m}/\partial Y$ are unknown. We need to add an artificial boundary where $s_{w,m}$ is known. We extend the interval of interest, for example to 5, and we should make sure that water does not break through at the new outlet during the whole process of waterflooding so that we can set $s_{w,m}$ to be $s_{wi,m}$ at the new outlet.

For parabolic transport problems, another commonly used boundary condition at outlet is convective outflow. Diffusion is set to be zero at outlet in this case. Bjørnarå and Aker (2008) includes capillary pressure in the both 1D and 2D waterflooding problems and applies convective outflow boundary condition. However, in our work, we stick to the method of artificial boundary.

Under small gravity numbers, when Eq. (5.17) may be reduced to Eq.(5.18), the corresponding system of one-dimensional equations becomes hyperbolic and is greatly simplified:

$$\Phi_m\frac{\partial s_{w,m}}{\partial T}+\frac{\partial}{\partial X}\left(F_m\frac{\Lambda_{X,m}V_{inj}}{\sum_{n=1}^{N}\Lambda_{X,n}\alpha_n}\right)-\frac{G_m\sum_{j=1}^{m}\alpha_j\frac{\partial}{\partial X}\left(\frac{\Lambda_{X,j}V_{inj}}{\sum_{n=1}^{N}\Lambda_{X,n}\alpha_n}\right)-G_{m-1}\sum_{j=1}^{m-1}\alpha_j\frac{\partial}{\partial X}\left(\frac{\Lambda_{X,j}V_{inj}}{\sum_{n=1}^{N}\Lambda_{X,n}\alpha_n}\right)}{\alpha_m}$$

$$-E_aE_g\left(1-E_\rho\right)\frac{\Lambda_{o,m}F_m-\Lambda_{o,m-1}F_{m-1}}{\alpha_m}=0$$

(5.21)

The choice of G_m is done in the similar way as for Eq.(5.20). Positive value of $\bar{U}_{Y,m}$ means outflow from layer m to layer $m+1$. In this case, we should set $G_m = F_m$. Otherwise this term describes the inflow from layer $m+1$ to layer m. Then we should be set $G_m = F_{m+1}$. G_{m-1} is determined in a similar way.

An initial condition and a boundary condition are needed for solving each hyperbolic equation generalized by Eq. (5.21). The initial condition is: $s_{w,m}(X,0) = s_{wi,m}$, where $s_{wi,m}$ is initial (most commonly, irreducible) water saturation in layer m. At the inlet ($X = 0$), we set $s_{w,m}(0,T) = 1 - s_{or,m}$, where $s_{or,m}$ is the residual oil saturation in layer m.

5.3 Numerical Study

In sections 5.3.2-5.3.4, we only consider small value of E_g resulting negligibly small value of $E_g(1-E_\rho)$, since the value of $E_g(1-E_\rho)$ is mainly determined by the value of E_g. The reduced form of equations (Eq.(5.21)) is therefore used in our 1D calculation. Section 5.3.5 extends the calculations onto mediate gravity effect by using mediate value of E_g and large value of E_a respectively. The complete system (Eq. (5.20)) is used for cases with mediate value of E_g. The results are compared with the complete 2D simulation of waterflooding, which is carried out by application of COMSOL solving the system of equations Eq. (3.12), (5.5),(5.8), (5.9). Average water saturation is given by Eq.(3.31). The dimensional parameters of our 2D model of reservoir are listed in Table 5.1.

5.3.1 Practical Aspects of Numerical Computations

An explicit finite difference method is applied to solve systems Eq. (5.20) and (5.21). The distance step is chosen to be $\Delta X = 0.01$ and the time step to be $\Delta T = 0.0025$. The method is implemented in the Intel Fortran program. Convergence is checked by varying the distance and the time steps. Corey power law (Eqs. (1.1)-(1.2)) is used to calculate relative permeabilities.

L (characteristic length, m)	200
H (characteristic height, m)	50
p_0 (characteristic pressure difference, Pa)	5×10^{6}
ϕ_0 (characteristic porosity)	0.2
k_{0x} (characteristic permeability, m^2)	2×10^{-13}
k_{0y} (characteristic permeability, m^2)	2×10^{-12}
μ_w (characteristic viscosity, $\frac{N\cdot s}{m^2}$)	1×10^{-3}
t_0 (characteristic time, s)	$\frac{L^2\mu_w\phi_0}{k_{0x}p_0}=8\times10^{6}$
ρ_w (density of water, $\frac{kg}{m^3}$)	1000
ρ_o (density of oil, $\frac{kg}{m^3}$)	800
v_{inj} (injection velocity, m/s)	5×10^{-6}

Table 5.1 Dimensional parameters of the two-dimensional model of reservoir.

5.3.2 A Single-Layer Reservoir

We first study the displacement in a single-layer homogeneous reservoir. Since gravity segregates flows in vertical direction, water saturation is different at different heights even in such a reservoir. Thus, in this study we can see the effect of gravity without the interlayer cross flow. Subdivision of the reservoir into small sub-layers is needed in order to catch the effect of gravity segregation. We divide the whole reservoir into 1, 2, 5, 10 uniform sub-layers respectively. The corresponding dimensionless parameters of Table 5.1 are shown in Table 5.2. The 2D saturation distribution generated by COMSOL is shown in Fig. 5.1. Results by our approach are compared with the results of two-dimensional simulations in Fig. 5.2.

Dimensionless parameters	Value
Fraction of thickness α	1
Irreducible water saturation s_{wi}	0.2
Residual oil saturation s_{or}	0.2
Relative water permeability at residual oil saturation kr_{wor}	0.8
Relative oil permeability at irreducible water saturation kr_{owi}	0.8
Dimensionless permeability in x-direction K_X	1
Dimensionless porosity Φ	1
Dimensionless dynamic viscosity of oil M_o	3
Dimensionless injection velocity V_{inj}	1
Anisotropy ratio E_a	160

Gravity-viscous ratio E_g	0.1
Density ratio E_ρ	0.8

Table 5.2 Dimensionless parameters of the one-layer reservoir.

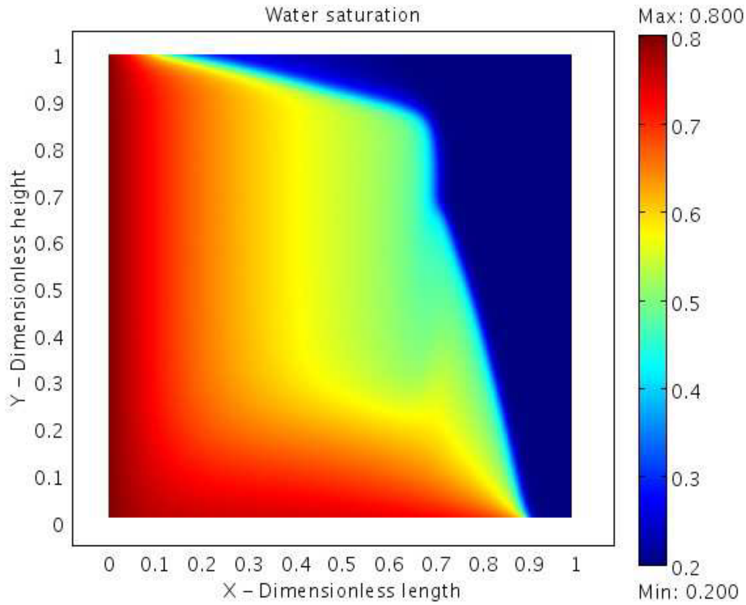

Fig 5.1 Water saturation distribution for 2D waterflooding simulation at one-layer homogeneous reservoir, time=0.3 pvi. The horizontal axis is the dimensionless distance along the reservoir, and the vertical axis is the dimensionless height (across the reservoir). E_a=160, E_g=0.1, E_ρ=0.8.

On the saturation profiles by 1 and 2 sub-layers algorithms (Fig 5.2a), there are fairly sharp displacement fronts (some smearing is due to numerical diffusion), which is very different from the averaged two-dimensional profiles. As the number of sub-layers increases to 5 and 10, smooth variation of the saturation becomes more and more obvious and the recovery becomes also closer to the results of 2D simulation (Fig. 5.2b). For the 10 sub-layer case, the recovery difference with the 2D simulation is less than 3%. Computations with even larger number of sub-layers are shown in Fig. 5.2c-d. Subdivision into 40 sub-layers clearly produces the best results, but the computations also consume much more CPU time (1.48s) than the computations for 10 sub-layers (0.21s). There is no reason to increase the number of sub-layers after 1% error in accuracy of recovery.

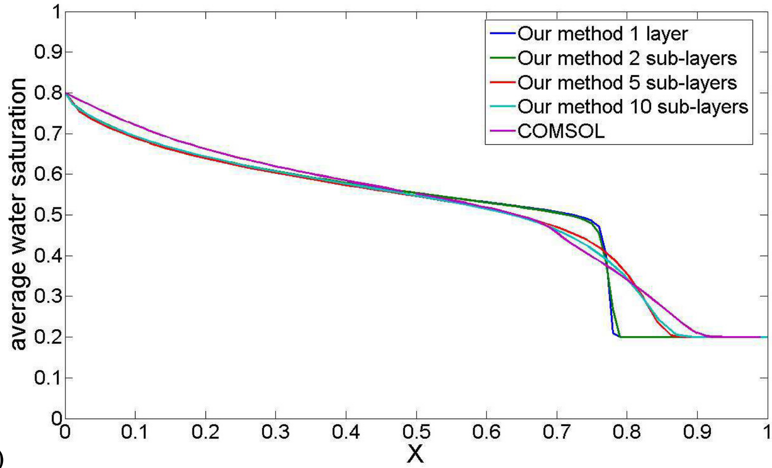

a)

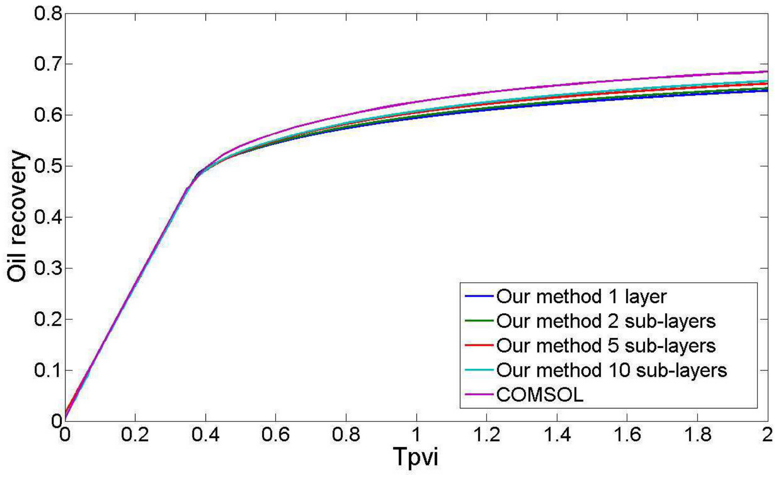

b)

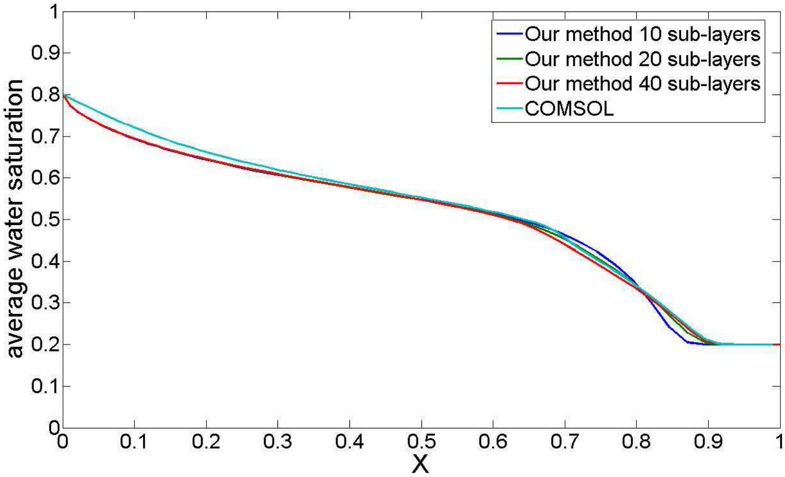

c)

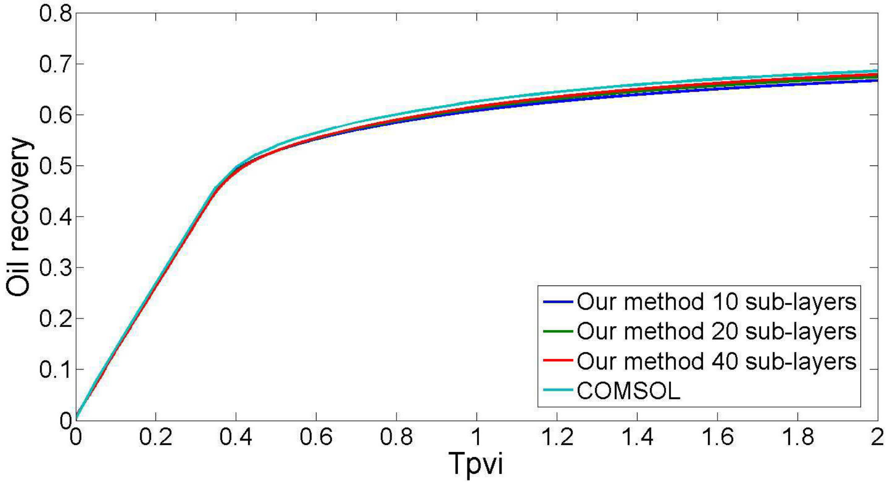

d)

Fig 5.2 Comparison of the results obtained by our method and that by the 2D simulation of a one-layer homogeneous reservoir. E_a =160, E_g=0.1, E_ρ =0.8. (**a**), (**c**) Average water saturation profiles at time=0.3 pvi, (**b**), (**d**) oil recovery curves. "1 layer" means the result is based on the natural layer of the reservoir model, which is one layer.

1D simulations implemented in FORTRAN are much faster than the 2D computations by COMSOL. Injection of 0.3 porous volumes as computed for building Fig. 5.1 (direct UMFPACK solver in COMSOL) takes ca. 700 seconds, while the corresponding FORTRAN computations take only 1.48 seconds for the 40 sub-layer case.

It is also important to test the mass error for our discretization scheme. The mass error is equivalent to the volume error in these computations, since the flow is incompressible. It is calculated as: (current volume + production volume – initial volume – injected volume) / (initial volume + injected volume). For all the results shown in Fig. 5.2, the mass error is less than 1%.

5.3.3 A Two-Layer Reservoir

In this section, we study the gravity effect under existence of the inter-layer crossflow. We use the same parameters in Table 5.1 for the two-layer communicating reservoir, so that E_a, E_g, E_ρ are the same as in the previous case. Other dimensionless parameters are listed in Table 5.3. The 2D saturation distribution is shown in Fig. 5.3.

We divide layer 1 (the small layer) into1, 3 and 6 uniform sub-layers and divide layer 2 (the large layer) into 1, 6 and 12 uniform sub-layers correspondingly. From Fig. 5.4, it is seen that our approximate approach produces the saturation profiles close to those of the 2D simulation when the number of total sub-layers exceeds 9, which corresponds to 3 sub-layers for layer 1 and 6 sub-layers for layer 2. The height fraction of each sub-layer is around 0.1.

Dimensionless parameters	Layer 1	Layer 2
Fraction of thickness α	0.33	0.67
Irreducible water saturation s_{wi}	0.2	
Residual oil saturation s_{or}	0.2	
Relative water permeability at residual oil saturation kr_{wor}	0.8	0.8
Relative oil permeability at irreducible water saturation kr_{owi}	0.8	0.8
Dimensionless permeability in X -direction K_X	0.6	1.2
Dimensionless porosity Φ	1	
Dimensionless dynamic viscosity of oil M_o	3	
Dimensionless injection velocity V_{inj}	1	
Anisotropy ratio E_a	160	
Gravity-viscous ratio E_g	0.1	
Density ratio E_ρ	0.8	

Table 5.3 Dimensionless parameters of the two-layer reservoir.

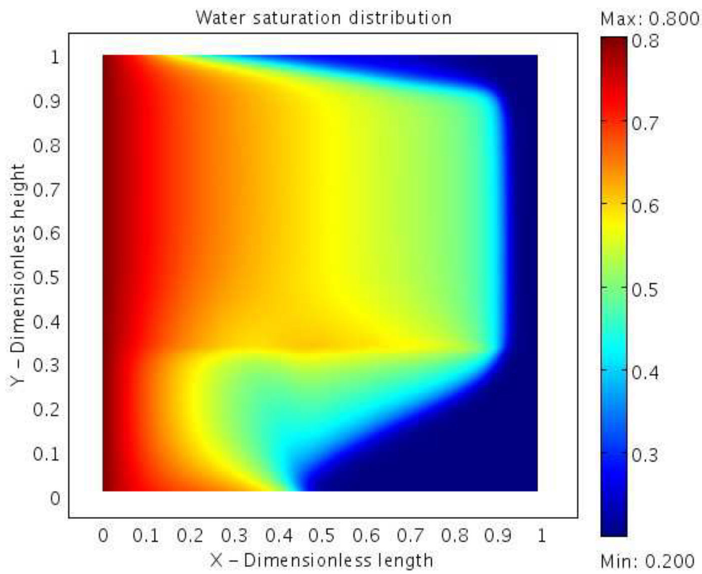

Fig 5.3 Water saturation distribution for 2D waterflooding simulation at a reservoir consisting of two fully communicating layers, time=0.3 pvi. The horizontal axis is the dimensionless distance along the reservoir, and the vertical axis is the dimensionless height (across the reservoir). E_a=160, E_g=0.1, E_ρ=0.8

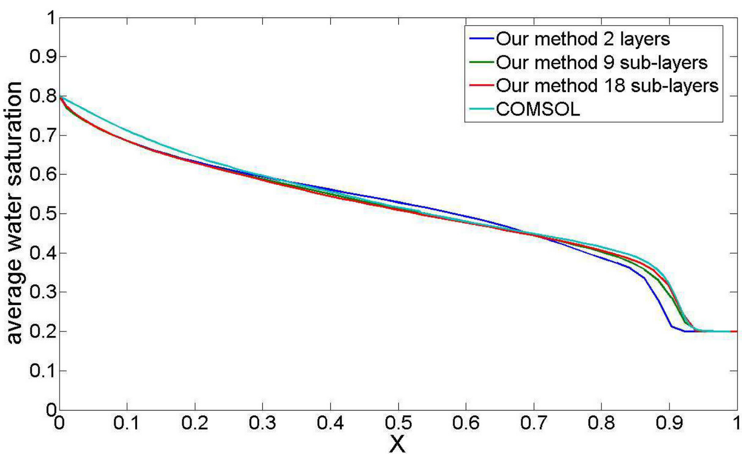

a)

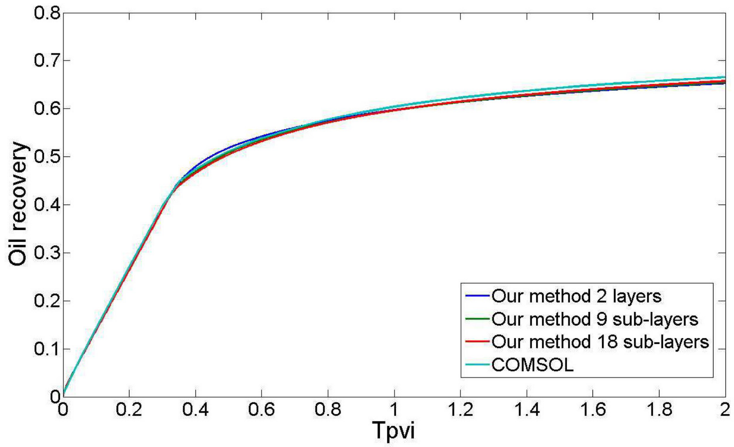

b)

Fig 5.4 Comparison of the results obtained by our method and that by the 2D simulation of a two-communicating-layer reservoir. E_a =160, E_g=0.1, A=0.8 (**a**) Average water saturation profiles at time=0.3 pvi, (**b**) oil recovery curves. "2 layers" means the result is based on the natural layers of the reservoir model, which are two layers.

Sections 5.3.2 and 5.3.3 show that the more sub-layers we use the better results we get. When the height fraction of each sub-layer does not exceed ca. 0.1 of the total height, our approach produces acceptable results.

5.3.4 A Ten-Layer Reservoir

As a better approximation to a more realistic case, we study the saturation distribution in a ten-layer reservoir with permeability increasing from the bottom to the top. We use the basic parameters from Table 5.1, and the dimensionless parameters are listed in Table 5.4.

Dimensionless parameters	Value
Fraction of thickness α	0.1
Irreducible water saturation s_{wi}	0.2
Residual oil saturation s_{or}	0.2
Relative water permeability at residual oil saturation kr_{wor}	0.8
Relative oil permeability at irreducible water saturation kr_{owi}	0.8
Dimensionless permeability in X -direction K_X	0.5; 0.6; 0.7; 0.8; 0.9; 1.1; 1.2; 1.3; 1.4; 1.5
Dimensionless porosity Φ	1
Dimensionless dynamic viscosity of oil M_o	3
Dimensionless injection rate V_{inj}	1
Anisotropy ratio E_a	160
Gravity-viscous ratio E_g	0.1
Density ratio E_ρ	0.8

Table 5.4 Dimensionless parameters of the ten-layer reservoir.

The reservoir is split into 10 and 20 sub-layers. Comparison of the results obtained by our 1D method and the results from the complete 2D simulation is shown in Fig. 5.6. Splitting the reservoir into 20 sub-layers gives better approximation to the averaged saturation profile and recovery prediction than in the case of 10 sub-layers. But the results obtained in the latter case are acceptable, with recovery difference less than 3%.

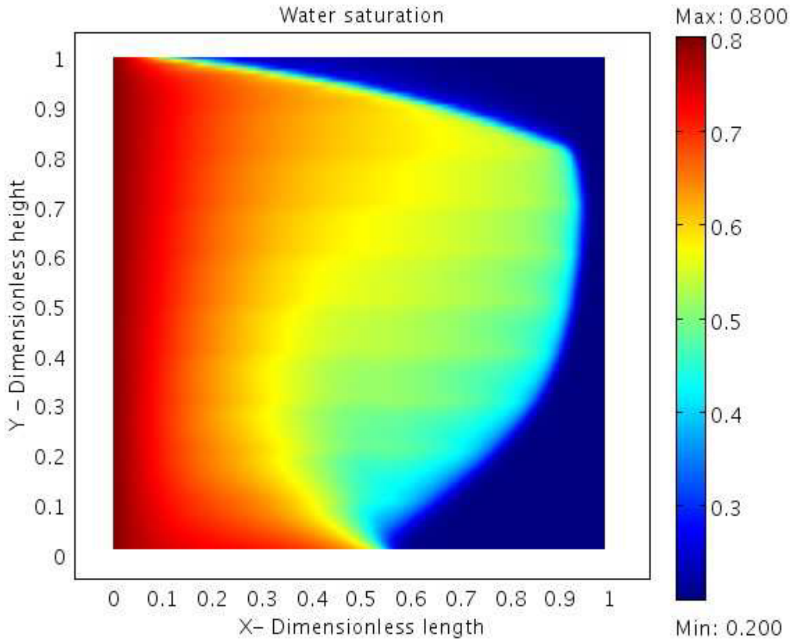

Fig 5.5 Water saturation distribution for 2D waterflooding simulation at a reservoir consisting of ten fully communicating layers, time=0.3 pvi. The horizontal axis is the dimensionless distance along the reservoir, and the vertical axis is the dimensionless height (across the reservoir). E_a=160, E_g=0.1, E_ρ=0.8

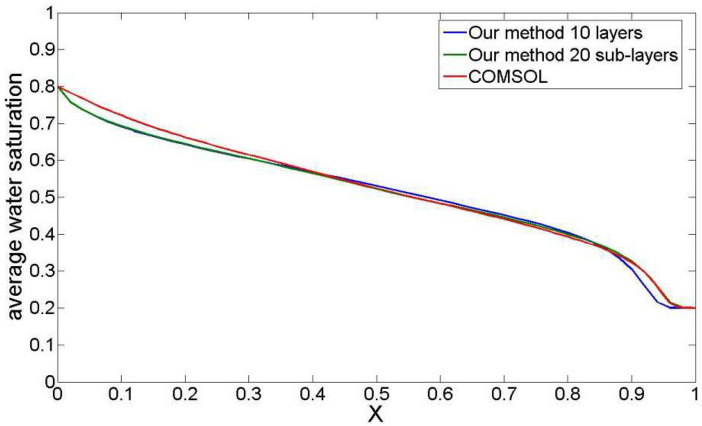

a)

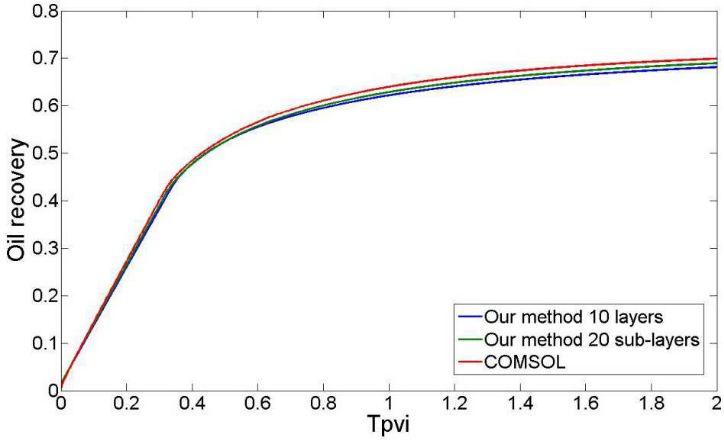

b)

Fig 5.6 Comparison of the results obtained by our method and that by the 2D simulation of a ten-communicating-layer reservoir. E_a =160, E_g=0.1, E_ρ =0.8 (**a**) Average water saturation profiles at time=0.3 pvi, (**b**) oil recovery curves. "10 layers" means the result is based on the natural layers of the reservoir model, which are ten layers.

5.3.5 Larger Gravity Effect

In this section, we study cases with large gravity effect, by comparing the computations with small E_g but large $E_aE_g\left(1-E_\rho\right)$ by solving Eq. (5.21) and the computations with mediate E_g by solving the complete system (Eq.(5.20)). We also compare the effect on flow behavior produced by terms having only $E_g\left(1-E_\rho\right)$ and term having $E_aE_g\left(1-E_\rho\right)$. All simulations are based on one-layer homogeneous reservoir model. Its dimensional parameters of properties are listed in Table 5.1. When E_g is small, the gravity effect is only related with the terms whose characteristic scale is $E_aE_g\left(1-E_\rho\right)$. This value is equal to 3.2 in simulations represented in Fig 5.1 and 20 in simulations shown in Fig 5.7. The value of $E_g = 0.1$ is the same in both cases.

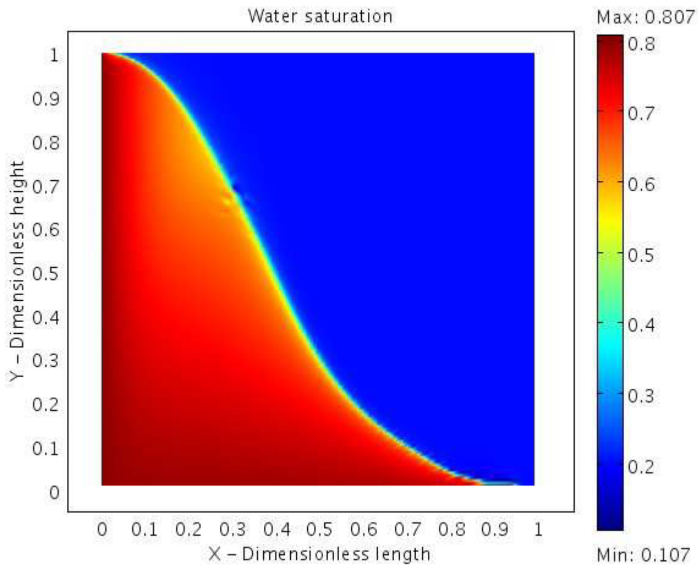

Fig 5.7 Water saturation distribution for 2D waterflooding simulation at one-layer homogeneous reservoir, time=0.2 pvi. The horizontal axis is the dimensionless distance along the reservoir, and the vertical axis is the dimensionless height (across the reservoir). E_a=1000, E_g=0.1, E_ρ=0.8.

Comparing Figs 5.1 and 5.7, we see that when $E_a E_g(1-E_\rho)$ increases, smooth variation of saturation due to gravity effect becomes more obvious. In Fig 5.7, there is some numerical error on the displacement front, because when gravity effect increases, the displacement process becomes unstable.

However, when $E_a E_g(1-E_\rho)$ is too large, water and oil become completely separated by gravity. At the height where $Y \le h$, there is only water; where $Y > h$, there is only oil. The macroscopic interface h is a function of X and T. The water saturation is expressed as

$$s_w = \begin{cases} s_{wi} & 0 \le Y \le h(X,T) \\ 1-s_{or} & 1 \ge Y > h(X,T) \end{cases}$$

Since in the limit of infinite buoyancy displacement is reduced to motion of the water-oil interface, for the conditions approaching this limit the two-dimensional simulations based on finite differences may experience problems. In particular, when the value of $E_a E_g(1-E_\rho)$ is above 30, convergence in the COMSOL simulations described above cannot be obtained.

Now let us consider the case where E_g is of the order of 1. In Fig 5.8, the product of $E_a E_g(1-E_\rho)$ is the same as in Fig 5.1, but E_g is ten times as larger, which corresponds to, for example, one fifth p_0 and two times H from Table 5.1, and E_a is one tenth as the case shown in Fig 5.1. We notice that the difference between the Fig 5.1 and Fig. 5.7 is much larger than that between Fig 5.1 and Fig 5.8. Thus, the buoyancy term proportional to $E_a E_g(1-E_\rho)$ has more influence on the flow than the remaining gravity terms.

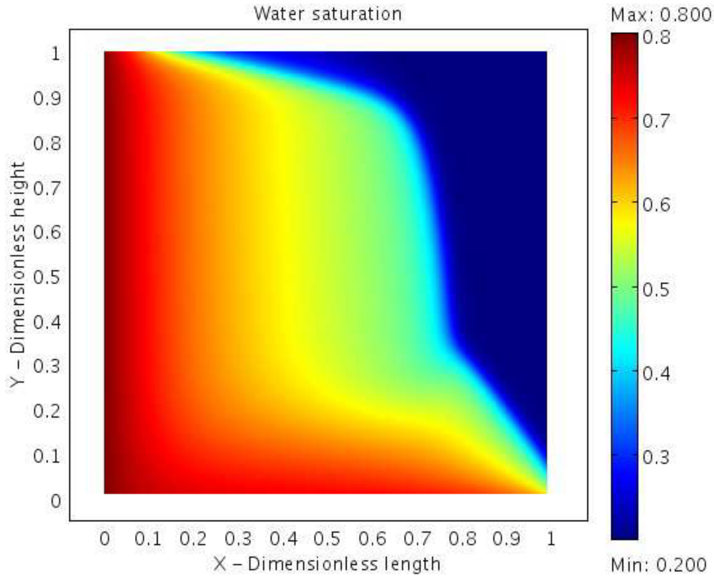

Fig 5.8 Water saturation distribution for 2D waterflooding simulation at one-layer homogeneous reservoir, time=0.3 pvi. The horizontal axis is the dimensionless distance along the reservoir, and the vertical axis is the dimensionless height (across the reservoir). E_a=16, E_g=1, E_ρ =0.8.

The saturation profile presented in Fig 5.9 is based on $E_a = 50$, which is the lowest value of anisotropy ratio for the validity of perfect inter-layer communication or equivalently vertical equilibrium (See Fig 3.9). $E_g\left(1-E_\rho\right)$ is equal to 0.2, which is comparable to other terms. $E_aE_g\left(1-E_\rho\right)$ is equal to 10. 20 sub-layers are used for the 1D calculation. Results by our 1D method are compared with those by 2D simulation in Fig 5.10. The oil recovery curve fits well to the 2D simulation (Fig 5.10b). On average water saturation profile (Fig 5.10a), full equation (Eq.(5.20)) generates more “smoothing” variation on displacement front than reduced equation (Eq.(5.21)).

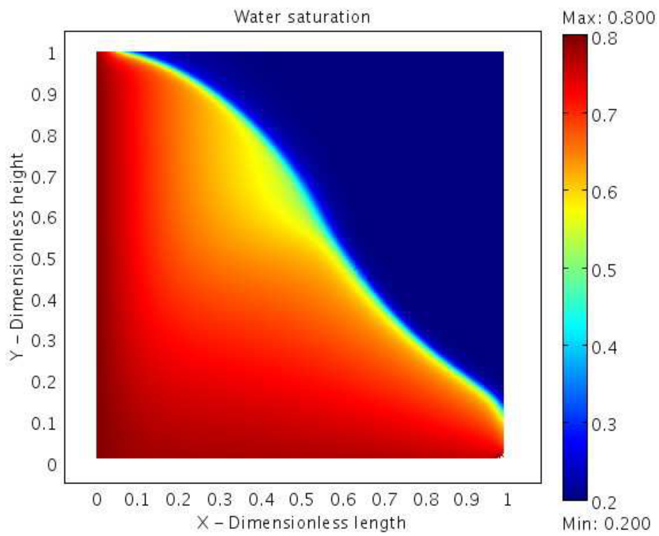

Fig 5.9 Water saturation distribution for 2D waterflooding simulation at one-layer homogeneous reservoir, time=0.3 pvi. The horizontal axis is the dimensionless distance along the reservoir, and the vertical axis is the dimensionless height (across the reservoir). E_a=50, E_g=1, E_ρ=0.8.

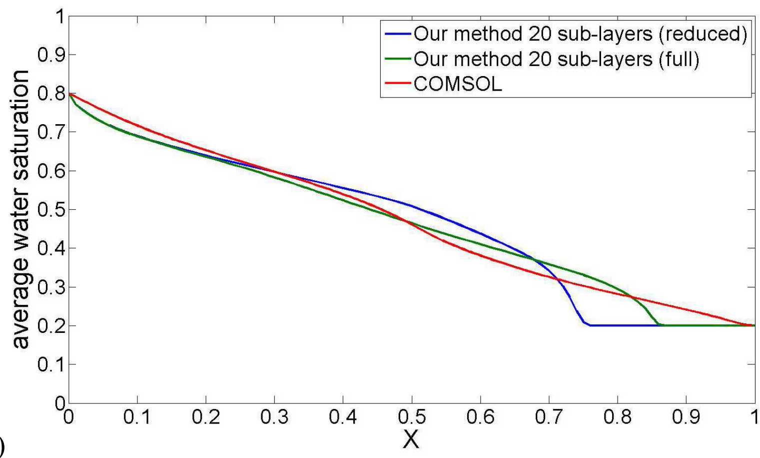

a)

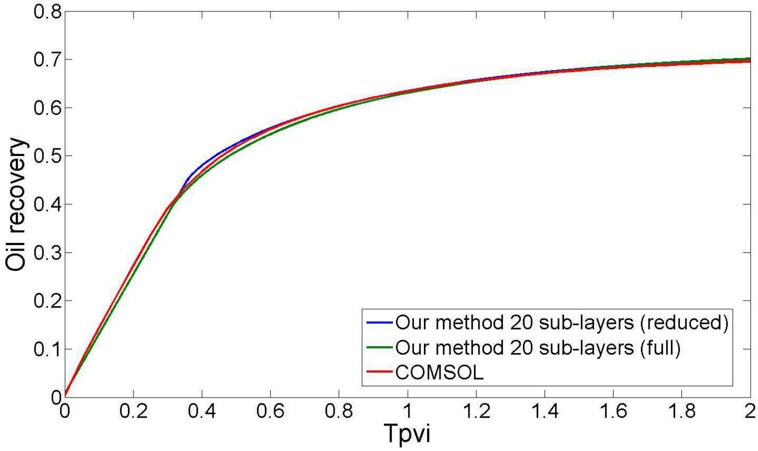

b)

Fig 5.10 Comparison of the results obtained by our method and that by the 2D simulation of a one-layer homogeneous reservoir. E_a=50, E_g=1, E_ρ=0.8 (**a**) Average water saturation profiles at time=0.25 pvi, (**b**) oil recovery curves. "reduced" means the solution is based on reduced form of the flow equation (Eq. (5.21)); "full" means the solution is based on full form of the flow equation (Eq.(5.20)).

5.4 Summary

We have developed a fast semi-analytical 1D upscaling method for two-phase immiscible incompressible flows in a stratified reservoir of a viscous dominant regime with gravity effect. The method is applied to the cases of high anisotropy ratios (very good communication between layers), small to moderate gravity numbers. For the waterflooding problems in well-defined multilayer reservoirs, the results obtained by our method are close to the results obtained by the complete 2D displacement simulation. As gravity effect becomes large, the error of our method increases, but is still within an acceptable range. Partly it is explained by the fact that the gravity effect changes the type of an averaged 1D system for flow in the layers. This system is hyperbolic for negligibly small gravity numbers, but it becomes parabolic for moderate gravity numbers. In this sense, the average gravity acts similar to diffusion (or the Taylor dispersion). This creates problems and instabilities in the simulations (also in the simulations based on the commercial software like COMSOL). Generally, the contribution of the whole term $E_g E_a (1 - E_\rho)$ is higher than the contribution of the term $E_g (1 - E_\rho)$.

Subdivision onto many sub-layers is needed to catch the effect of gravity segregation within each single layer. Our calculations indicate that when the height fraction of each sub-layer is around 0.1 of the total height, the results are comparable with the results of the complete 2D simulations.

Chapter 6 Streamline Simulation

In Chapter 3 and Chapter 5, a method for reduction of two-dimensional displacement problem into multiple one-dimensional problems in a well-defined layer-cake reservoir model under the assumption of perfect vertical communication (or equivalently vertical equilibrium) is introduced. In this chapter it is shown that it is possible to extend this method onto three-dimensional reservoir models by application of streamline simulation.

The streamline simulator used in this thesis is made by the Chemical Engineering Department, University of Southern California, USA. It is only used for generating streamline paths. The rest of the algorithm was specially produced for this thesis.

6.1 Introduction

The key idea of the streamline simulation method is to reform the governing system of equations for fluid motion on a full 3D space into a number of 1D problems, by transformation of the 3D problem from space domain to the domain of time-of-flight (TOF). The application of TOF eliminates the necessity of keeping track of the geometry. The space coordinate in conventional streamline simulation is the time-of-flight variable (Datta-Gupta (2000)).

The number of the 1D problems is equal to the number of streamlines. The 1D equations are to be solved along streamlines. Solution for the pressure field generates the paths of the streamlines. Flows are moved along the natural streamline grids rather than between discrete background grid blocks, as in conventional methods. The main advantage of the streamline technique is that very large time steps can be taken for updating pressure field, which means that the pressure field, equivalently the streamline paths, only needs to be updated a few times throughout a displacement process. In this sense, streamline simulation method is orders of magnitude faster than conventional methods (King and Datta-Gupta (1998)).

The TOF concept has been used in the ground water study as a method for calculating the capture radii of wells (Shafer (1987)). King et al. (1993) and Datta-Gupta and King (1995) have used the TOF concept for modeling flow in oil reservoirs. The details of development in the streamline approach can be found in Batycky (1997) and Thiele (1991). Datta-Gupta (2000) produced an excellent review on the application of streamline simulators.

Streamline simulation is able to solve the problems of multiphase displacement, tracer flow (Batycky (1997)) and multicomponent flow (Mallison (2004); Nielsen (2010)).

The accuracy of streamline simulation depends not only on the algorithm applied to equations along streamlines, but also the techniques for mapping variables, for example saturations, between regular and irregular grids on streamlines and between streamlines and background grid blocks. Mallison (2004) make a thorough comparison of various mapping methods and introduce Kriging interpolation into the mapping from streamlines to background grid blocks. This reduces the mass error and the numerical diffusion.

One phenomenon that often acts across the streamlines is the effect from gravity, but the propagation of the fluids along the streamlines does not account for the gravity effect. Therefore, the conventional streamline simulators often underestimate the gravity effect. To properly account for the gravity crossflow, operator splitting is a commonly used approach. (Batycky (1997); Berenblyum (2004); Nielsen (2010); Jessen and Orr (2004)).

In this chapter, the vertical upscaling method for two-phase immiscible flows (Chapter 3 and Chapter 5) is applied to streamline simulation. In this way, we are able to solve a full 3D problem by means of 1D equations under the assumption of perfect inter-layer communication. However, the application of streamlines in our study is different from the conventional ways. We produce streamlines basing on the vertically averaged properties of the 3D reservoir model and thus treat single streamline as a cross-section surface, which is a 2D geometry, of the 3D model. The previously developed upscaling method is then implemented to each cross-section surface. Emanuel and Milliken (1997) propose a similar implementation for a 2D layered streamtube model of reservoir. But the layers are assumed to be non-communicating and the displacement problem is solved by the Dykstra-Parsons method.

It should be noted that the calculation carried along streamlines is based on the arc length of streamlines, but not TOF. Therefore gravity can be included without the application of the operator splitting approach. The cases where the gravity is included and where it is excluded are studied in this chapter.

The chapter is organized as follows. Section 6.2 describes briefly the theory of streamline simulation. Section 6.3 describes the implementation of the vertical upscaling method to streamline simulation, including the change of flow equations because the volume of streamline is not uniform along the path of streamline. Section 6.4 shows comparison of the computational results by the combined streamline method and 3D finite difference method. Conclusions are drawn in Section 6.5.

6.2 Brief Introduction into the Streamline Simulation Method

The streamline simulation method can solve multidimensional flow problems. First, the pressure field is found basing on the known/initial saturation field. Then the velocity field is calculated and the streamline paths are generated. The saturation field is advanced along streamlines. The values of the renewed saturation field need to be mapped from the streamlines to the real geometry in order to calculate the new pressure field, to update streamlines and so on.

In this section, we show how the streamlines are located on the background grid blocks in the reservoir. We also introduce the concepts of the time-of-flight and the volume of a streamtube, as well as the mapping method for saturation between streamlines and background grid blocks.

6.2.1 Streamline and Streamtube

Streamlines are a family of curves that are instantaneously tangent to the velocity vector of the flow. They show the direction a fluid element will travel in at any point in time. It is a numerical description of the flow paths from a source (injector) to a sink (producer) in a reservoir model. In two dimensions the streamlines may be found from a stream function equation. The lines of constant stream function values form the streamlines and the boundaries of streamtubes (Emanuel and Milliken (1997)).

In streamline simulation, streamlines are located in the flow domain which is usually divided into a number of grid blocks for the purpose of calculation. In this thesis, we call them background grid blocks, which may be 1D, 2D or 3D geometry, to distinguish them from the grids on streamlines, which are one-dimensional. See Fig 6.1 for more details. The segments of streamlines are usually approximated as straight lines.

The principal developments of streamtube methods were first applied to model displacement process in porous media by Higgins and Leighton (1962).

In our work, a 3D reservoir model is studied, so the streamtubes are produced in three dimensions. The flow domain is divided into a number of streamtubes (Datta-Gupta (2000)). The volumes of all the streamtubes sum up to be the volume of the whole flow domain. In the streamline simulation, streamlines are considered as central curves of the corresponding streamtubes (Batycky (1997)). So the number of streamlines in a specific flow domain is equal to the number of streamtubes. Fig 6.2 is the illustration of streamtubes and streamlines.

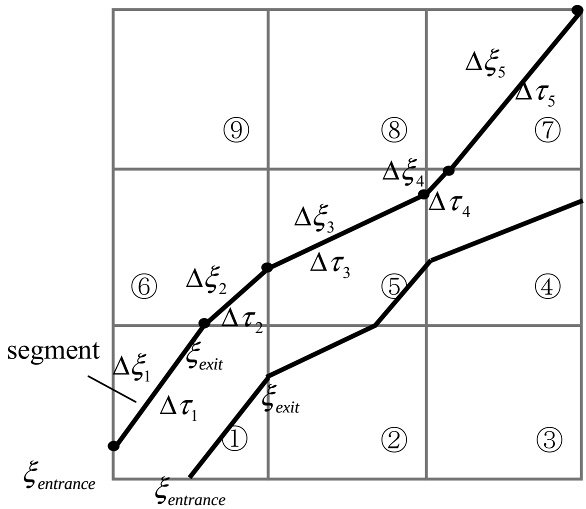

Fig 6.1 Illustration of background grid blocks in of the reservoir model and paths of streamlines. Blue squares, which are numbered by ①-⑨, represent background grid blocks in the reservoir model. The black lines represent segments of the streamline. They form the path of streamlines. $\Delta\xi$ is arc length of the segments, while $\Delta\tau$ is the TOF that the flow need to travel the distance of $\Delta\xi$. $\xi_{extrance}$ is the location of arc length on streamlines where

flow goes into the background grid. ξ_{exit} is the location of arc length on streamlines where flow goes out of the background grid.

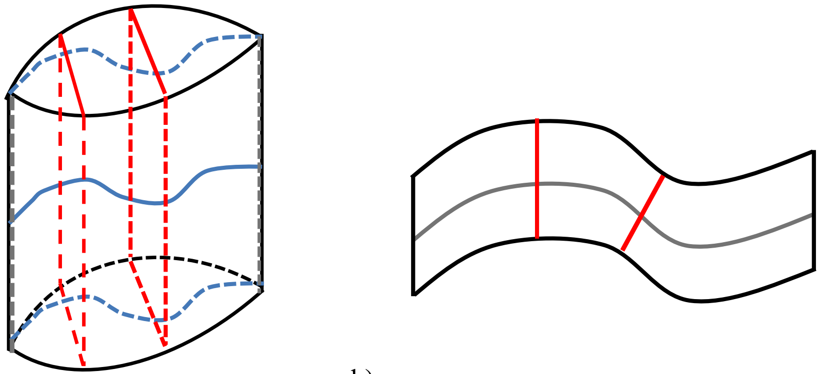

a) b)

Fig 6.2 Illustration of streamtube and streamline. The object formed by black lines is a streamtube, which is a) three dimensional or b) two-dimensional. The solid blue lines represent streamline, which is taken as the central axis of corresponding streamtube. Dashed blue lines form the cross-section surface of the reservoir. The red lines form the cross-section plane of the streamtube, which is perpendicular to the streamline.

6.2.2 Time-of-Flight

The time-of-flight (TOF) is the time required for total flow, water and oil in this chapter, to propagate from location ξ_1 to location ξ_2 along a streamline based on the velocity field along the streamline. Mathematically, TOF, τ , is defined as:

$$\tau_{\xi_1 \to \xi_2} = \int_{\xi_1}^{\xi_2} \frac{\phi(\xi)}{\left|\vec{U}(\xi)\right|} d\xi \tag{6.1}$$

where ξ is arc length of streamline, $\vec{U}(\xi)$ is the total velocity of all phases of the flow and $\phi(\xi)$ is porosity. Operator $|\;|$ means the length of a vector. $\vec{U}(\xi)$ is a vector, whose dimension in Cartesian coordinates is equal to the dimension of the reservoir model. According to definition of a streamline, $\vec{U}(\xi)$ is parallel to it. $\vec{U}(\xi)$ and $\phi(\xi)$ may vary along the streamline.

6.2.3 Volume of a Streamtube

The geometry of streamtubes depends on the flow path. The area of the streamtube cross-section $A^{st}(\xi)$ may vary along the central streamline.

When the flowrate carried by streamtubes (or corresponding streamlines) needs to be quantified, the volume of streamtubes is needed. The volume of streamtube from a location ξ_1 to location ξ_2 on the streamline is given by:

$$V^{st}_{\xi_1 \to \xi_2} = \int_{\xi_1}^{\xi_2} \phi(\xi) A^{st}(\xi) d\xi \tag{6.2}$$

where ξ is arc length of the streamline, the area of cross-section of streamtube $A^{st}(\xi)$ and porosity $\phi(\xi)$ may vary along the streamline. Superscript st indicates streamtube.

Let us distinguish between the two concepts: cross-section of the reservoir and cross-section of a streamtube. Fig 6.2 tells the difference. All the cross-sections of a streamtube are perpendicular to the corresponding streamline.

Calculation of streamtube volume has been greatly facilitated by the introduction of the TOF concept that has eliminated the need to keep track of the streamtube geometry (Datta-Gupta (2000)). For incompressible immiscible flows, volume flow rate in each streamtube is constant,

$$q^{st} = A^{st}(\xi)U(\xi) \tag{6.3}$$

so Eq.(6.2) can be rewritten as:

$$V^{st}_{\xi_1 \to \xi_2} = \int_{\xi_1}^{\xi_2} \phi(\xi) \frac{q^{st}}{U(\xi)} d\xi = q^{st} \tau_{\xi_1 \to \xi_2} \tag{6.4}$$

6.2.4 Mapping Saturation from Streamlines to Background Grid Blocks

The properties of background blocks must be calculated based on the multiple streamlines that pass through them. For example, in Fig 6.1, since two streamlines pass through grid block ①, the properties of grid block ① should be average values of the properties of these two streamlines. The average saturation for a background grid block θ, $s^{gb}_{w,\theta}$, is defined as the weighted average saturation of all streamlines passing through this grid block

$$s^{gb}_{w,\theta} = \sum_{d=1}^{n^{sl}_{gb}} \omega_{d,\theta} \bar{s}^{sl}_{w,d} \tag{6.5}$$

where $\bar{s}^{sl}_{w,d}$ is the average water saturation of the segment on the d^{th} streamline in grid block θ, $\omega_{d,\theta}$ is the weighting factor for segment on the d^{th} streamline in grid block θ, n^{sl}_{gb} is the number of streamlines passing through grid block θ.

Volume fraction of the streamtube represented by the d^{th} streamline with respect to all the n^{sl}_{gb} streamlines that pass the grid block θ is often used as the weight factor $\omega_{d,\theta}$.

$$\omega_{d,\theta} = \frac{V_{d,\theta}^{st}}{\sum_{e=1}^{n_{gb}^{sl}} V_{e,\theta}^{st}} \tag{6.6}$$

where $V_{d,\theta}^{st}$ is the streamtube volume of the segment on the d^{th} streamline in grid block θ.

Volume of each streamtube $V_{d,\theta}^{st}$ is accounted from the entrance location on streamline $\xi_{entrance}$, where the streamline goes into the grid block θ, to the exit location on the streamline ξ_{exit}, where the streamline exits the grid block θ. See Fig 6.1, grid block ①. It should be noted that $\xi_{entrance}$ and ξ_{exit} may differ for different streamlines, for example, in Fig 6.1, the two streamlines passing through grid block ① have different $\xi_{entrance}$ and ξ_{exit}. Referring to Eq.(6.4), $V_{d,\theta}^{st}$ in Eq. (6.6) is calculated as:

$$V_{d,\theta}^{st} = q_d^{st} \tau_{d,\xi_{entrance} \to \xi_{exit}} \tag{6.7}$$

Similar to the way for calculating $V_{d,\theta}^{st}$, $\overline{s}_{w,d}^{sl}$ is also only accounted for the part of streamline that lays inside the grid block θ, [$\xi_{entrance}$, ξ_{exit}].

$$\overline{s}_{w,d}^{sl} = \frac{1}{\xi_{exit} - \xi_{entrance}} \int_{\xi_{entrance}}^{\xi_{exit}} s_{w,d}^{sl}\, d\xi \tag{6.8}$$

After mapping saturation from streamlines to background grid blocks, resulting in the saturation distribution in the Cartesian grids along a reservoir, we finish one global step of calculation.

6.2.5 Mapping Saturation from Background Grid Blocks to Streamlines

When a new global step of calculation starts with updated streamline path, we need to map saturation from background grid blocks to the new streamlines. The common approach is to assume that the saturation is piecewise constant on the background grid blocks and to assign saturation value for each gird block to all streamline segments that lay inside it. For example, grid block θ has water saturation $s_{w,\theta}^{gb}$. The number of streamlines passing through θ is n_{gb}^{sl}. For the segment between $\xi_{entrance}$ and ξ_{exit} of the d^{th} streamline, water saturation $\overline{s}_{w,d}^{sl}$ is assigned to be that of the grid block θ.

$$\overline{s}_{w,d}^{sl} = s_{w,\theta}^{gb} \quad d = 1,2.....n_{gb}^{sl} \tag{6.9}$$

When we map saturation from background grid blocks to the new streamlines, we can also assume that saturation is piecewise linear on the grid blocks. That means, for example, that the derivative of saturation with respect to x at background grid block θ is calculated as:

$$\left.\frac{\partial s_w^{gb}}{\partial x}\right|_{\theta} = \frac{s_{w,\theta+1}^{gb} - s_{w,\theta}^{gb}}{\Delta x}$$

The derivatives with respect to y and z are calculated similarly. Here values Δx, Δy, Δz are the sizes of the grid block.

After knowing the derivatives in all directions, we can calculate the value of water saturation at the points $\xi_{entrance}$ and ξ_{exit} for each streamline in the grid block, instead of the average value for the whole segment. In this sense, the position of streamline defines the saturation value mapped to the streamline.

Bratvedt, F. et al. (1996) provide a method to find the saturation values for new streamlines by using the old streamlines that are closest to them. This method gives more accurate saturation profiles than Eq.(6.9), but it also requires more computational time.

6.2.6 Mapping between Irregular Grids and Regular Grids

As shown in Fig 6.1, the segments of a streamline usually are not of the same size. They form a domain of irregular grids. However, the calculation of saturation along the streamlines prefers regular spaced grids in order to obtain better stability. The need for mapping saturation from irregular grids to regular grids arises. That should be done after saturation values on the irregular grids are obtained from the background grid blocks (Eq.(6.9)). The calculation of segment value (Eq.(6.8)) is actually the mapping from regular girds to irregular grids. Fig 6.3 shows the scheme of irregular grids and regular grids for the same streamline.

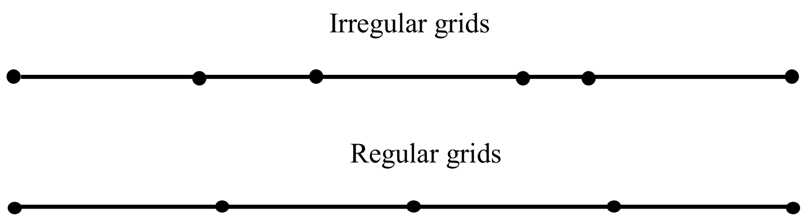

Fig 6.3 Scheme of irregular grids and regular grids for the same streamline.

Both mapping methods should obey mass balance. Fig 6.4 generalizes the relation between irregular grids and regular grids. When we consider the large interval (the interval between the two large dots) as a regular grid, we treat the small intervals (the interval between short vertical lines) as irregular grids. When we consider the large interval as an irregular grid, we treat the small intervals as regular grids.

Fig 6.4 Illustration of irregular and regular grids on streamlines. $\Delta\xi$ is the length between two adjacent points, while $s_{w,a}^{reg/irr}$ is the point value of water saturation. The superscript reg/irr means regular/irregular grids.

Water saturation can be assumed to be constant or linear on each interval $\Delta\xi$ (Fig 6.4). An average value of saturation on each interval $\Delta\xi$, for example $\bar{s}_{w,a}^{reg/irr}$, should be used to calculate the average saturation for the whole large segment, $\bar{s}_{w}^{irr/reg}$, which is the value on irregular/regular space grids. For the beginning and end of the large segment, we should only use the average value for $\Delta\xi_{left}$ and $\Delta\xi_{right}$. The averaged saturation for this large interval is calculated in the following way:

$$\bar{s}_{w}^{irr/reg} = \frac{\Delta\xi_{left}\cdot\bar{s}_{w,left}^{reg/irr} + \Delta\xi_a\cdot\bar{s}_{w,a}^{reg/irr} + \ldots\Delta\xi_{b-1}\cdot\bar{s}_{w,b-1}^{reg/irr} + \Delta\xi_{right}\cdot\bar{s}_{w,right}^{reg/irr}}{\Delta\xi_{left} + \Delta\xi_a + \ldots\Delta\xi_{b-1} + \Delta\xi_{right}}$$

When saturation is assumed to be piecewise constant on the space grids of $\Delta\xi$, $\bar{s}_{w,a}^{reg/irr}$ is equal to point value $s_{w,a}^{reg/irr}$. The equation above is changed into

$$\bar{s}_{w}^{irr/reg} = \frac{\Delta\xi_{left}\cdot s_{w,a-1}^{reg/irr} + \Delta\xi_a\cdot s_{w,a}^{reg/irr} + \ldots\Delta\xi_{b-1}\cdot s_{w,b-1}^{reg/irr} + \Delta\xi_{right}\cdot s_{w,b}^{reg/irr}}{\Delta\xi_{left} + \Delta\xi_a + \ldots\Delta\xi_{b-1} + \Delta\xi_{right}} \qquad (6.10)$$

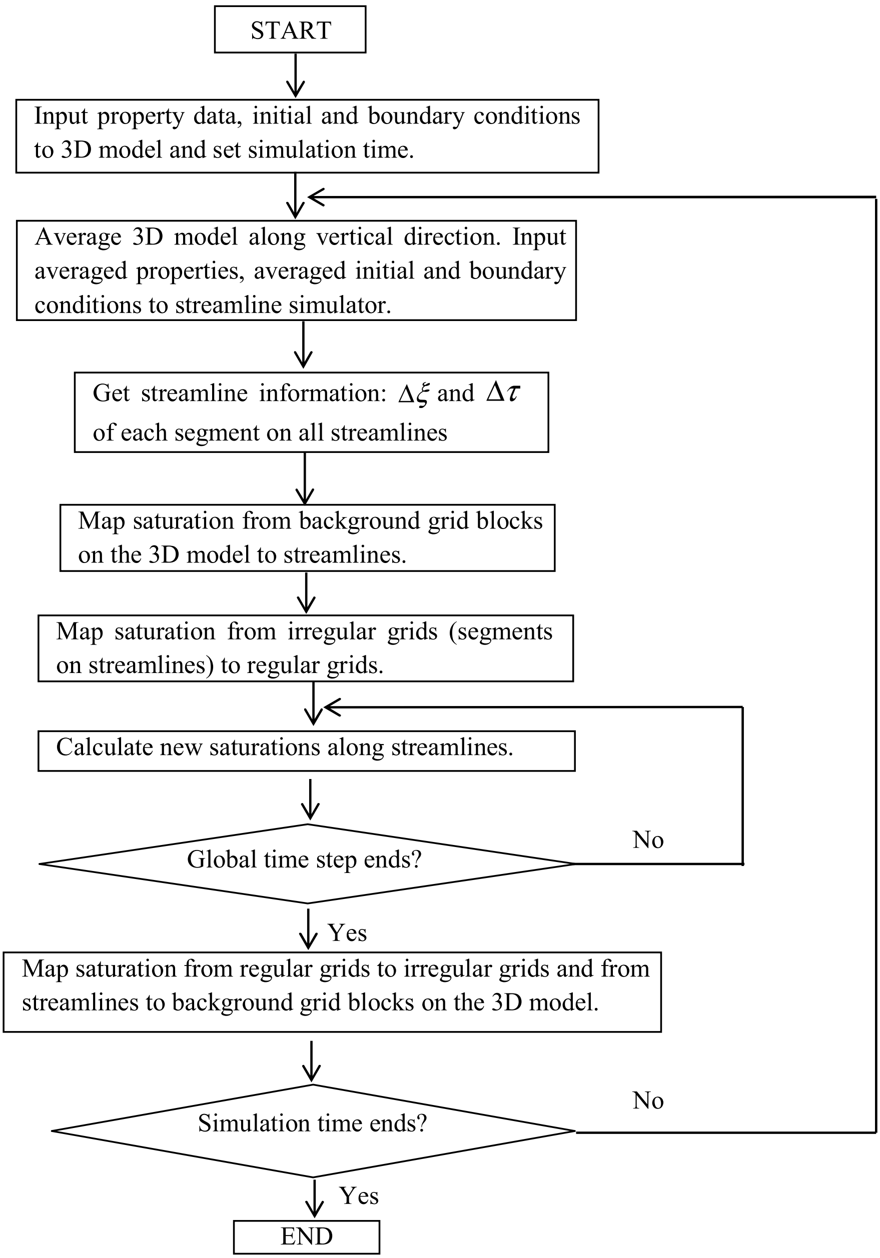

Fig 6.5 Flow chart of the implementation of our vertical upscaling method in streamline simulation.

6.3 Implementation of Vertical Upscaling Method to Streamlines

Fig 6.5 is the flow chart of the implementation of our vertical upscaling method in streamline simulation. It includes the implementation of 3D reservoir model as well as the 1D calculations.

6.3.1 Implementation of the 3D Model to Streamline Simulator

We firstly reduce the 3D layered reservoir described in Fig 3.1 to a homogeneous 2D model by averaging its natural properties: absolute permeability field, porosity field, initial water saturation and residual oil saturation, along vertical direction. Then we input the vertically averaged model, which has only one layer characterized by averaged properties, to the streamline simulator and produce a set of streamlines that go from the injector to the producer parallel to the horizontal extent of the reservoir. Each streamline represents a vertical cross-section surface of the reservoir consisting of N layers. Lengths of the streamlines and the total flow velocity $U(\xi)$ along the streamlines are known. The arc length of a streamline is equivalent to the x-axis of the 2D reservoir model described in Section 3.2.1. Thus it should replace the x-axis in the equations in Section 3.2.7.

The assumption of perfect inter-layer crossflow allows the application of a single streamline, which is based on the vertically averaged properties of the 3D reservoir model, to all layers of the reservoir on the cross-section surface. This streamline can also be considered as an averaged streamline for all the layers.

The streamline simulator generates lengths and Cartesian coordinates of the segments, like $\Delta\xi_1, \Delta\xi_2...$ in Fig 6.1, as well as the TOF for total flow to pass each segment of the streamline, like $\Delta\tau_1, \Delta\tau_2...$ in Fig 6.1 A ratio of the segment length to the TOF, like $\Delta\xi_1/\Delta\tau_1, \Delta\xi_2/\Delta\tau_2...$, is the total flow velocity in this segment $U(\xi)$. Considering the property of averaged streamlines, $U(\xi)$ is the averaged total velocity of all the layers represented by the same streamline. The streamline simulator may also compute the streamline field on the basis of the injection rate (volume per unit time) assigned from injector to each streamtube q^{st}.

6.3.2 Implementation of Vertical Upscaling Method to 2D Cross-Section Surface Described by Streamlines

Under the assumption of vertical equilibrium or, equivalently, perfect inter-layer communication, the vertical upscaling method introduced in Chapter 3 and Chapter 5 can be applied to the 2D models represented by streamlines. Different from Eq. (3.23), the averaged total velocity $U(\xi)$ is not equal to injection velocity v_{inj} because of the irregular geometry of the streamtube (Fig 6.2a). $U(\xi)$ should replace all terms involving v_{inj} in dimensional expressions for waterflooding process.

We also need to take into account the area of cross-section of a streamtube, since it may be nonuniform along the streamline (Fig 6.2). According to Eq.(6.3), the area of cross-section of a streamtube is equal to volume rate divided by total flow velocity. For example, for the streamline d

$$A_d^{st}(\xi) = \frac{q_d^{st}}{U_d(\xi)}$$

There exist N equations corresponding to the N layers of the reservoir model, similar with Eq.(3.33) but in dimensional form for the case of negligible gravity, saturation equation for layer m is:

$$\phi_m \frac{\partial s_{w,m}}{\partial t} \frac{q_d^{st}}{U_d(\xi)} + q_d^{st} H \frac{\partial}{\partial \xi} \left(\frac{\lambda_m^{sl}}{\sum_{j=1}^{N} \lambda_j^{sl} h_j} F_m \right) - q_d^{st} H \frac{G_m \sum_{j=1}^{m} \frac{\partial}{\partial \xi} \left(\frac{\lambda_j^{sl}}{\sum_{n=1}^{N} \lambda_n^{sl} h_n} \right) h_j - G_{m-1} \sum_{j=1}^{m-1} \frac{\partial}{\partial \xi} \left(\frac{\lambda_j^{sl}}{\sum_{n=1}^{N} \lambda_n^{sl} h_n} \right) h_j}{h_m} = 0 \quad (6.11)$$

It should be stressed that since we calculate saturation along the path of streamlines, mobilities in these equations should be taken along streamline λ^{sl} , so the absolute permeability along streamline k^{sl} should be used instead of the horizontal permeabilities k_x or k_z. k^{sl} usually changes along streamlines in anisotropic medium and it is difficult to calculate it. For simplicity, we assume that all layers of the reservoir are isotropic in the horizontal areal extent that $k_x = k_z$. So we have k^{sl} equal to k_x or k_z.

Similar modification also applies for cases with non-negligible gravity effect (Chapter 5). The full form of equation (Eq.(5.20)) is expressed as:

$$
\begin{aligned}
&\phi_m \frac{\partial s_{w,m}}{\partial t}\frac{q_d^{st}}{U_d(\xi)} + q_d^{st} H \frac{\partial}{\partial \xi}\left[F_m \frac{\lambda_m^{sl}}{\sum_{n=1}^{N}\lambda_n^{sl} h_n} + (\rho_w - \rho_o) g F_m \left(\lambda_m^{sl} B_m - \frac{\lambda_m^{sl}\sum_{n=1}^{N}\lambda_n^{sl} B_n h_n}{\sum_{n=1}^{N}\lambda_n^{sl} h_n}\right)\right] \\
&-q_d^{st} H \left\{ G_m \sum_{j=1}^{m} h_j \frac{\partial}{\partial \xi}\left[\frac{\lambda_m^{sl}}{\sum_{n=1}^{N}\lambda_n^{sl} h_n} + (\rho_w - \rho_o) g \left(\lambda_m^{sl} B_m - \frac{\lambda_m^{sl}\sum_{n=1}^{N}\lambda_n^{sl} B_n h_n}{\sum_{n=1}^{N}\lambda_n^{sl} h_n}\right)\right]\right. \\
&\qquad \left. - G_{m-1} \sum_{j=1}^{m-1} h_j \frac{\partial}{\partial X}\left[\frac{\lambda_m^{sl}}{\sum_{n=1}^{N}\lambda_n^{sl} h_n} + (\rho_w - \rho_o) g \left(\lambda_m^{sl} B_m - \frac{\lambda_m^{sl}\sum_{n=1}^{N}\lambda_n^{sl} B_n h_n}{\sum_{n=1}^{N}\lambda_n^{sl} h_n}\right)\right]\right\} / h_m \\
&-(\rho_w - \rho_o) g \frac{q_d^{st}}{U_d(\xi)} \frac{\lambda_{o,m}^{sl} F_m - \lambda_{o,m}^{sl} F_{m-1}}{h_m} = 0
\end{aligned}
\tag{6.12}
$$

B_m is defined to be

$$
B_m = \int_0^y \frac{\partial F_m}{\partial \xi} dy' \tag{6.13}
$$

The reduced equation (Eq. (5.21))

$$\phi_m \frac{\partial s_{w,m}}{\partial t}\frac{q_d^{st}}{U_d(\xi)} + q_d^{st} H \frac{\partial}{\partial \xi}\left(\frac{\lambda_m^{sl}}{\sum_{j=1}^{N}\lambda_j^{sl} h_j} F_m\right) - q_d^{sl} H \frac{G_m \sum_{j=1}^{m} h_j \frac{\partial}{\partial \xi}\left(\frac{\lambda_j^{sl}}{\sum_{n=1}^{N}\lambda_n^{sl} h_n}\right) - G_{m-1}\sum_{j=1}^{m-1} h_j \frac{\partial}{\partial \xi}\left(\frac{\lambda_j^{sl}}{\sum_{n=1}^{N}\lambda_n^{sl} h_n}\right)}{h_m}$$
$$-\left(\rho_w - \rho_o\right) g \frac{q_d^{st}}{U_d(\xi)} \frac{\lambda_{w,m}^{sl}\left(1-F_m\right) - \lambda_{w,m-1}^{sl}\left(1-F_{m-1}\right)}{h_m} = 0$$

(6.14)

Another remark is that Eqs.(6.11)-(6.14) should be calculated on regular grids of a streamline.

6.3.3 Mapping between the Streamlines and 3D Background Grid Blocks

We assume that the saturation is piecewise constant on the streamlines and the background grid blocks, so that we can use Eq.(6.10) to map saturation between regular grids and irregular grids on streamline, Eq.(6.9) to map saturation from background grid blocks to streamlines and Eq.(6.5) to map saturation from streamlines to background grid blocks. This mapping method can be applied to all the layers for the same streamline. As written at the beginning of section 6.3.1, the vertically averaged model of reservoir, which is used in the streamline simulator, has only one layer with averaged properties of the real reservoir model. Therefore each grid block consists of N layers. The saturation values on all layers in the streamlines are mapped to corresponding layers in the grid blocks, vice versa. In this way, we manage to map saturations between streamlines and the real 3D reservoir model.

6.4 Case Study and Results

In this section, we study the cases of 2-layer and 10-layer communicating reservoirs in absence and in presence of gravity. The sample reservoir models are a quarter of a five spot well pattern. This well pattern is illustrated in Fig. 6.6. The layers of the reservoir model are arranged in an increasing order from bottom to top of the reservoir and characterized by their absolute permeabilities listed below. Other parameters are listed in Table 6.1. We assume that porosity ϕ, irreducible water saturation s_{wi}, residual oil saturation s_{or}, relative water permeability at residual oil saturation kr_{wor}, relative oil permeability at irreducible water saturation kr_{owi} do not change across the layers.

All the cases are implemented in the streamline simulation combined with the vertical upscaling method and full 3D finite difference method. The finite difference solver UTCHEM is developed by University of Texas, Austin. Results by these two methods are compared. Water saturation profiles are all produced for the moment of 0.2 pvi. Oil recovery is calculated up to 2 PVI.

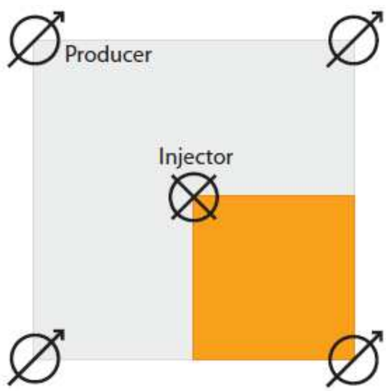

Fig 6.6 Five spot well pattern is shown as the gray area, where one injector is located in the center and four producers are located in each corner. The quarter of a five spot well pattern is the orange area. Adapted from Nielsen (2010).

Dimensional parameters	Values
Length (m)	200
Width (m)	200
Height (m)	50
Location of injector x,z,top*-bottom** (m)	(0,0,0-50)
Location of producer x,z,top-bottom (m)	(200,200,0-50)
Injection volume rate q (m^3/day)	200
Production pressure p_{pro} (KPa)	22500
Size of grid block ($m \times m \times m$)	10×10×10
Porosity ϕ	0.2
Irreducible water saturation s_{wi}	0.2
Residual oil saturation s_{or}	0.2
Relative water permeability at residual oil saturation kr_{wor}	0.8
Relative oil permeability at irreducible water saturation kr_{owi}	0.8
Density of water ρ_w (kg/m^3)	1000
Density of oil ρ_o (kg/m^3)	800
*: Top vertical coordinate of the wells **: Bottom vertical coordinate of the wells Wells extend from the top coordinate to bottom coordinate in the vertical direction	

Table 6.1 Parameters of the 3D reservoir

6.4.1 Numerical Computation

An explicit finite difference method is applied to solve saturation equation along streamlines. Each streamline is discretized into 80 uniform grid steps. No modification about streamline paths needs to be made. The local time step, which is used for calculation along streamlines, is set to be 1 day. The global time step, which is related with pressure and streamlines update, is selected to be 800 days. In one global time step, streamlines do not change. This corresponds to 0.4 pvi in our work. The program is run for 5 times to simulation the injection process of 2 pvi. Thus a piecewise oil recovery curve is expected.

However, we use 400 days (corresponds to 0.2 pvi) as global time step to generate water saturation profiles, since water already breaks through after it is injected for 800 days.

The method is implemented in the Intel Fortran program. Convergence is checked by varying the distance and the time steps.

Average water saturation s_w^* is given by Eq.(3.31) .

6.4.2 Two-Layer Communicating Reservoir with Negligible Gravity Effect

Permeability field and height of each layer are listed in Table 6.2. These parameters result in anisotropy ratio E_a about $\frac{200^2+200^2}{50^2}\times 10 = 320$ (Eq. (3.9)), which is large enough for the assumption of vertical equilibrium or equivalently perfect inter-layer communication. Eq.(6.11) is valid for this case. Saturation distribution on grid blocks of the 3D reservoir and oil recovery curve by our method and full finite difference are given in Fig 6.7. For water saturation distribution on each individual layer (Fig 6.7 a)-d)) and the vertically averaged saturation profile (Fig 6.7 e)-f)), streamline method gives very close results to 3D finite difference. Due to the very good inter-layer communication, waterflooding for the two layers generate only one displacement fronts instead of two individual fronts. The good fit of these two methods is also shown on oil recovery curve (Fig 6.8).

The maximum pressure difference between injector and producer is around $4.7Mpa$ in this case. It decreases as the displacement proceeds.

Dimensional parameters	Layer 1	Layer 2
Horizontal absolute permeability k_x or k_z (mili Darcy)	100	200
Vertical absolute permeability k_y (mili Darcy)	1000	2000
Height h (m)	25	25

Table 6.2 Permeability field and heights of a two-layer reservoir

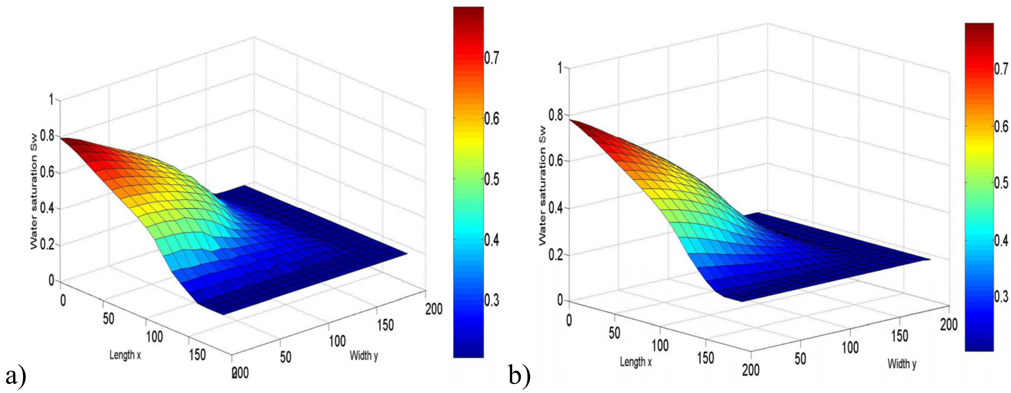

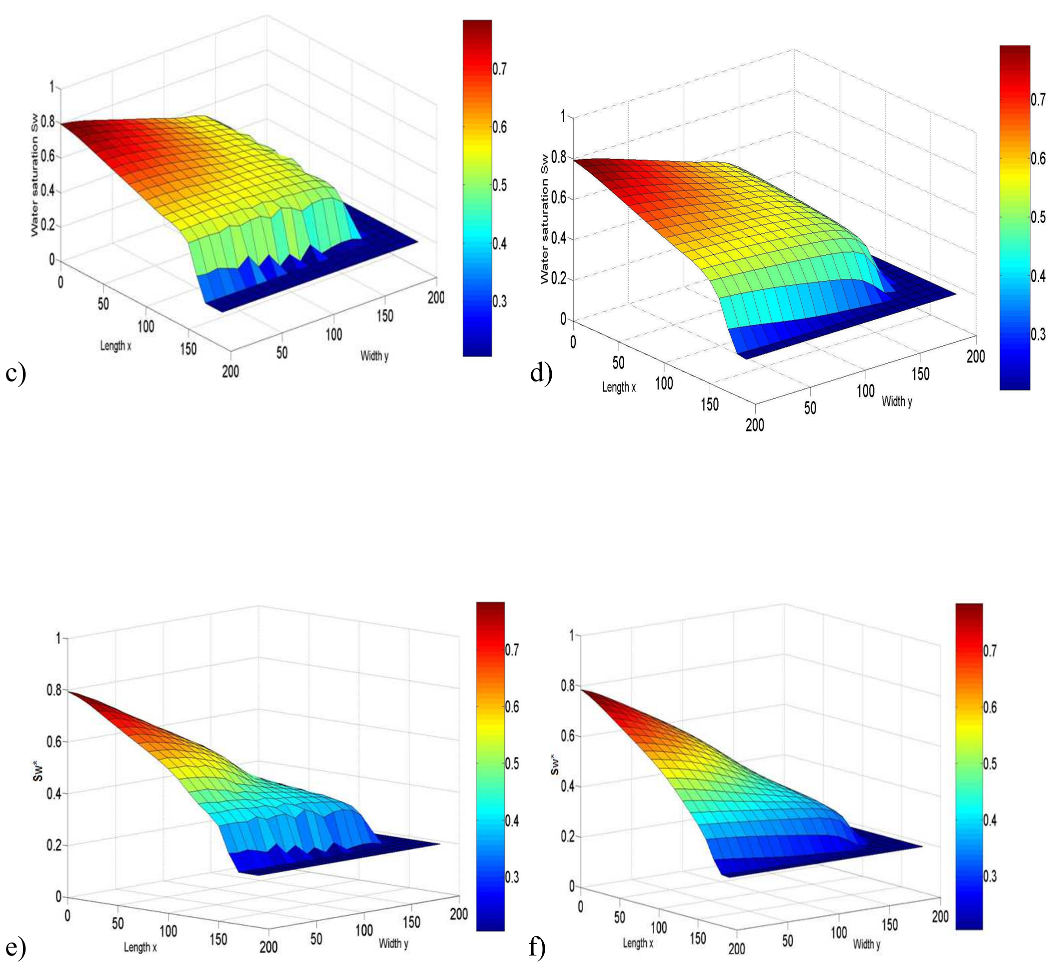

Fig 6.7 Water saturation distribution in a two-layer fully communicating reservoir without inclusion of gravity, at time=0.2 pvi. a)-e) by our method with streamline simulation; b)-f) by 3D finite difference method. a)-b) water saturation on the first (bottom) layer; c)-d) water saturation on the second (top) layer; e)-f) vertically averaged saturation.

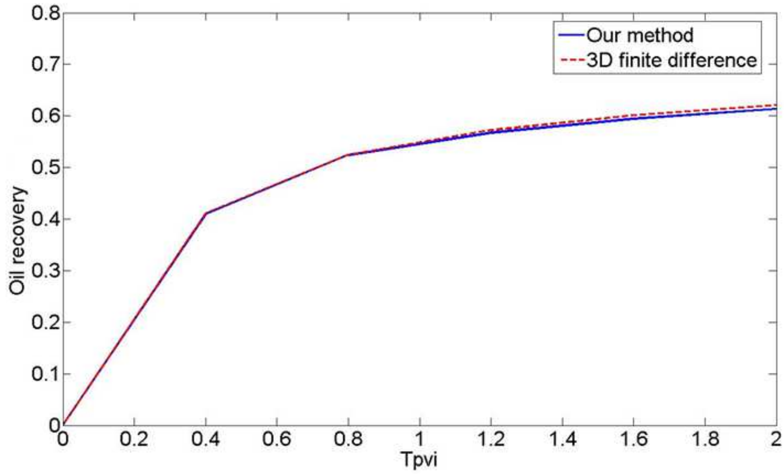

Fig 6.8 Comparison of oil recovery curve by our method with streamline simulation and 3D finite difference method, in two-layer communicating reservoir model without inclusion of gravity.

6.4.3 Ten-Layer Communicating Reservoir with Negligible Gravity Effect

Permeability field and height of each layer are listed in Table 6.3. These parameters result in anisotropy ratio E_a about $\frac{200^2+200^2}{50^2}\times 10 = 320$ (Eq. (3.9)), which is large enough for the validity of Eq.(6.11) in this case. Results are given in Figs 6.9-6.10. We only compare the vertically averaged water saturation profiles by our method (Fig 6.9a) and the finite difference simulation (Fig 6.9b). Oil recovery curves obtained by our vertical upscaling method combined with streamline simulation and by 3D finite difference method are drawn in Fig 6.10. Results by these two methods fit well with each other. The maximum pressure difference between injector and producer is around $3.7Mpa$ in this case. It decreases as the displacement processes.

Dimensional parameters	Values (from layer 1 to layer 10)
Horizontal absolute permeability k_x or k_z (mili darcy)	100,120, 140, 160, 180, 200, 220, 240, 260,280
Vertical absolute permeability k_y (mili darcy)	1000,1200, 1400, 1600, 1800, 2000, 2200, 2400, 2600,2800
Height h (m)	5 for all layers

Table 6.3 Permeability field and heights of a ten-layer reservoir.

a)

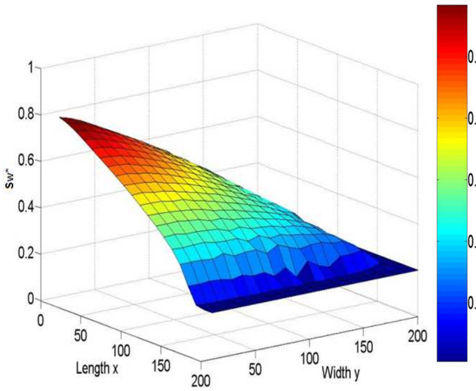

b)

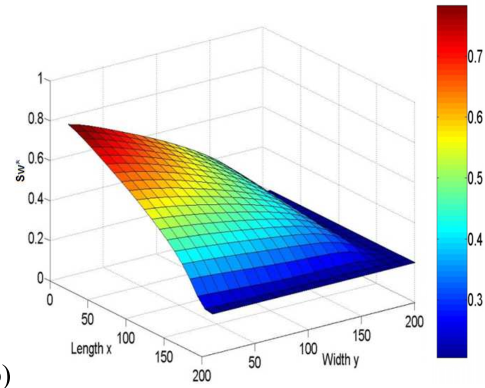

Fig 6.9 Vertically averaged water saturation distribution in a ten-layer fully communicating reservoir without inclusion of gravity at time=0.2 pvi. a) by our method with streamline simulation; b) by 3D finite difference method.

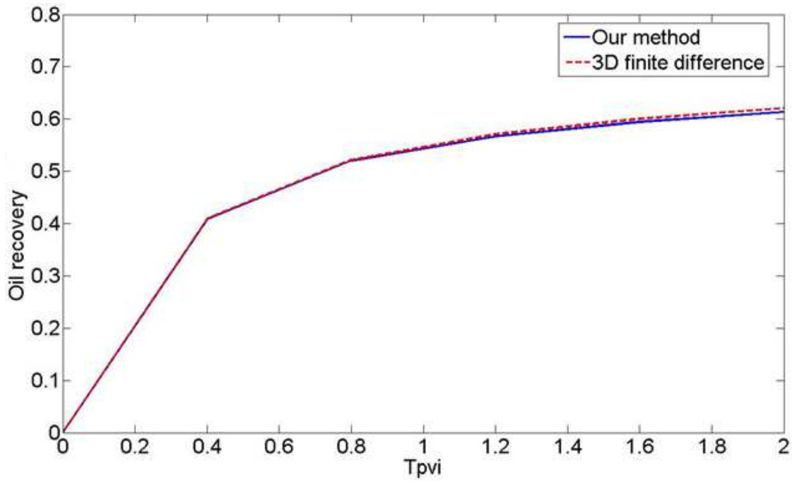

Fig 6.10 Comparison of oil recovery curve by our method with streamline simulation and 3D finite difference method, in ten-layer communicating reservoir model without inclusion of gravity.

6.4.4 Two-Layer Communicating Reservoir with the Gravity Effect

We use the permeability and height parameters in Table 6.2 and include gravity in this case. These parameters result in density ratio E_ρ equal to 0.8. E_g is in the order of 0.1, because in section 6.4.2 we get the pressure difference between injector and producer p_0 around $4.7Mpa$. Thus $E_g(1-E_\rho)$ is in the order of 0.01. According to the analysis in Chapter 5, the reduced equation for water saturation in presence of gravity (Eq.(6.14)) is used for this case. Small sub-layers are used in each big layer, in order to catch the gravity segregation. We split each geological layer into 5 uniform sub-layers. The height of each sub-layer is 5 *m*. Results are given in Figs 6.11-6.12. The difference between result by our method and result by finite difference method is larger than in the cases without gravity inclusion. For oil recovery curve, the largest difference is around 4%, which is acceptable and can be reduced by application of more sub-layers. Large difference between the oil recovery curves made by these two methods happens after injection of 0.8 pvi.

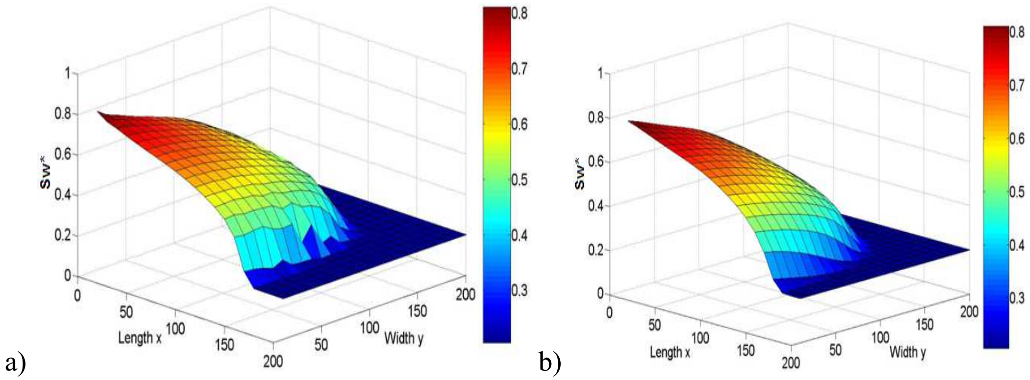

Fig 6.11 Vertically averaged water saturation distribution in a two-layer fully communicating reservoir with inclusion of gravity, at time=0.2 pvi. a) by our method with streamline simulation; b) by 3D finite difference method.

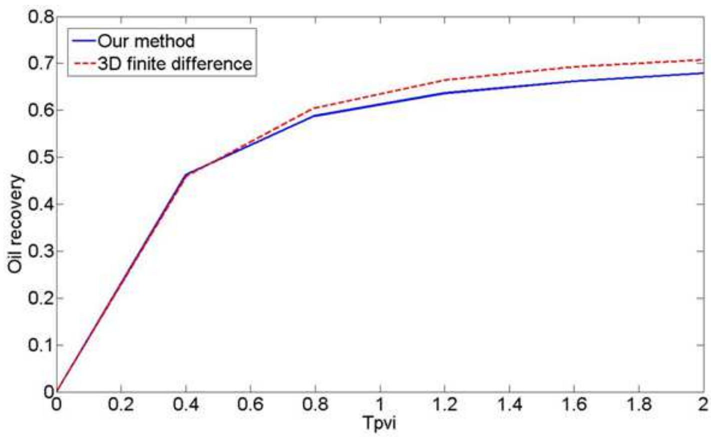

Fig 6.12 Comparison of oil recovery curve by our method with streamline simulation and 3D finite difference method, in two-layer communicating reservoir model with inclusion of gravity.

Compared with the case without gravity (Fig 6.8), oil recovery is around 10% higher in this case, because gravity pulls water down from the fast layer, which is at top, and makes displacement front more uniform (See Fig 11 a)-b) and Fig 7 e)-f)). That increases oil recovery.

6.4.5 Ten-Layer Communicating Reservoir with the Gravity Effect

We use the permeability and height parameters in Table 6.3 and include gravity in this case. These parameters result in density ratio E_ρ equal to 0.8. E_g is in the order of 0.1, because in section 6.4.3 we get the pressure difference between injector and producer p_0 around $3.7Mpa$. Thus $E_g(1-E_\rho)$ is in the order of 0.01. According to the analysis in Chapter 5, the reduced equation for water saturation in presence of gravity (Eq.(6.14)) is used for this case. Results are given in Fig 6.13-6.14.

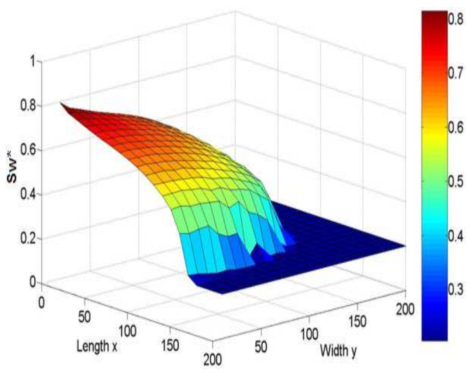

a)

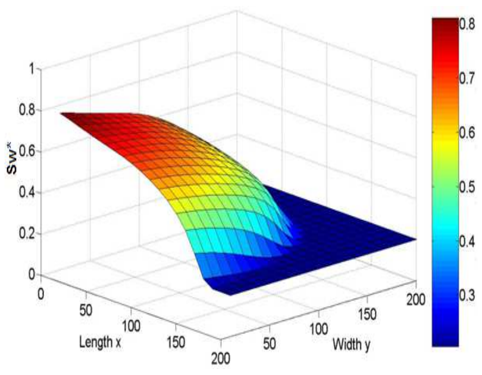

b)

Fig 6.13 Vertically averaged water saturation distribution in a ten-layer fully communicating reservoir with inclusion of gravity, at time=0.2 pvi. a) by our method with streamline simulation; b) by 3D finite difference method.

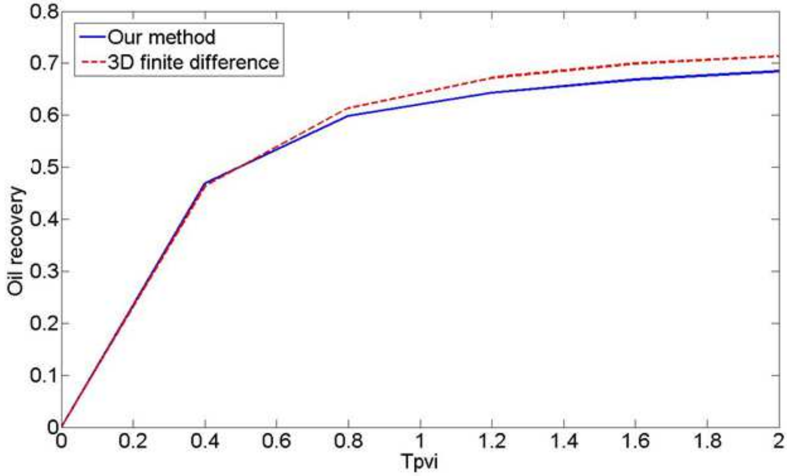

Fig 6.14 Comparison of oil recovery curve by our method with streamline simulation and 3D finite difference method, in ten-layer communicating reservoir model with inclusion of gravity.

The difference between the results produced by our method and the finite difference method is larger than in the cases without gravity inclusion. For the oil recovery curve, the largest difference is around 5%, which is acceptable and can be reduced by application of more sub-layers. The largest difference between the oil recovery curves produced by these two methods appears after injection of 0.8 pvi.

We also get around 10% higher oil recovery in this case compared to the case of the absence of gravity (shown in Fig 6.10).

6.5 Summary

In this chapter, we combine the vertical upscaling method for the two-phase immiscible incompressible flows with the streamline simulation under the assumption that the reservoir is of a layered structure and in vertical equilibrium. In this way, we are able to solve a full 3D problem by means of multiple 1D equations without transforming the problem into the TOF domain. In conventional streamline simulation methods, multiple pseudo 1D problems are written in the TOF domain, which is one-dimensional. Thus the technique of operator splitting is needed for taking gravity term into the final result. However, our 1D problems are written along the paths of streamlines, which are in the space domain. The coordinate along arc length of streamline ξ replaces the coordinate x in two-dimensional space. Vertical coordinate in the description based on streamlines is equivalent to that in two-dimensional space. So cases with gravity effect can be solved directly, without application of operator splitting. But sub-layers with smaller height are needed in order to catch gravity the segregation. The number of sub-layers affects the results.

The cross-sections of the streamtubes may be non-uniform along the arc lengths of the streamlines, so all the 1D equations based on Buckley-Leverett theory should be modified by taking into account the areas of cross-section of the streamtubes.

Our method creates very close results to the finite difference method for cases without inclusion of gravity effect (or negligible gravity effect). For the cases where gravity is not negligible, the error of our method increases, but the results are still acceptable since they have very similar breakthrough times and the saturation profiles compared to the finite difference method. It was also demonstrated that when fast layers, which have higher permeabilities, are on top of slow layers, which have lower permeabilities, gravity helps oil recovery, because it pulls water down and makes displacement fronts more uniform.

Chapter 7 Conclusion

In this PhD project, we have developed a fast semi-analytical 1D simulation method for two-phase immiscible incompressible flow in a layer-cake reservoir. It may be used for upscaling of waterflooding in a stratified reservoir of a viscous dominant regime. We have studied the cases without and with gravity effect included. Capillary pressure is assumed to be negligible.

The essence of the proposed method is to reduce the problem of 2D two-phase immiscible incompressible flow to the multiple 1D flow equations under the assumption of perfect inter-layer communication or, equivalently, vertical equilibrium. By combining with the streamline simulation, our 1D upscaling method may also be applied to the 3D problems. However, the 3D reservoir conditions must be qualified for the assumption of a viscous or gravity-viscous dominant regime with good vertical communication.

For the cases where the gravity effect is negligible, the results obtained by our method are all very close to the results obtained from the complete 2D displacement simulation, in both well defined multilayer reservoir models, as well as the models with log-normal distributed permeabilities. The saturation profile calculated by our method is slightly different from the 2D simulation results. However, the difference is within the degree of approximation and the positions of the displacement fronts are almost the same.

The method developed for upscaling is advantageous over the classical Hearn method, since it refrains from some of the assumptions of the Hearn method and takes into account mass exchange between the layers. Our approach produces more realistic smooth saturation profiles, and is better at predicting positions of displacement fronts and oil recovery curves. Simulations show that different arrangements of the layers lead to different displacement patterns. Since our method does not rely on assumptions of exchangeability of the layers, it is superior to Hearn's procedure.

Inter-layer crossflow affects the overall displacement profiles. It makes displacement profiles more even and smoother in a communicating layer-cake reservoir than those in a non-communicating layer-cake reservoir. In a communicating layer-cake reservoir, larger (larger than 1) values of the end-point mobility ratio (oil to water) lead to more even displacement profiles. With small values of the mobility ratio ($M < 1$), water banks behind the displacement fronts and transition zones before them may be observed. Analysis of the mathematical model and the modeling results indicates that water tends to flow from the less permeable to the more permeable layers behind displacement fronts, while water tends to flow from the more permeable to the less permeable layers ahead of the slower displacement fronts, forming water banks and transition zones.

Inter-layer crossflow also affects oil recovery efficiency. For mobility ratios (oil to water) $M > 1$, more oil is produced by waterflooding from a communicating stratified reservoir than from a non-communicating stratified reservoir. For mobility ratios (oil to water) $M < 1$, the effect is opposite.

For the cases where gravity effect is non-negligible, our 1D method is only applicable where this effect is small to moderate, or where the two phases of flow are not completely separated by gravity. These cases corresponds to small to moderate gravity numbers E_g For the waterflooding problems in well-defined multilayer reservoirs, the results obtained by our method are close to the results obtained by the complete 2D displacement simulation. As gravity effect becomes large, the error of our method increases, but is still within an acceptable range. Partly this is explained by the fact that the gravity effect changes the type of an averaged 1D system for flow in the layers. This system is hyperbolic for negligibly small gravity numbers, but it becomes parabolic for moderate gravity numbers.

Combination of the streamline simulation and our 1D upscaling method enables us to solve a full 3D problem, reducing it to multiple 1D equations. Unlike conventional streamline simulation method, we carry on calculation along the natural paths of the streamlines in the space domain, instead of transforming the problem into the domain of times-of-flight (TOF). The cases with gravity effect can be solved directly, without application of operator splitting. Sub-layers with smaller heights have to be introduced in order to model the gravity segregation more precisely. The number of sub-layers affects the results.

Our method produces very close results to the full finite difference method for the cases without inclusion of the gravity effect (or negligible gravity effect). For the cases where gravity is not negligible, the error of our method increases, but the recovery is still calculated with a reasonable accuracy. When “fast” layers, which have higher permeabilities, are located on top of “slow” layers, gravity helps oil recovery, because it pulls water down and makes displacement more uniform.

Chapter 8 Suggestion for Future Work

The 1D upscaling method presented in this thesis considers only viscous forces and gravity. Inclusion of the capillary pressure in the system would be an important subject for future work. It will make the problem more complicated, since it creates dispersion-like fluxes in all the directions. However, under the assumption of gravity-capillary equilibrium, the problem may probably be simplified.

Our 1D method can only solve problems under small to moderate gravity effect. Improvements and modifications in order to solve the cases under large gravity effect might be another future extension of the method. The macro interface between two phases needs to be accounted in the system of equations. Injection rate will affect the flow behavior when gravity is included. As we know, when a fast layer (with high permeability) is located below a slow layer (with low permeability), gravity tends to make the displacement process unstable, resulting in early breakthrough and low oil recovery efficiency. High injection rate can partly overcome the bad effect from gravity. So a more detailed study of the effect of injection rate is also of interest.

The most obvious continuation of the work is generalization onto the different practically important cases and processes. In the work of Yuan et al. (2011), the method was applied to study the effects of fine migration and re-deposition on recovery under injection of water of the different salinity. This work may further be developed. The improved method may be applied to gas injection or other methods of enhanced oil recovery. Another application is carbon dioxide sequestration for underground storage.

References

Barker, J.W., Thibeau, S.: A Critical Review of the Use of Pseudorelative Permeabilities for Upscaling. In: European 3D Reservoir Modeling Conference, Stavanger. 16-19 April (1996)

Batycky, R. P.: A three-dimensional two-phase field scale streamline simulator. Ph. D. thesis, Department of Petroleum Engineering, Stanford University, California, USA (1997)

Bear, J.: Dynamics of Fluids in Porous Media. American Elsevier Publishing Company (1972)

Bedrikovetsky, P.: Mathematical Theory of Oil and Gas Recovery-with Applications to Ex-ussr Oil and Gas Fields. P3-7, P12, P22, P428-533, Kluwer Academic Publishers (1993)

Berenblyum, R. A.: Streamline Simulation with Capillary Effects Applied to Petroleum Engineering Problems. Ph. D. thesis, Department of Chemical Engineering, Technical University of Denmark, Denmark (2004).

Bird, N. R. A., Perrier, E., and Rieu, M.: The Water Retention Function for A Model of Soil Structure with Pore and Solid Fractal Distributions, Eur. J. Soil Sci., 51: 55–63 (2000)

Bjørnarå, T.I., Aker, E.: Comparing Equations for Two-Phase Fluid Flow in Porous Media. In: COMSOL Conference. Hannover, Germany (2008)

Bondino, I., McDougall, S. R. and Hamon, G.: Pore-Scale Modeling of the Effect of Viscous Pressure Gradients during Heavy Oil Depletion Experiments. SPE 144467 (2010)

Boyer, R.L., Morgan, F., Muskat, M.: A New Method for the Measurement of Oil Saturation in Cores. Journal of Petroleum Technology, January (1947)

Bratvedt, F., Gimse, T., Tegnander, C.: Streamline Simulation for Porous Media Flow Including Gravity. SPE J. (January) (1996)

Buckley, S.E. and Leverett, M. C.: Mechanism of Fluid Displacement in Sands. Transport in Porous Media, AIME 146, 107-116 (1941)

Burdine, N. T., Gournay, L. S. and Reichertz, P. P.: Pore Size Distribution of Petroleum Reservoir Rocks. In: Branch Fall Meeting, San Antonio, Texas, USA. 5-7 October (1949)

Cardwell, W.T., Parsons, R.L.: Gravity Drainage Theory. Journal of Petroleum Technology, November (1948)

Chen, Y., Durlofsky, L. J., Gerritsen, M., Wen, X. H.: A Coupled Local-Global Upscaling Approach for Simulating Flow in Highly Heterugeneous Formations. Advances in Water Resources 26, 1041-1060 (2003)

Corey, A.T., Rathjens, C.H.: Effect of Stratification on Relative Permeability. Journal of Petroleum Technology (1956)

Coats, K.H., Dempsey, J.R., Henderson, J.H.: The Use of Vertical Equilibrium in Two-Dimensional Simulation of Three-Dimensional Reservoir Performance. In: the Second Symposium on Numerical Simulation. Dallas, USA (1970)

Craig, F. F. Jr.: The Reservoir Engineering Aspects of Waterflooding, P15-16. Society of Petroleum Engineering of AIME, New York (1971)

Dake, L.P.: Fundamentals of Reservoir Engineering, P343-365. Elsevier Science B. V. (1978)

Datta-Gupta, A. and King, M.J.: A Semianalytical Approach to Tracer Flow Modeling in Heterogeneous Permeable Media. Advance in Water Resources, 18, 9-24 (1995)

Diaz-Viera, M.A., Lopez-Falcon, D.A., Moctezuma-Berthier, A., Ortiz-Tapia, A.: COMSOL Implementation of a Multiphase Fluid Flow Model in Porous Media. In: COMSOL Conference. Boston, US (2008)

Dietz, D.N.: A Theoretical Approach to the Problem of Encroaching and Bypassing Edge Water. Konikl. Ned. Akad. Wetenschap. (1953)

Dullien, F.A.L.: Porous Media Fluid Transport and Pore Structure. P251, Academic Press (1979)

Dykstra, H.: The Prediction of Oil Recovery by Gravity. Journal of Petroleum Technology, May (1978)

Dykstra, H., Parsons, R.L.: The Prediction of Oil Recovery by Waterflooding. Secondary Oil Recovery of Oil in the United States, 2nd edition, API, 160-174 (1950)

Ekström, T. and Linden, K.: Oil Discharge and Transport in a Natural River. In: COMSOL Users Conference, Stockholm, Sweden (2005)

El-Khatib, N.: The Effect of Crossflow on Waterflooding of Stratified Reservoirs. In: SPE Middle East Oil Technical Conference and Exhibition. Manama (1983)

El-Khatib, N.: Waterflooding Performance of Communicating Stratified Reservoir with Log-Normal Permeability Distribution. SPE Reservoir Eval. & Eng. 2(6), 542-549 (1999)

Elliot, K.T., Kovscek, A.R.: A Numerical Analysis of the Single-Well Steam Assisted Gravity Drainage (SW-SAGD) Process. Report for National Energy Technology Laboratory, National Petroleum Technology Office, U.S. Department of Energy, Tulsa, Oklahoma, July (2001)

El-Sayed, M. S., and Dullien, F .A. L.: Investigation of Transport Phenomena and Pore Structure of Sandstone Samples. In: 28th Annual Technical Meeting Petroleum Society, Edmonton, May 10 – June 3 (1977)

Emanuel, A. S. and Milliken, W. J.: Application of Streamtube Techniques to Full-Field Waterflood Simulation. In: SPE Annual Technical Conference and Exhibition, Dallas, 3-6 October (1995)

Fayers, E J. and Muggeridge, A. H.: Extensions to Dietz Theory and Behavior of Gravity Tongues in Slightly Tilted Reservoirs. SPE Reservoir Engineering, 487-494. (1990)

Gelfand, I. M.: Some problems of the theory of quasi-linear equations. Usp. Mat. Nauk. 24, 2(86), 87-158 (1959)

Guedes, S.S., Schiozer, D.J.: An Implicit Treatment of Upscaling in Numerical Reservoir Simulation. In: SPE Reservoir Simulation Symposium, Houston, USA, 14-16 February (1999)

Halder, A. and Datta, A. K.: Boundary Conditions in Multiphases, Porous Media Transport Models. In: COMSOL Conference, Boston, USA (2009)

Hales, H. B., Cook, K. M.: The Mechanism of Flow in Reservoir Regions Dominated by Gravity Segregation. In: The 10th Canadian International Petroleum Conference, Calgary, 16-18 June (2009)

Hearn, C.L.: Simulation of Stratified Water Flooding by Pseudo Relative Permeability Curves. SPE 2929, (1971)

Hiatt, W.N.: Injected-Fluid Coverage of Multi-Well Reservoir with Permeability Stratification. In:Spring Meeting of the Pacific Coast District, Division of Production. Los Angeles, USA (1958)

Higgins, R. V. and Leighton, A. J.: A Computer Method to Calculate Two-Phase Flow in Any Irregular Bounded Porous Medium. In: The 32nd Annual California Regional Meeting of SPE, Bakersfield, California, USA, 2-3 November (1961)

Huang, Z.: Modeling Two-Phase Flow in Strongly Heterogeneous Porous Media. In: COMSOL Conference, China (2010)

Hunt, A.G.: Percolation Theory for Flow in Porous Media. P33, The Lecture Notes in Physics, Springer, Berlin Heidelberg (2005)

Jacks, H.H., Smith, O.J.E., Mattax, C.C.: The Modeling of a Three-Dimensional Reservoir with a Two-Dimensional Reservoir Simulator-The Use of Dynamic Pseudo Functions. In: SPEAIME 47th Annual Fall Meeting. San Antonio, USA (1972)

Javad, S., Oskouei, P., Maini, B., Moore, R.G., Mehta, S.A., Yazdani, A. J.: Effect of Initial Gas Saturation on Steam Assisted Gravity Drainage Process. In: SPE EUROPEC/EAGE Annual Conference and Exhibition, Vienna, Austria, 23-26 May (2011)

Jessen, K. and Orr, F. M.: Gravity Segregation and Compositional Streamline Simulation. In: The IOR Symposium, Tulsa, Oklahoma, USA, 17– 21 April (2004)

Kanevskaya, R.D.: Asymptotic Analysis of the Effect of Capillary and Gravity Forces on the Two-Dimensional Transport of Two-Phase Systems in a Porous Medium. Fluid Dynamics 4, 557-563 (1988)

King, M.J., Blunt, M.J., Mansfield, M., Christie, M.A.: Rapid Evaluation of the Impact of Heterogeneity on Miscible Gas Injection. In: Western Regional Meeting. Anchorage, AK. (1993)

King, M. J. and Datta-Gupta, A.: Streamline simulation: A current perspective. In Situ 22, P91–140 (1998)

Koval, E. J. 1963, A method for predicting the performance of unstable miscible displacement in heterogeneous media, Soc. Petroleum Eng. J., 3, 145-I55.

Kufus, H.B., Lynch, E.J.: Linear Frontal Displacement in Multi-Layer Sands. Prod. Monthly 24, No. 12, 32, December (1959)

Kurbanov, A.K.: On Some Generalization of the Equations of Flow of a Two-Phase Liquid in Porous Media. Collected Research Papers on Oil Recovery, VNINeft, 15, 32-38 (1961)

Kurbanov, A.K., Atanov, G.A.: On the Problem of Oil Displacement by Water from Heterogeneous Reservoirs. Oil and Gas of Tyumen, Collected Research, 13, 36-38 (1972)

Kyte, J.R., Berry, D.W.: New Pseudofunctions to Control Numerical Dispersion. SPE Journal 269, August (1975)

Lake, L. W.: Enhanced Oil Recovery, Chapter 6. Prentice Hall, Englewood Cliffs, NL (1989)

Lake, L. W. and Hirasaki, G. J.: Taylor's Dispersion in Stratified Porous Media. SPE Journal, 21,459-468. (1981)

Lamine, S., Edwards, M.G.: Multidimensional Cell Based Schemes for Hyperbolic Systems with Gravity in Porous Media on Structured and Unstructured Grids. In: SPE Reservoir Simulation Symposium, Woodlands, Texas, USA, 21-23 February (2011)

Leverett, M. C.: Capillary Behavior in Porous Solids. Trans., AIME 142, 152. (1941)

Longino, B.L. and Kueper, B.H.: Retention of Dense Nonaqueous Phase Liquid (DNAPL) In Fractured Rock, In: 2nd North American Rock Mechanics Symposium, June, Montreal, Quebec, Canada (1996)

Lopez-Falcon, D.A., Diaz-Viera1, M.A. and Ortiz-Tapia1, A.: Transport, Growth, Decay and Sorption of Microorganisms and Nutrients through Porous Media: A Simulation with COMSOL. In: COMSOL Conference, Boston, USA (2008)

Mahfoudhl, J. E., Enlck, R. M.: Extension of the Generalized Dykstra-Parsons Technique to Polymerflooding in Stratified Porous Media. SPE Reservoir Engineering, August (1990)

Mallison, B.T.: Streamline-Based Simulation of Two-Phase Multicomponent Flow in Porous Media. Ph. D. thesis, The Program in Scientific Computing and Computational Mathematics, Stanford University, USA (2004)

Martin, J.C.: Partial Integration of Equations of Multiphase Flow. SPE J. (December), 370-380 (1968)

Melcher, A. F.: Determination of Pore Space of Oil and Gas Sands. In: Lake Superior Meeting. August (1920)

Muskat, M., Taylor, M.O.: Effect of Reservoir Fluid and Rock Characteristics on Production Histories of Gas-Drive Reservoirs. Journal of Petroleum Technology, September (1945)

Nielsen, S.M.: Microbial Enhanced Oil Recovery– Advanced Reservoir Simulation. Ph. D. thesis, Department of Chemical and Biochemical Engineering, Technical University of Denmark, Copenhagen, Denmark (2010)

Orr, F. M.: Theory of gas injection processes. TIE-LINE Publications (2007)

Pau, G.S.H., Bell, J.B., Pruess, K., Almgren, A.S., Lijewski, M.J., Zhang K.: High-Resolution Simulation and Characterization of Density-Driven Flow in CO2 Storage in Saline Aquifers, Advances in Water Resources 33 (2010) 443-455

Reznik, A. A., Enick, R. M., Panvelker, S. B.: An Analytical Extension of the Dykstra-Parsons Vertical Stratification Discrete Solution to a Continuous, Real-Time Basis. SPE Journal, December, 643 (1984)

Rittirong, A., Kelkar, M.: Analytical Upgridding of Geocellular Model to Preserve Dynamic Flow Behavior in the Presence of Gravity Dominated Displacement. In: SPE Improved Oil Recovery Symposium, Tulsa, Oklahoma, USA, 24-28 Apr (2010)

Sarkar, A., G. Georgiou, and M. Sharma.: Transport of Bacteria in Porous Media: II. A Model for Convective Transport and Growth. Biotechnol Bioeng 44, 499–508. (1994)

Scheidegger, A.E.: The Physics of Flow through Porous Media, P56-57, P248. Univ. of Toronto Press (1974)

Shafer, J.M.: Reverse Pathline Calculation of Time-Related Capture Zones in Nonuniform Flow. Ground Water (May-June), 25, No.3, 283-289 (1987)

Snyder, R. W., Ramey, H. J.: Application of Buckley-Leverett Displacement Theory to Non-Communicating Layered Systems. In: SPE Rocky Mountain Regional Meeting, Casper, Wyo, USA. 22-29 May (1967)

Spivak, A.: Gravity Segregation in Two-Phase Displacement Processes. In: SPE-AIME 48th Annual Fall Meeting, Las Vegas, Nevada, USA, 30 Sep- 3 Oct (1973)

Stevens, J. G.: The Effect of a Trailing Zone on the Generalized Dykstra-Parsons Vertical Stratification Analysis. MS thesis, University of Pittsburgh, Pittsburgh, PA, USA (1985)

Stiles, VM. E.: Use of Permeability Distribution in Water Flood Calculation. In: Division Fall Meeting. Dallas, Texas, USA. 4-6 October (1948)

Stone, H.L.: Rigorous Black Oil Pseudo Functions. In: The 11th SPE Symposium on Reservoir simulation, Anaheim, USA. 17-20 February (1991)

Suarez-Rivera, R.: Multiphysics Modeling for Petroleum Geomechanics. In: COMSOL Conference, Las Vegas, USA (2006)

Thiele, M. R.: Modeling Multiphase Flow in Heterogeneous Media Using Streamtubes. Ph. D. thesis, Department of Petroleum Engineering, Stanford University, USA. (1991)

Todd, M. R., Longstaff, W. J.: The Development, Testing and Application of a Numerical Simulator for Predicting Miscible Flood Performance. Journal of Petroleum Technology, 874-82. (1972)

Tyler, S. W., and Wheatcraft , S. W.: Fractal Processes in Soil Water Retention. Water Resource. Res. 26: 1045–1054. (1990)

Tyler S. W., and Wheatcraft, S. W.: Fractal Scaling of Soil Particle Size Distributions - Analysis and Imitations, Soil Sci. Soc. Am. J., 56: 362–369 (1992)

Weber, K.J.: How Heterogeneity Affects Oil Recovery. Reservoir Characterization. Academic Press Inc. P487- 544 (1986)

Weber, K.J., van Geuns, L.C.: Framework for Constructing Clastic Reservoir Simulation Models. Journal of Petroleum Technology, October (1990)

Welge, H. J.: A Simplified Method for Computing Oil Recovery by Gas or Water Drive. In: Petroleum Branch Fall Meeting. Oklahoma City, USA. 3-5 October (1952)

Yokoyama, Y., and Lake, L.W.: The Effects of Capillary Pressure on Immiscible Displacements in Stratified Porous Media, paper SPE 10109 presented at the Society of Petroleum Engineers Fall Technical Conference and Exhibition, San Antonio, Texas (1981)

Yortsos, Y.C.: A Theoretical Analysis of Vertical Flow Equilibrium. In: The 66th SPE Annual Fall Meeting, Dallas, Texas, USA, 6-9 October (1991)

Yortsos, Y.C.: Annlytical Studies for Proceses at Vertical Equilibrium. In: The 3rd European Conference on the Mathematics of Oil Recovery, Holland, 17-19 June (1992)

Yuan,H., Zhang, X., Shapiro, A., Stenby, H.E.: Water Banks in Viscous Dominant Regimes of Displacement. Journal of Petroleum Science and Engineering (2011)

Yuan, H. and Shapiro, A.A.: Induced Migration of Fines during Waterflooding in Communicating Layer-cake Reservoirs. Journal of Petroleum Science and Engineering (2011)

Zapata, V.J., and Lake, L.W.: A Theoretical Analysis of Viscous Crossflow, paper SPE 10111 presented at the Society of Petroleum Engineers Fall Technical Conference and Exhibition, San Antonio, Texas (1981)

Zhang, X., Shapiro, A., Stenby, E. H.: COMSOL Implementation for Upscaling of Two-Phase Immiscible Flows in Communicating Layered Reservoir. In: COMSOL Conference, Paris (2010)

Zhang, X., Shapiro, A., Stenby, E. H.: Upscaling of Two-Phase Immiscible Flows in Communicating Stratified Reservoirs, Transport in Porous Media, 1287 (2011)

Center for Energy Resources Engineering
Department of Chemical and
Biochemical Engineering
Technical University of Denmark
Søltofts Plads, Building 229
DK-2800 Kgs. Lyngby
Denmark

Phone: +45 4525 2800
Fax: +45 4525 4588
Web: www.cere.dtu.dk

ISBN : 978-87-92481-54-2